Contour Method: Procedure Optimization

Daniel Filipe Oliveira Braga

060504113

Master in Mechanical Engineering Dissertation

Supervisors: Dr. Valentin Richter-Trummer

Prof. Paulo Manuel Salgado Tavares de Castro



Faculdade de Engenharia da Universidade do Porto

Master in Mechanical Engineering

January 2012

Abstract

A destructive residual stress measurement technique, the contour method, was studied along this work. Residual stress fields in different specimens were measured using this technique in order to examine each step of the method. This allowed understanding the overall influence of the different required parameters. Improvements for the technique were searched.

Throughout this dissertation it is shown how to achieve trustworthy residual stress measurements with the contour method by showing how each parameter should be chosen. The limitations of the method and potential sources of errors are also discussed.

The contour method was used to study the effect of a post weld rolling technique by comparing two geometrically similar specimens, one without post-welding treatment and the other subjected to a heavy post-welding rolling process.

Results from the contour method were compared with residual stress measurements performed by neutron diffraction on the same specimens, for validation purposes.

Some economic and legal remarks were provided in order to pave the way for a future application of the technique in an industrial environment.

Resumo

Ao longo deste trabalho foi estudada uma técnica de medição de tensões residuais designada 'método *contour*'. Diferentes amostras foram estudadas recorrendo a esta técnica com o objectivo de examinar cada fase do processo procurando perceber quais são os parâmetros envolvidos, qual é o seu efeito nos resultados medidos e também encontrar potenciais melhoramentos para o método.

No decorrer desta dissertação é demonstrado como obter medições de tensões residuais com o método *contour* ao exemplificar como cada paramêtro deve ser escolhido. Também são mostradas limitações da técnica e potenciais fontes de erros.

O método *contour* foi utilizado para estudar o efeito da PWRT (post weld rolling technique) utilizando duas amostras com geometrias semelhantes tendo só uma delas sido submetida ao tratamento de redução de tensões residuais por PWRT.

Resultados obtidos com o método *contour* foram comparados com resultados obtidos por difracção de neutrões realizadas nas mesmas amostras com o objectivo de validar o método.

São apresentados alguns comentários relativos a considerações económicas e legais com o intuito de estabelecer uma ponte para futuras aplicações desta técnica experimental em ambiente industrial.

Acknowledgments

I would like to thank Dr. Valentin Richter-Trummer and Professor Paulo Manuel Salgado Tavares de Castro, supervisors of this dissertation, for the availability and assistance provided throughout the entire work.

I would also like to extend this acknowledgment to Sérgio Tavares and Daniel Peixoto for all the assistance provided especially regarding the different software used throughout this dissertation, such as MATLAB, ABAQUS, LYX and INKSCAPE.

I am grateful to the staff at Autoconceptus and CATIM for their availability to perform the necessary work and to solve challenges regarding the WEDM cuts and CMM measurements.

This dissertation is a result of a suggestion, received from Cranfield University by Valentin Richter-Trummer, to compare their neutron diffraction measurements of residual stress with contour results to be obtained in Porto.

I would like to thank Harry E. Coules and Paul Colegrove from Cranfield University, UK for all the information shared regarding the diffraction measurements and specimen specifications. Tata Steel Europe sponsored the Cranfield University work that is included, for comparison purposes, in this thesis.

The work presented in this thesis is part of the development of residual stress measurement techniques, involved in project PTDC/EME-PME/100204/2008 of the Portuguese FCT - Fundação para a Ciência e Tecnologia.

I am very grateful to my family for their incentive and support throughout my life.

Contents

1 Introduction **1**

1.1 Motivation, Problem Statement and Research Question 1

1.2 Dissertation Synopsis 2

2 Introduction to Residual Stress **3**

2.1 Basic Concepts and Terminology 3

2.1.1 Effect of Residual Stress on Crack Initiation and Growth 5

2.1.2 Residual Stresses and Distortion in Welds 6

2.2 Measurement of Residual Stress 8

2.2.1 Curvature 10

2.2.2 Hole drilling 11

2.2.3 Crack compliance 13

2.2.4 Diffraction 14

2.2.4.1 Laboratory X-Ray Diffraction Technique 15

2.2.4.2 Neutron Diffraction Technique 16

2.2.5 Contour Method 17

2.3 Residual stress treatments 20

3 Technology Requirements of the Contour Method **23**

3.1 Wire electrical discharge machining 23

3.2 Finite Element Method 25

4 Experimental Procedure **27**

4.1 Specimen Details 27

4.2 CT Specimen 30

4.2.1 Parametric study of smoothing operation 33

4.2.2 Parametric study of the CMM measurement grid 42

4.3 Welded Plate Specimens 44

4.3.1 WEDM cutting parameters 44

4.3.2 Parametric study of the smoothing operation 49

4.3.3 Parametric study of the CMM measurement grid 52

4.3.4 FEM considerations 54
4.4 Rolling Technique 57

5 Neutron Diffraction Comparison 59

6 Economic and Legal Considerations 61
6.1 Cost Analysis 61
6.2 Legal Remarks 63

7 Concluding Remarks and Future Works 65
7.1 Conclusions 65
7.2 Future Works 67

References 69

A CT specimen 73

B MATLAB contour method code for welded plate specimen 83

C Fabrication drawings for the clamping system 97

D Residual stress effect on stress intensity factor 101

List of Figures

2.1 Types I, II and III of stresses, Gregory [2008] 4
2.2 Schematic representation of the changes in temperature and stress during bead-on-plate welding, Masubuchi [2005] 7
2.3 Curvature technique (a) layer adding, (b) layer removal, Withers and Bhadeshia [2001] 10
2.4 Strain gauge rosette for hole drilling method, HBM [2011] 11
2.5 Hole drilling and ring coring techniques, Gregory [2008] 12
2.6 Schematic diagram of deep hole drilling, Gregory [2008] 13
2.7 Schematics of crack compliance method, Prime [1999] 13
2.8 Changes in spacing between the rows of atoms are recorded as a shift in the associated diffraction peak - to lower angle for tension as here, or to higher angle for compression, Withers and Webster [2001] 14
2.9 Bueckner's superposition principle, Prime et al. [2009] 18
2.10 Contour method along a line, Prime [2001] 19

3.1 Simple schematics of WEDM, Gregory [2008] 24
3.2 Nomenclature of ABAQUS elements, Simulia [2010] 25

4.1 Geometry of the CT specimen 28
4.2 Plane of cut of CT specimen in the contour method 28
4.3 Welded plate specimen 29
4.4 Measured data of both cut surfaces 30
4.5 Measured data (both cut surfaces) in an interpolated grid 31
4.6 Average plane represented over the interpolated surfaces 31
4.7 Plane rotation 31
4.8 Average plane 32
4.9 Smoothed surface 32
4.10 Residual stress map in MPa for minimum number of smoothing knots {1,1} 34
4.11 Residual stress map in MPa for maximum number of smoothing knots {107,28} 34
4.12 GOF variation with different smoothing knots 35

4.13 Difference between measured stress (MPa) for {5,5} and {10,10} smoothing knots . . . 36
4.14 Surface relaxation for optimum number of smoothing knots (non-smoothed on the left and smoothed on the right) . . . 36
4.15 Residual stress through the thickness for different values of smoothing knots 37
4.16 2-D schematics of the interpolation containing the interpolation grid . . . 38
4.17 2-D Schematic of the smoothing operation . . . 38
4.18 GOF variation with different interpolation densities . . . 39
4.19 Interpolated surfaces using knots {5,5} for the extreme interpolation densities . . . 40
4.20 Smoothed surface relaxation using "linear" interpolation . . . 41
4.21 Smoothed surface relaxation using "cubic" interpolation . . . 41
4.22 Difference in residual stress (MPa) between "v4" and "nearest" interpolation method . . . 42
4.23 Measurement grid scheme . . . 43
4.24 Difference of residual stress (MPa) between the original measurement grid and one with half the density in both directions . . . 44
4.25 Specimen positioning in the WEDM machine using in house clamping system . . . 45
4.26 First successful specimen cut . . . 46
4.27 Mounting and alignment of clamping system . . . 47
4.28 Residual stress measured at plate mid thickness . . . 48
4.29 Scheme showing zone cutting path and direction . . . 48
4.30 Interpolation grid over smoothed average surface deformation [mm] . . . 49
4.31 GOF for different numbers of smoothing knots . . . 50
4.32 Stress map [MPa] using {41-1} smoothing knots and 2x0,5 mm interpolation grid density . . . 50
4.33 Residual stress measured at mid thickness . . . 51
4.34 Average interpolated surface . . . 52
4.35 Stress maps [MPa] using different CMM measurement grids, a) removing points along the thickness and length, b) removing points along the length, c) removing points along the thickness, d) removing interlock points . . . 53
4.36 Difference in measured stress between using the entire CMM measurement grid and removing the points along the thickness . . . 54
4.37 FEM model of quarter plate . . . 55
4.38 FEM model using wedge elements . . . 55
4.39 Difference in measured residual stress [MPa] between using optimized and original FEM mesh . . . 56
4.40 Residual stress (MPa) for rolled (a) and unrolled (b) specimen . . . 57

4.41 Residual stress measured at mid thickness for both rolled and unrolled plate 58

5.1 Residual stress measurement using contour method and neutron diffraction for unrolled plate (a) and rolled plate (b) 60

C.1 Clamping system 97

D.1 Residual stress field 102
D.2 Scheme of infinite plate under remote tension 103
D.3 Stress intensity factor evolution with crack length 104

List of Tables

2.1 Summary of different methods for residual stress measurement, Withers [2001b], ASTM [2008b] 9

4.1 Chemical composition of the S355NL steel, Miranda [2010] 27
4.2 Welding parameters 29

6.1 Contour method approximated costs per measurement 62

Acronyms and Symbols

Symbols

ΔK Stress intensity factor variation

ΔT Temperature variation

σ_{Res} Residual stress

σ_x Stress in x direction

V Volume

da/dn Crack growth rate

R-ratio Minimum to maximum stress ratio

S-N Curve of cyclic stress against the number of cycles to failure

Tm Melting point temperature

Acronyms

AFM Atomic force microscope

BM Base material

CMM Coordinate measuring machine

CPU Central processing unit

EDM Electric discharge machining

FEM Finite element method

GMAW Gas metal arc welding

GOF Goodness of fit

HAZ Heat affeted zone

ILL Institut Laue-Langevin, Grenoble, France

MAG Metal active gas welding

MIG Metal inert gas welding

PWRT Post weld rolling technique

RAM Random access memory

SSD Solid state drive

WEDM Wire electric discharge machining

Chapter 1

Introduction

1.1 Motivation, Problem Statement and Research Question

Residual stresses play a critical role in the failure of mechanical systems due to fatigue, creep, wear, stress corrosion cracking, fracture, buckling, and more. Adding to the concern of potential early failure there is the eventuality of dimensional instability caused by residual stresses after heat treatment or after machining. For these reasons the capability of measuring residual stresses is of fundamental importance for the design and maintenance of present and future mechanical parts and systems.

Residual stresses tend to be of special relevance in parts or systems subjected to strict tolerances, or those highly loaded. Industries where these requirements exist and are therefore interested in measuring these stresses are, for example, aeronautical, aerospace or automotive industries, but also general mechanical construction. Measuring these stresses can be of extreme importance especially where welding is used in the production chain as it generates considerable residual stresses.

The topic of this dissertation is linked to the measurement of residual stresses, more specifically it studies the contour method, which is a recently developed destructive technique able to create a two dimensional map of residual stresses (stresses normal to the cutting plane) on a plane of interest.

The author of this work feels motivated by the developments in this field of science, more specifically the developments studied in this work. Furthermore, bridging the industry and the research centers where this method was invented and developed, which this thesis aims at, is a very rewarding work.

The contour method has been used until now in some laboratories and institutes around the world and provides the challenge for this work; is it possible to optimize this technique? How can it be made ready to be provided as service to industry? For this purpose the effect of several parameters of this experimental method will be studied in order to obtain the best relation between cost and accuracy of measurement. An additional goal is to produce a

practical guide to the contour method.

1.2 Dissertation Synopsis

The research done along this dissertation had the goal of studying residual stress measurement techniques, more specifically a new emerging technique called the contour method.

This dissertation is organized in six chapters including this first one that serves as an introduction to the work. In this chapter the guidelines for the dissertation are defined, the overall goal of the work is stated, and the strategy to achieve that goal is proposed.

The second chapter compiles bibliographic information regarding the main subject studied in this work, residual stress. Residual stress is described and characterized, its effects on fatigue and crack propagation are discussed, and several methods for residual stress measurement including the contour method are mentioned. Older and more established techniques and also some techniques that present similar characteristics to the contour method are also mentioned. The aim of this section is to show the advantages and disadvantages of these methods in relation to the contour method. Finally some treatment techniques used in order to reduce residual stress are mentioned.

The third chapter presents a bibliographic research on technological needs of the experimental work involved in the contour method, such as cutting techniques, more specifically wire electric discharge machining, and finite element method treatment.

In the fourth chapter the experimental procedures performed during this work are described. Firstly the different specimens used in the contour method measurements are described, showing their geometry and other relevant information. Different studies performed with each specimen are then described showing the obtained results.

Economical and legal remarks are made in the sixth chapter. A rough cost analysis is presented in this chapter.

Comparison between results obtained in Porto with contour method and supplied by Cranfield University using neutron diffraction is presented in chapter five.

The seventh chapter presents the final remarks with the most important conclusions from this work. Proposals for future works are made in this section.

Chapter 2

Introduction to Residual Stress

2.1 Basic Concepts and Terminology

With the use of modern analytical and computational techniques, it is often possible to estimate the stresses to which a part is subjected during its life, but this in itself is not enough to determine the component performance along its service life, Withers [2001b]. For a more reliable prediction it is necessary to take into account the residual stresses that may be present in the analyzed component.

> *"Residual stress is the stress that remains in a body that is stationary when all applied stresses have been removed. It is of great relevance to be able to define and quantify these stresses, as they combined with applied stresses can cause failure at levels below that at which failure would occur from applied stresses alone."* Withers [2001b]

Although of great importance, it is also of great difficulty to assess the residual stresses, as they are self-equilibrating and so, unlike applied stresses, they cannot be calculated from the forces, impulses, and couples experienced by material, component, or assembly.

The residual stresses may be categorized in different manners, by cause (e.g., thermal mismatch stresses), according to the methods by which they can be measured (destructive, semi-destructive, non-destructive), or by the scale over which they self-equilibrate (e.g., macro- or microstresses), Withers and Webster [2001], Withers [2001b].

Residual stresses originate from misfits, and they can span over large distances creating macrostresses or they can be accommodated over relatively short distances, creating microstresses. Real materials, in addition to being inhomogeneous on the scale of atoms, can be inhomogeneous on larger scales as well. Examples of this can be dislocations, precipitates, separate grains, reinforcing particles or fibers, and pores or inclusions. These inhomogeneities disrupt the stress field. Thus, measured stress may be recorded as uniform for larger areas, but becomes highly nonuniform as the sampling area approaches the size of the inhomogeneities.

Since by definition residual stresses exist in the absence of external loading, then they must balance to zero within a confined volume, as given by equation 2.1.

$$\int_V \sigma_{Res}\, dV = 0 \tag{2.1}$$

The dimensions of the smallest volume V over which the residual stresses will balance defines a characteristic length that can be used to differentiate between macrostresses and microstresses. Macrostresses are those that balance to zero when integrated over a cross section of the component, so the characteristic length for macrostresses is on the order of the component's dimension. In the case of macrostresses, the material can thus be considered homogeneous, Winholtz [2001].

Residual microstresses result from the presence of inhomogeneities on a small scale and therefore residual microstresses are those between grains in polycrystalline materials, between phases in multiphase materials, (e.g., between matrix and reinforcement in composites), or around other microstructural features such as dislocations or precipitates. Microstresses are then defined as the local variations of stress from the macrostress value within the inhomogeneities of the material. Microstresses will thus balance to zero over a characteristic length of the order of the microstructural features giving rise to them, Winholtz [2001].

For general engineering purposes the effect of the macrostresses are more relevant as they impose noticeable effects on the overall loadings of solid or structures. Microstresses can also have important effects locally, for example in surface treatment.

It is recurrent to categorize residual stress as type I, II and III. Type I are the residual macrostresses, which are the ones that balance themselves over a large length (considering 1-D stress for simplicity purposes). Type II are residual microstresses that balance over a scale comparable to the grain size. Type III are also residual microstresses, but they originate from dislocations and point defects within grains, and will balance to zero over a characteristic length smaller than the grain dimensions. These three types of residual stresses are schematically shown in the Figure 2.1.

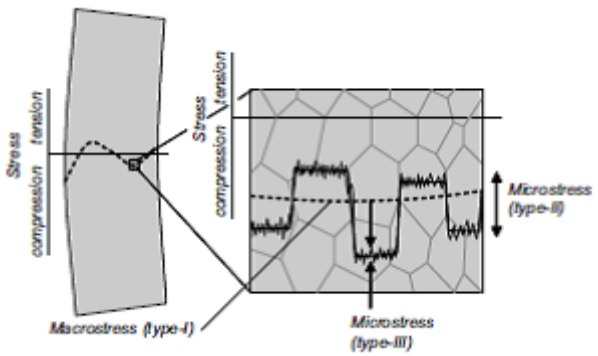


Figure 2.1: Types I, II and III of stresses, Gregory [2008]

Tensile residual stresses are generally regarded as adversely affecting fatigue life and increase stress corrosion and crack propagation in materials. Compressive stresses, on the other hand, can have a beneficial effect in these areas, by inhibiting crack nucleation and growth. For example the compressive stresses induced in shot peening improve fatigue resistance, Gregory [2008].

In the case of brittle materials, the mechanical behavior can be significantly improved with the intelligent use of residual stress. As example of this smart use there is the thermally toughened glass and prestressed concrete. In the first example, rapid cooling of the glass from elevated temperature generates compressive surface stresses which are counterbalanced by tensile stresses in the interior, preventing the initiation of cracks. On the other hand when a defect does penetrate the tensile interior a crack can grow quickly and catastrophically to give the characteristic shattered mosaic-like pattern. Concrete, like glass, is a brittle material and so it has a very low tensile strength, but prestressed concrete can be used in tensile structures, such as cantilever beams. Concrete is prestressed in compression by the tensile members, Withers [2001b].

2.1.1 Effect of Residual Stress on Crack Initiation and Growth

As mentioned before, residual stress has a high influence in many failure processes; one of those is cracking. The influence of residual stress on fatigue-crack initiation life depends on the magnitude and sign (compressive or tensile) of the residual stress, and the cyclic deformation behavior of the structural region of interest, Bouchard [2001].

When a certain component is subjected to cyclic loads and where the local stress-strain response is linear-elastic, the presence of residual stress can either raise or lower crack propagation time. If a crack is subjected to tensile residual stress, it reduces fatigue life. On the other hand if a crack is positioned in a location subjected to compressive residual stress the fatigue life is increased, Bouchard [2001]. The retardation/acceleration effect of compressive/tensile residual stress is also referred in Nelson [1982]. This reference also mentions that a growing fatigue crack will generate its own residual stress field, both in front of and in the wake of the tip. If compressive residual stress are left in the wake of the tip of the fatigue crack it will generate a phenomenon called crack closure, which is responsible for crack growth retardation.

Mean stress is usually characterized in terms of the *R-ratio*, that is the minimum to maximum stress ratio. The effect of *R-ratio* on high-cycle fatigue behavior can be quantified using well-known constant-life models in conjunction with *S-N* (stress-life) curves for the material, geometry and surface finish of interest. This stress-based assessment approach is commonly applied to rotating machinery, welded components, pressure vessels, and aircraft structures subjected to alternating loads, Bouchard [2001].

In the case of components subjected to elevated temperatures such as welded parts, there

is the problem of time-dependent plasticity, or creep, which becomes important at temperatures greater than 0,3 Tm (melting point temperature). The failure mode is often characterized by void growth on grain boundaries. Commonly observed failure modes include stress-relief cracking, reheat-crack initiation, transverse weld cracking, and various types of heat-affected zone cracking in ferritic welds. Relaxation of residual stress associated with a welded joint can have a crucial influence on the susceptibility of a structure to these failure modes. Different assessment procedures for creep-crack initiation in steel components are available, for example in the *"R6 Assessment of the integrity of structures containing defects"* by the British Energy, Bouchard [2001], Milne et al. [1988].

The residual stresses' influence on stable cyclic fatigue crack growth in metallic materials depends on different factors, such as crack size, mechanical load variables, crack closure effects, and the environment. The growth rate per cycle (*da/dN*) of long cracks can be characterized by the stress intensity factor range, $\Delta K = (K_{max} - K_{min})$ of the load cycle. For most engineering alloys, a plot of *log(da/dN)* versus $log\,(\Delta K)$ exhibits a sigmoidal variation having three regions: a threshold regime, an intermediate Paris-Law regime, and a high growth rate regime. Tensile residual stresses in the crack area increase the load *R-ratio* ($R = K_{min}/K_{max}$), and this increases crack growth rates in all three behavior regimes, Bouchard [2001].

2.1.2 Residual Stresses and Distortion in Welds

The developments in mechanical technology and in the use of metals for mechanical systems and parts, led to a continuous development of joining processes for metal alloys, existing today over one hundred of these processes. These techniques include adhesives, fixings, welding (oxyacetylene welding, resistance welding, friction welding, etc.), brazing and soldering, as well as many others. Welded joints present several benefits in comparison to other joining procedures, such as, water and air tightness, and low fabrication costs. For these reasons welding is extensively used in different industries, such as shipbuilding, off-shore structures, steel bridges, and pressure vessels, Teng et al. [2001], Joseph et al. [2005], Masubuchi [2005].

Welding metal alloys involves localized heating and subsequent rapid cooling, which may cause residual stress to appear on the welded component. As the temperature distribution in the weld is nonuniform and changes as welding progresses, it produces complex nonelastic strains in the weld metal and base metal regions near the weld. These nonelastic strains cause residual stresses after the weld cools down to the initial temperature. In this process shrinkage and distortion also occurs. Controlling the resurgence of residual stress and also shrinkage and distortion are major concerns in the development of welding technologies, Teng et al. [2001], Joseph et al. [2005], Masubuchi [2005].

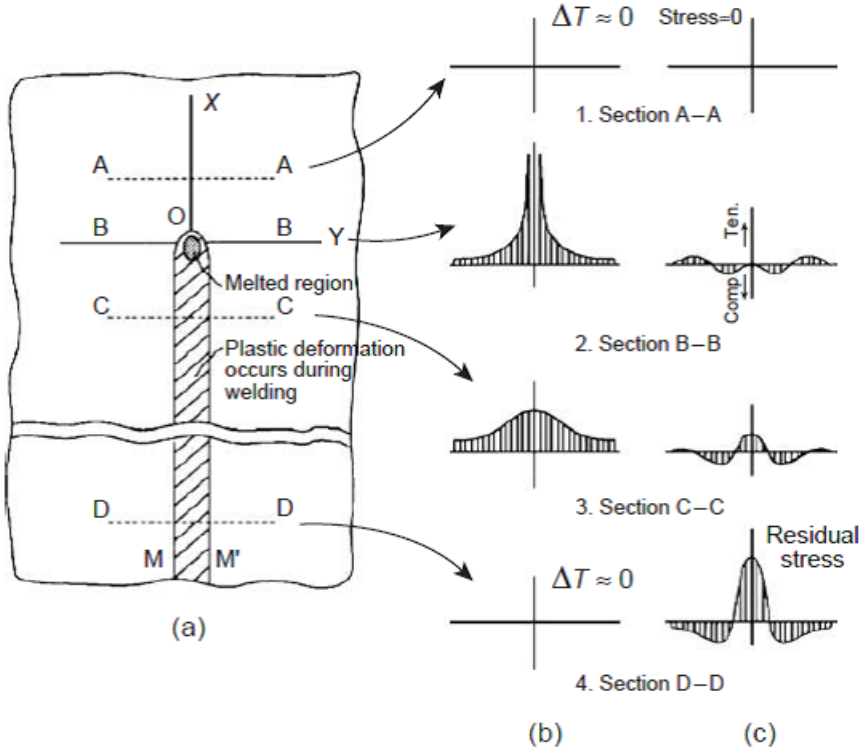


Figure 2.2: Schematic representation of the changes in temperature and stress during bead-on-plate welding, Masubuchi [2005]

In the schematic representation of a bead-on-plate weld shown in Figure 2.2, the weld is being made along the x-axis by a welding arc. Figure 2.2(a) shows the region where plastic deformation occurs during the welding cycle, as cross-hatched area, the region where the metal is melted is shown by the egg-shaped area, and the region outside the cross-hatched area remains elastic during the entire welding thermal cycle, Masubuchi [2005].

Figure 2.2(b) shows the temperature distribution in several cross sections. Cross section A-A is ahead of the welding arc. Section B-B crosses the welding arc. C-C is a cross section at some distance behind the welding arc, and D-D is the cross section behind the arc. In section A-A the temperature difference (ΔT) due to welding is negligible. Along B-B, temperatures in regions near the arc are very high, while temperatures in regions away from the arc are still relatively low having a very steep temperature gradient. Along C-C temperatures in the region near the arc are decreasing, while temperatures in regions away from the arc are still increasing. Along D-D the temperature changes due to welding diminish to nearly zero, Masubuchi [2005].

Figure 2.2(c) shows the stress distribution in the x-direction (σ_x) along the cross sections described above. Along A-A, as this cross-section is before the welding arc, it is theoretically stress free. Along B-B, stresses immediately beneath the welding arc are close to zero because molten metal cannot support loading. Near to the arc, stresses are compressive because the expansion of this area is restrained by surrounding metal at lower temperatures.

Since the temperatures of the heated areas are high and the yield stresses of the material is low, stresses in these areas is limited by the yield stress of the base metal at corresponding temperatures. The magnitude of compressive stress passes through a maximum with increasing distance from the weld or with decreasing temperature. However, stresses in areas away from the weld are tensile and balance with compressive stresses in areas near the weld. Along section C-C, tensile stresses are formed in regions close to the weld, as the the weld metal and base metal have cooled and try to shrink. As the distance from the weld increases, the stresses first change to compressive and then may even become tensile. Along D-D, there is an intensification of the stress field present in section C-C, as high tensile stresses are produced in regions near the weld, while compressive stresses are produced in regions away from the weld. After the welding procedure these stresses will remain on the body and become residual stresses, Masubuchi [2005].

In sum, high tensile stress induced by welding makes the entire applied stress reversal cycles contribute to fatigue, Cheng et al. [2003].

2.2 Measurement of Residual Stress

As mentioned before, residual stresses must self-equilibrate over a characteristic area. For a multiphase material the characteristic area over which the stresses sum to zero will depend on the microstructure. In order to be able to measure the residual stresses on a certain given part it is necessary that the resolution of the technique used to measure those stresses is finer than the characteristic area. As an example, in the case of the hole drilling method, there is a resolution of about 0,1 mm and therefore it is usually insensitive to intergranular stresses, because unless the grain size is very large, their characteristic area is much smaller, Withers [2001b].

In the following table different techniques for measuring residual stress are listed with their corresponding resolution, as well as other relevant information. Over the next sections of this chapter several experimental methods for measuring residual stress will be described, including the one dealt with in this work, the contour method.

Table 2.1: Summary of different methods for residual stress measurement, Withers [2001b], ASTM [2008b]

	Method	Penetration	Spatial resolution	Principle	Comments
Destructive techniques	Curvature	A few mm	1/20 of thickness No lateral resolution	Measures in plane stresses by changes in curvature of strip	Accuracy limited by minimum measurable curvature
	Contour Method	Full plane of interest	Dependent on measu-rement technique and FEM mesh used	Bueckner's superposition princple	Destructive Only suitable for measuring stress normal to the plane of interest
	Hole drilling	< hole diameter	50 μm depth ≈1 mm laterally	Measures in plane stresses by stress relaxation	Semidestructive
Non-destructive techniques	X-ray diffraction	< 50 μm (Al) < 5 μm (Ti)	20 μm depth 1 mm laterally	Atomic strain gauge	Requires layer removal for depth sensitivity
	Hard X-ray diffraction	50 mm (Al)	20 μm depth 1 mm laterally	Atomic strain gauge	Availability Microstructure sensitive
	Neutron diffraction	100 mm (Al) 4 mm (Ti)	500 μm	Atomic strain gauge	Availability Microstructure sensitive
	Ultrasonics	>10 cm	5 mm	Stress-related changes in elastic wave velocity	Microstructure sensitive
	Magnetics	300 μm	1 mm	Stress-related magnetic domain behavior	Magnetic materials only - microstructure sensitive
	Photoelasticity	A few mm	50 μm	Stress-related changes in optical properties	Only for transparent photoelastic materials or coatings
	Thermoelasticity	1 mm	500 μm	Stress-related changes in temperature	Only suitable for cyclic loading
	Raman	Surface unless transparent	1 μm	Stress-related shifts in Raman peaks	Stress-related magnetic domain behavior – microstructure sensitive

2.2.1 Curvature

The curvature technique is a method for measuring residual stress frequently used in the measurement of stress in coatings and layers. Stress can be induced when a layer is deposited, which causes the substrate to curve. This curvature can be measured and therefore make it possible to calculate the corresponding variations in stress as a function of the deposit thickness. Measurement of the curvature can be achieved by direct contact (e.g. profilometry, strain gauges, CMM) or without direct contact (e.g. video, laser scanning, grids, double crystal diffraction topology), allowing curvatures down to about 0,1 mm^{-1} to be routinely characterized. Measurements of the curvature are usually made on narrow strips (width/ length <0,2) to avoid multiaxial curvature and mechanical instability, Withers and Bhadeshia [2001].

Besides measuring the curvature with layer addition it can also be done with layer removal, thus the curvature technique may be used *post-mortem*. This has been done for metallic and polymeric composites, and for thin coatings produced using plasma or chemical vapor deposition and physical vapor deposition, Withers and Bhadeshia [2001].

This process was already used at FEUP to determine the residual stress field, *post-mortem*, for 6 cm thick aluminum rolled plates.

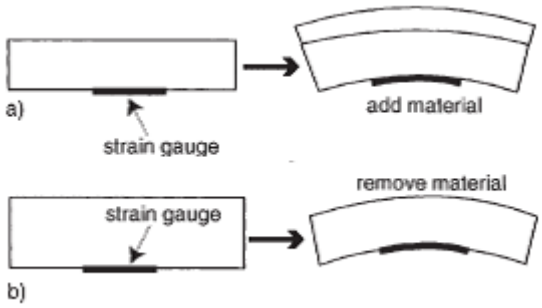


Figure 2.3: Curvature technique (a) layer adding, (b) layer removal, Withers and Bhadeshia [2001]

2.2.2 Hole drilling

Drilling a small hole in a sample, the removal of material will permit stress relaxation around the hole. This is the principle of the hole drilling technique. The measurement of the strains associated with this material relaxation is measured by specially designed triple strain gauge rosette. The gauge rosette, shown in Figure 2.4, permits an estimation of the in-plane stresses that were present in the drilled material from the measured strain relaxations (ε_1,ε_2, ε_3) using the general guiding formula, Withers and Bhadeshia [2001], Gregory [2008], Schajer [1988].

$$\sigma_{max}, \sigma_{min} = -\frac{E}{2}\left(\frac{\varepsilon_3 + \varepsilon_1}{(1+\nu)\,\bar{a}} \pm \frac{\sqrt{(\varepsilon_3 - \varepsilon_1)^2 + (\varepsilon_3 + \varepsilon_1 - 2\varepsilon_2)^2}}{\bar{b}}\right) \tag{2.2}$$

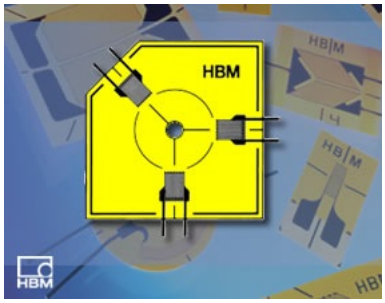


Figure 2.4: Strain gauge rosette for hole drilling method, HBM [2011]

where the values of $\bar{a}$ and $\bar{b}$ are geometrically determined and are tabulated for a number of different setups. This approach is used when the stress field is expected to be uniform with depth, but this is often not the case, particularly when surface treatments have been used. There are a number of non-uniform calculations available for these problems where the hole is drilled incrementally, and strains measured for each depth steps, procedures which are also included in the ASTM standard, Gregory [2008], Schajer [1988], ASTM [2008b].

Hole drilling method is a 'semi-destructive' procedure because although the technique involves material removal, the quantity is quite small, and repairs may be made to the component tested without compromising their integrity, Gregory [2008].

The hole drilling technique is a very mature method for measuring residual stress, as it is over 70 years old, and so, there are a multiplicity of approaches, including different drilling techniques, calibration routines, and analysis tools. Due to its maturity it is very commonly used for measuring residual stress, dealt with in an ASTM standard, Gregory [2008], ASTM [2008b].

The strengths of this technique are its simplicity, common usage, and ability to be used in the field with not too expensive equipment. However, as any experimental technique it also presents weaknesses, such as, the effect that the experience of the operator can have on the accuracy of the results, since depending on who is doing the procedure the results may vary. Also a concern with this technique is that the hole itself causes a stress concentration

that limits the stress that can be measured, although this limit can be extended using strain gauges with four grids. Another concern is that the measurement depth over which it is possible to measure reliably is around 1mm (depending on the hole diameter), due to the decreased sensitivity of the strain gauges mounted on the surface to stress relief at increasing depths, Gregory [2008].

Extensive work about this technique was performed at FEUP by Ribeiro [2006].

There are two major techniques that in essence vary from the hole drilling method, ring coring and deep hole drilling.

In ring coring, shown in Figure 2.5, the strain gauges are attached to the sample and a pedestal is created by trepanning around them. This allows for a bigger depth measurement but introduces a series of experimental problems, such as the need to detached and reattached the strain gauges for every drilling increment, Gregory [2008].

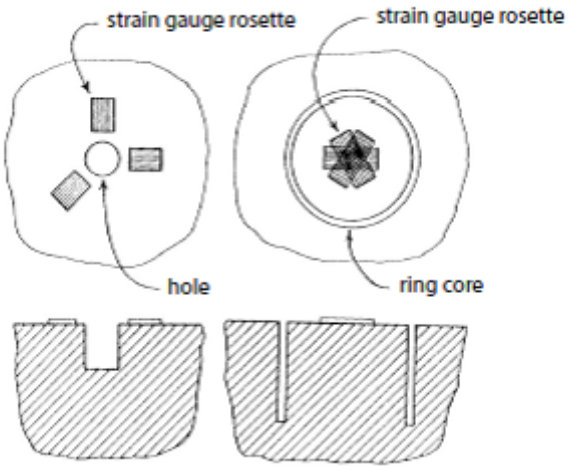


Figure 2.5: Hole drilling and ring coring techniques, Gregory [2008]

Deep hole drilling is another technique derived from the hole drilling method and it permits a through-thickness measurement of stress. This technique can be seen as a combination between the hole drilling and the contour method, as it uses some of the same principles. First, a reference hole is drilled through the sample under examination. The diameter of this hole is then measured, both as a function of angular position, and of depth, using an air probe. Then a cylindrical core, coaxial to the hole, is trepanned, during which any axial extension of the central hole may be measured. After the core has been cut, the reference hole is measured again, and distortion radial to the hole is recorded. This allows the determination of residual stresses in a plane normal to the axis of the hole using elasticity solutions, Gregory [2008]. This method presents high values of penetration but is not valid for measurements at the surface making it invalid for small thickness specimens like the welded plates studied in this work.

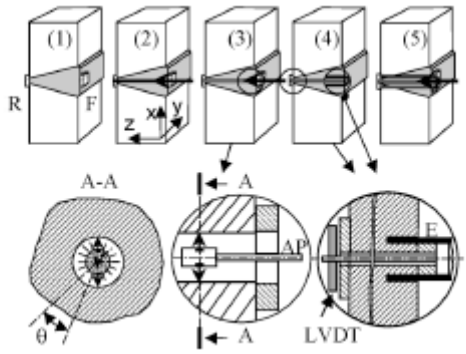


Figure 2.6: Schematic diagram of deep hole drilling, Gregory [2008]

2.2.3 Crack compliance

Crack compliance method is a technique for measurement of residual stress using successive extension of a slot. In this method, as a slit is deepened while strain gauges mounted on each side of the long axis of the slit measure the strains. These measured strains permit the back-calculation of the residual stresses originally present. Crack compliance is sensitive to stresses normal to the cutting direction, due to the geometry of the slit. It is implicit in this technique that the stress field is uniform along the width of the crack (z direction in Figure 2.7), Gregory [2008], Prime [1999].

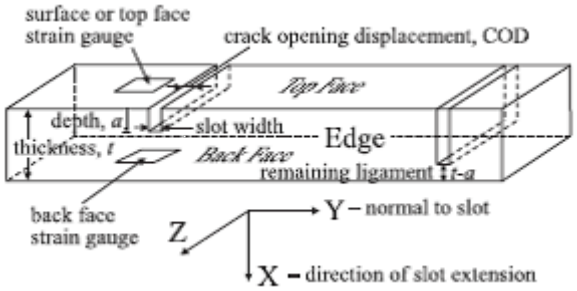


Figure 2.7: Schematics of crack compliance method, Prime [1999]

Crack compliance is still not a very commonly used method, as there is no applicable standard, like there is for hole drilling for example, and therefore it requires a certain degree of experience to determine the relative location of the slit and gauge; however it is a more flexible method than hole drilling or ring coring, as the geometric constrains are much less rigorous, Gregory [2008].

2.2.4 Diffraction

Diffraction based techniques provide the opportunity for mapping residual strain and stress distributions within polycrystalline materials non-destructively. This method is based upon the principle of using the crystalline lattice as an atomic strain gauge. Increases or decreases in the lattice spacing are recorded as angular shifts in the diffraction peak positions. Since diffraction is sensitive primarily to the elastic component of strain, the strains can be used to infer a measure of the stress using appropriate elastic constants. In order to measure three main types of radiation are available, x-ray, photon and neutron beams. These three beams provide very different levels of penetration into crystalline materials and so their applications are quite different, Gregory [2008], Withers and Webster [2001], Withers [2001a].

Diffraction occurs when a wave impinges upon a regular array of scattering objects, provided that the distance between the objects is of the same order of magnitude as the length of the incoming wave. The scattering of the incident wave by this array results in many of the scattered waves being out of phase with each other, leading to destructive interference. However, when the waves are in phase, constructive interference leads to a distinct outgoing wave. This behavior is described by Bragg's law, which relates the wavelength of the incoming wave (and its multiples) $n\lambda$, the spacing of the planes in the scattering array d, and the angle of incidence and diffraction θ, Gregory [2008], Withers [2001a], Withers and Webster [2001], Withers [2007].

$$n\lambda = 2d\sin(\theta) \tag{2.3}$$

Figure 2.8 shows schematically this effect.

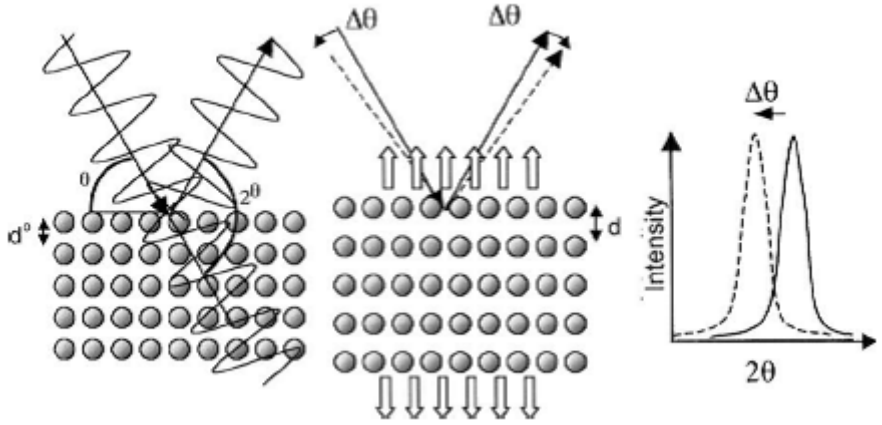


Figure 2.8: Changes in spacing between the rows of atoms are recorded as a shift in the associated diffraction peak - to lower angle for tension as here, or to higher angle for compression, Withers and Webster [2001]

Since elastic strain (ε) results in an increase or decrease in lattice spacing, it can be deduced from shifts in the position of the Bragg peaks.

$$\varepsilon = \frac{d - d^0}{d^0} \tag{2.4}$$

where d^0 is the "stress-free" lattice spacing. Obtaining d^0 is a complex problem, as it is difficult to assure that a certain component is in fact "stress-free", this means that this can be a source of errors in diffraction techniques. It is not possible every time to obtain the "stress-free" lattice spacing in a non destructive way challenging the great advantage of these methods, Withers and Webster [2001].

The unique advantage of the diffraction methods over others is their ability to provide non-destructively, residual strain information internally as a function of position. Their principal limiting feature is the limited access to facilities with capability to provide this methods of residual stress measurement, Withers and Webster [2001].

Within the diffraction techniques those most used for residual stress measurement are the laboratory x-ray and neutron diffraction; both will be briefly discussed next.

2.2.4.1 Laboratory X-Ray Diffraction Technique

Laboratory x-ray diffraction is one of the most commonly used diffraction techniques, due to the fact that a nuclear reactor is not required to perform this experimental technique, but only specialized equipment which in terms of cost is in reach of most research laboratories. In these equipments, x-rays are usually obtained by colliding a stream of energetic electrons, which have been generated by heated filament within an evacuated chamber, with a metal target, Gregory [2008].

The x-ray diffraction technique is based on the principle that when a metal is under stress, the resulting elastic strains can cause the atomic planes in the metallic crystal structure to change their spacing, Gregory [2008], Dronavalli [2004].

The technique uses repeated scanning of a selected peak with the specimen oriented at an increasing angle to the incident beam. The x-ray beam is directed onto the sample surface at the location of interest and the diffracted beam is detected by a position-sensitive proportional counter. The angular position (2θ) of the diffracted beam is used to calculate the distance (*d-spacing*) between parallel planes of atoms using Bragg's law, Dronavalli [2004]

The main strengths of using laboratory x-ray diffraction measurements is the availability of the method, as it is not only reserved for very special research institutes with access to a nuclear reactor but to a wide array of research departments willing to invest in the comparatively affordable equipment. A major disadvantage of this method is that it does not perform well with high degrees of texture or large grain sizes, as the small gauge volume gives a poor statistical measure of the type I stresses. Also it is very limited in terms of penetration, being mostly recommended for measuring the effect of surface treatments, Gregory [2008],

Richter-Trummer [2012].

2.2.4.2 Neutron Diffraction Technique

The neutron diffraction method relies on neutron particle bombardment. The distance between atoms is only about 0.1 nm, much smaller than the wavelength of light (400–700 nm), which renders light useless as an atomic strain gauge, but neutron along with electrons, are subatomic particles that act like waves with wavelengths similar to the distance between atoms, providing them with the capability of extracting the strain values present within the cristals. Another important characteristic of neutrons is that they are electrically neutral, unlike electrons, and therefore they can penetrate more into materials, and are of particular interest for magnetic materials. Penetration is a very important characteristic for non-destructive methods, as it allows greater usability, Gregory [2008], Dronavalli [2004], Hewat [2002].

This technique can provide a complete three-dimensional strain map with high spatial resolution of many engineering components, being mostly limited by the available beam time, which can be expensive, Dronavalli [2004].

Neutrons can be obtained in two different ways, one is by spallation, where a proton beam collides with a heavy metal target, and the other is from a nuclear reactor. This constitutes a limitation for this technique, since obtaining neutrons requires specialized facilities, equipment and specialized personnel, making the technique very expensive and with limited time available for industrial purposes and making the technique mostly viable for scientific research only. Also the size of the specimens studied is limited by the space available in the reactor. Another limitation of this technique is that it is sensitive to microstructural changes, possibly introducing errors in the measurement, Gregory [2008], Hewat [2002], Prime [2001].

2.2.5 Contour Method

With relaxation methods, residual stresses are determined from deformations measured after material removal. Analytical complexity generally limits such techniques to determination of one-dimensional stress variations. In order to perform a two-dimensional or three-dimensional map of residual stress with common relaxation techniques, it is necessary to cut a specimen into many pieces and take many deformation measurements, making this measurement prohibitively complex. The complexity of these measurements is due to conventional relaxation methods using deformations measured away from the location of the stress relief, Prime [2001].

The contour method is the experimental method studied in this work. It is a recently developed relaxation method for residual stress measurement due to Prime [2001]. This method is based on Bueckner's superposition principle and can determine residual stress variations directly from the measured deformations on the surface created by a cut, Gregory [2008], Prime [2001], Shin [2005].

The Bueckner's superposition principle can be best explained through Figure 2.9, where A shows the undisturbed part containing the residual stresses that are to be determined. The part is then cut in two, being represented in B one of the resulting halves. Each half deformes as residual stresses are released by the cut. At this point the surface contour is measured and in C displacement is applied to force the deformed shape back to a flat shape. Assuming elasticity, superimposing the partially relaxed stress state in B with the change in stress from C gives the original residual stress throughout the part, Prime et al. [2009], Prime [2001]:

$$\sigma^{(A)}(x,y,z) = \sigma^{(B)}(x,y,z) + \sigma^{(C)}(x,y,z) \tag{2.5}$$

The overall normal (σ) and shear (τ) stresses in B are not known but the ones acting on the free surface, σ_x, τ_{xy} and τ_{xz}, must be zero and thereforee, C by itself gives those stresses along the plane of the cut, Prime et al. [2009], Prime [2001]:

$$\sigma_x^{(A)}(0,y,z) = \sigma_x^{(C)}(0,y,z) \tag{2.6a}$$

$$\tau_{xy}^{(A)}(0,y,z) = \tau_{xy}^{(C)}(0,y,z) \tag{2.6b}$$

$$\tau_{xz}^{(A)}(0,y,z) = \tau_{xz}^{(C)}(0,y,z) \tag{2.6c}$$

Although in practice, only the normal stress component σ_x, can be experimentally determined, as the measurement of the contour only provides information about the displacements in the normal direction, not those in the transverse directions. therefore, the surface is displaced back to the flat configuration in the x-direction only. The shear stresses τ_{xy} and τ_{xz} are constrained to zero in the solution for C. This stress-free constraint on the surface is auto-

matically enforced in most structural finite-element analysis if the transverse displacements are left unconstrained.

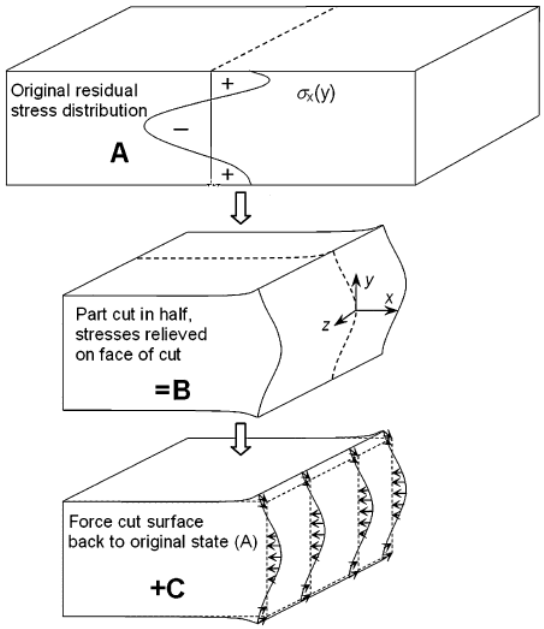


Figure 2.9: Bueckner's superposition principle, Prime et al. [2009]

The contour method is able to determine two-dimensional variations in residual stress directly from the measured deformations. This fact makes the method exceedingly simple in theory. When compared to other methods that are also able to perform a two-dimensional stress measurement, like neutron diffraction for example, it presents itself as more affordable and simple making it a more viable solution for an industrial application. Although the contour method is a more viable solution for industrial applications, they are limited by the need to cut the sample as well as the difficulties in choosing parameters in order to obtain consistent results. This work focuses on decreasing these difficulties, Prime [2001].

The implementation of this technique in the study of manufacturing processes has been a focus of several works. Many manufacturing processes that can be studied using the contour method are quite universal and present a big range of applications, for example laser peening, friction stir welding and fusion welding, but also there are some applications studied by this technique are quite unique, such as, the mapping of residual stress in a railroad rail, in the region of an individual laser peening pulse and under an impact crater, proving the versatility of this technique, Prime et al. [2009].

As mentioned above, the contour method is based on the Bueckner's superposition principle. Figure 2.10 shows the application of the contour method along a line for simplicity, although it can be applied to an entire surface. Cutting the component along the plane in which it is intended to measure the residual stress, relaxes the surface and deforms the body. This superposition principle assumes that the material behaves elastically during the relaxation of residual stress and that the material removal process does not introduces stresses

of sufficient magnitude to affect the measured displacements. The deformation is then measured for both cut halves using a coordinate measuring machine or a laser surface noncontact measuring machine. With both halves measured, it is now necessary to average them in order to remove the effect of transverse stress, as the contour method can only measure normal stress, as well as removing cut induced errors. Finally FEM is used for calculating the stress required to deform the surface back to a flat shape. This calculated stress is equal to the prior residual stress, Prime [2001], Prime et al. [2004], Prime [2009].

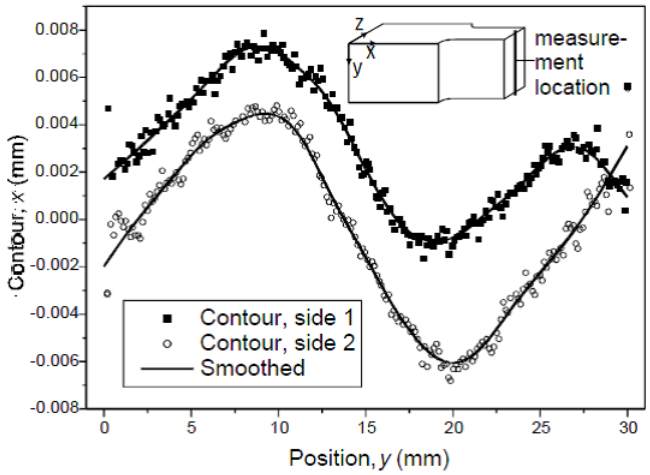


Figure 2.10: Contour method along a line, Prime [2001]

Although the contour method is quite simple in principle, it presents challenges and certain criteria must be guaranteed in order to obtain a reliable measurement. While cutting there are three criteria for a suitable cutting technique: it must make a flat cut, it should remove as little (and as constant) an amount of material as possible, and should cause a minimum of plastic deformation. In order to fulfill these requirements there is currently only one cutting technique available, which is the wire electro discharge machining (WEDM), Prime [2001], Gregory [2008].

The spatial resolution of the contour method is determined by the resolution of the surface metrology. For metals having stresses of hundreds of MPa, the variation of the surfaces can typically be measured in tens of microns across tens of millimeters laterally, so a great number of techniques are either too limited in working volume (atomic force microscopy) or not sufficiently accurate (structured light scanners). The measurements need to be accurate in both lateral location and height. Represented as a dataset, the measurements are always discrete, and it is important to recognize that while the measurement may have been made in a continuous or analog fashion, it will be stored and processed as a series of discrete points, Gregory [2008].

In order to measure surface topography, three broad categories of techniques exist: tactile, optical, and electromagnetic. The tactile category is that of the coordinate measurement machine, or CMM, an instrument in widespread use for quality assurance of fabricated parts.

Much of the initial works on the contour method, such as Prime [2001], used CMMs as they are readily available in many machine shops, operate over large working volumes whilst maintaining precision at the micron level. The optical category contains devices such as triangulating laser probes, confocal microscopes, and interferometers. In particular, the triangulating laser probe is capable of measurements that, although are less accurate than a CMM on a single point basis, when coupled with the higher rate of measurement leads to very large datasets with accuracy that (by virtue of increased counts/unit area) is equivalent to that of the tactile probe. These measurement devices were already used in previous contour method works, such as Prime et al. [2004], proving that they can be used in this method with gains in measuring time. The electromagnetic domain is typified by the atomic force microscope (AFM). The AFM is not suitable for the application of the contour method to engineering samples due to the very limited working volume and slow speed, Gregory [2008], Prime et al. [2004].

For this work, a CMM available at CATIM (Centro de Apoio Tecnológico à Indústria Metalomecânica) was used, which was already used in previous works with the contour method done at FEUP, Richter-Trummer and de Castro [2011], Richter-Trummer et al. [2008].

2.3 Residual stress treatments

As mentioned before in section 2.1.2., the presence of tensile residual stress in welds is an important factor contributing to fatigue crack development, and as such it is necessary for certain components to be treated before entering service in order to avoid premature failure. Induced compressive stress by post-weld treatment can improve service life by reducing tensile stress and introducing compression residual stress in areas of interest which improves fatigue strength of welded structures. Although residual stress self-equilibrates (and so the induced compressive stress in certain areas will result in tension stress in other) with well performed post weld treatments the areas with induced tension stress will be the non critical areas, Cheng et al. [2003].

Conventional post-weld treatment techniques include grinding, air hammer peening, shot peening, needle peening, laser shock peening, TIG (tungsten inert gas) remelting, ball/roller burnishing and deep cold rolling. Grinding and TIG dressing can well improve the weld toe profile and reduce stress concentration effects. However, tensile residual stresses remain due to the heat produced in the treatment operation. Mechanical surface treatments, such as peening treatments, ball/roller burnishing or deep cold rolling, induce plastic deformation in near-surface area of the components resulting in formation of compressive residual stresses, work hardening and changes in surface topography, Tolga Bozdana et al. [2005], Cheng et al. [2003].

Shot peening is a cold working process in which the surface of metal material is bom-

barded with small spherical shot. Each sphere that hits the target acts as a tiny peening hammer, creating a small indentation or dimple on the surface. Overlapping dimples develop an even layer of metal in compressive stress and cold works on the surface, which increases fatigue life, Cheng et al. [2003].

Deep cold rolling is one of the most used treatments for enhancing surface characteristics and service properties of titanium alloy components, and it consists in plastically deforming near-surface layers of the component using a spherical ball, which is pressed against the component surface and is rolled over along the surface to be treated. Compared with other treatment processes, deep cold rolling presents several advantages, such the generation of a deep and high compressive residual stresses and a work hardened microstructure as well as a relatively smoother surface finish. Although deep cold rolling is restricted to certain geometries, it is an inexpensive, fast and easy process. Compressive stresses induced in post weld roller tensioning are determine by the amount of roller force induced in the specimen being treated. In cases of higher roller loads the compressive stress induced may be significantly higher than the tension residual stress present in the weld and therefore compressive residual stresses are introduced which effectively slow down or stop crack propagation, Tolga Bozdana et al. [2005], Altenkirch et al. [2009].

Ultrasonic technology has been introduced to further improve the effect of conventional surface enhancement techniques. The use of ultrasonic vibrations reduces the amount of pressure to be applied on the part surface for achieving the required plastic deformation. For this reason, ultrasonically assisted surface enhancement processes are particularly beneficial for treatment of components with thin sections such as turbine blades and discs. Ultrasonic shot peening is one example of this application, in which the shots are accelerated by ultrasonic vibrations so that the impact effect of the shots on the part surface is increased, Tolga Bozdana et al. [2005].

Sandblasting is a surface treatment normally used to clean weld slags or to remove surface corrosion but it induces small compression stresses onto the treated surface and so it may cause an effect on present residual stress. Effective penetration of sandblasting has been presented in several published studies. Jiang et al. [2006] has shown that in titanium alloy sheets the compressive stresses had a penetration of 0,07 mm. Rhouma et al. [2001] have shown the depth under compression due to sandblasting for stainless steel alloys, which presented a larger value than in the case of titanium alloys since these present higher values of yield strength. The penetration shown was around 0,3 mm.

Chapter 3

Technology Requirements of the Contour Method

3.1 Wire electrical discharge machining

Electrical discharge machining (EDM) has become a well-established alternative to conventional machining, when the purpose is to machine complex geometries or hard metals. This type of machining operations went through a great technological evolution, as the interest in non-contact machining grew from a mere tool and die making process, to a machining alternative, and in that process attracting a considerable amount of research interest. The unique feature of EDM is the use of thermal energy to machine electrically conductive parts (or non conductive if coatings are used in some EDM techniques) regardless of hardness, which is a great advantage when compared to conventional machining processes, Ho and Newman [2003], Mohd Abbas et al. [2007].

In this machining technique the material removal is achieved by an erosion mechanism that makes use of the electrical energy and turns it into thermal energy through a series of discrete electrical discharges occurring between the electrode and work piece immersed in a dielectric fluid. The generated thermal energy causes the formation of a channel of plasma between the cathode and the anode at a temperature in the range of 8000 ºC to 12000 ºC initializing a substantial amount of heating and melting of material at the surface of each pole, Ho and Newman [2003].

Within the EDM techniques there is the wire electrical discharge machining (WEDM), which is a fast evolving machining technique, widely used in the aerospace and automotive industries. In WEDM, Figure 3.1, thin continuously travelling wire feeding is used through the work piece by a micro-processor, which eliminates the need for elaborate pre-shaped electrodes, required in EDM, thereforee making the process more affordable. The main reason for the proliferation of this machining process is its effectiveness cutting hard materials with intricate shapes. However due to the complicated stochastic process mechanisms in

WEDM a completely reliable model for the relationship between the cutting parameters and cutting performance is not available, even for the most sophisticated CNC WEDM machines, and so the selection of the cutting parameters can present itself as problem, Mohd Abbas et al. [2007], Tarng et al. [1995].

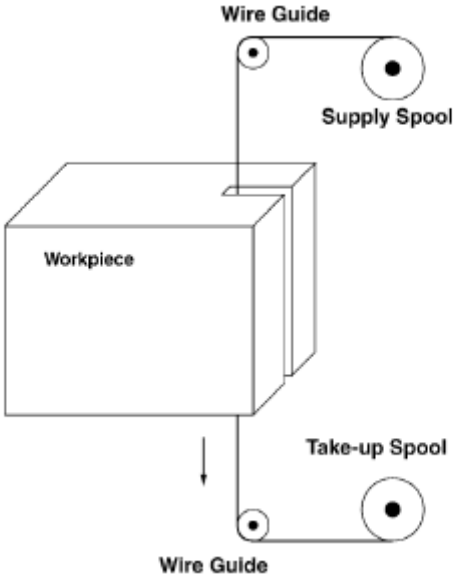


Figure 3.1: Simple schematics of WEDM, Gregory [2008]

In order to evaluate the performance in WEDM process, the removal rate, the cutting width and the surface finish should be taken into account, all of which are results of parameter variations. These parameters are discharge current, pulse duration, pulse frequency, wire speed, wire tension, dielectric flow rate and cutting speed. The computer control of the WEDM machine besides controlling the parameters also has to maintain a stable gap between wire and work piece (difference between cut width and wire diameter). This gap should be in the range from 0,025 to 0,075 mm, Mahapatra and Patnaik [2006].

Economics and rate of production of this machining process are largely determined according to the material removal rate, which is calculated by weight difference of the specimens before and after machining operations, Mahapatra and Patnaik [2006].

For the contour method high speed is not relevant, as the key issue is to guarantee that the cut is performed in one pass without the wire breaking. To ensure that the wire does not break and to improve the quality of the cut surfaces skim cut configuration is used, as it was already used in previous works of other authors, Gregory [2008], Prime et al. [2004], Richter-Trummer and de Castro [2011].

3.2 Finite Element Method

The advent of digital computers has permitted to obtain a solution within a reasonable time schedule even with large numbers of elements. This was a major factor in the development and proliferation of the use of the finite element method method, Zienkiewicz and Taylor [2000].

Finite element method is defined as a method or approximation to continuum problems such that:

> *a. "The continuum is divided into a finite number of parts (elements), the behavior of which is specified by a finite number of parameters,*
>
> *b. The solution of the complete system as an assembly of its elements follows precisely the same rules as those applicable to standard discrete problems"*,Zienkiewicz and Taylor [2000].

As mentioned in section 2.2.5 of this work it is necessary to use finite elements in order to obtain the stresses corresponding to the measured displacements in the contour method. In this work the commercial ABAQUS finite element package was used for reasons of availability and also due to its simplicity of use.

ABAQUS contains a very vast library of elements but for this work, only 3D solid elements of the "stress/displacement" element family were used. Figure 3.2 shows the nomenclature of these types of elements given by ABAQUS, Simulia [2010].

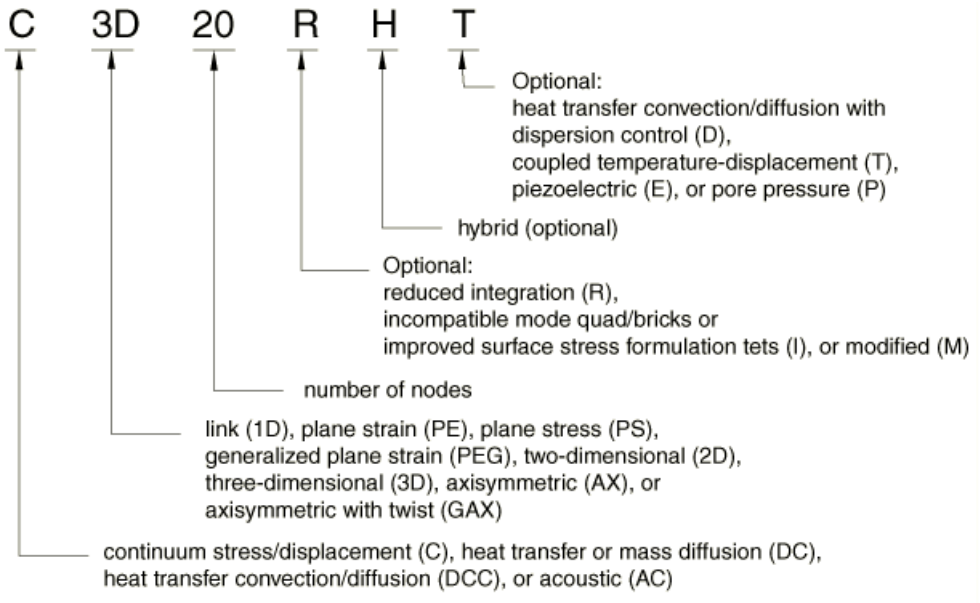


Figure 3.2: Nomenclature of ABAQUS elements, Simulia [2010]

The elements used in this work, according to the ABAQUS nomenclature, were the C3D8, C3D8R and C3D6H. Both C3D8 and C3D8R are 3D solid elements with 8 nodes

linear bricks, while C3D6H is a 3D wedge elements with 6 nodes. The only difference between the two linear brick elements is that C3D8R has reduced integration with hourglass control, which permits a faster calculation, due to the fact that the number of Gauss points is lower if reduced integration is used. Although the integration time is lower there is a cost in accuracy as a higher number of Gauss points leads to higher accuracy, up to a certain limit. Another problem present in reduced elements is the hourglass effect, in which elements become excessively flexible and therefore render the results useless, Sun [2006], Simulia [2010].

In order to apply measured data from the contour method to the FEM model, certain steps have to be followed, in order to guarantee that at least the first order derivative of the applied displacement distribution is continuous. These steps include, Richter-Trummer [2012]:

- The data measured of both halves has to be averaged, interpolating every point onto the same grid and in that way reducing the error in each point;
- The averaged data of both halves has to be smoothed and fitted to continuous functions with continuous first derivatives. Doing this procedure reduces errors in the interpolation of the node values to the Gauss points;
- The averaged and smoothed data has to be aligned to a plane that guarantees that the average displacement of the surface is zero.

Chapter 4

Experimental Procedure

4.1 Specimen Details

The first specimen used in this work was a compact tension specimen (CT) with the thickness of 32 mm and according ASTM [2008a], see Figure 4.1. This specimen was extracted from steel plates welded under similar conditions to those used for the new railway bridge in Alcácer do Sal in Portugal, Richter-Trummer [2012].

The base material used in these specimens was the steel grade S355NL, which is a normalized rolled structural steel according to EN 10025, EN 10163, with the chemical composition shown in Table 4.1, Miranda [2010].

Table 4.1: Chemical composition of the S355NL steel, Miranda [2010]

Steel grade	C (%)	Si (%)	Mn (%)	P (%)	S (%)	Al (%)
S355NL	Max 0,18	Max 0,5	Max 1,65	Max 0,025	Max 0,02	Max 0,02

N (%)	Cr (%)	Cu (%)	Ni (%)	Ti (%)	V (%)	Nb (%)
Max 0,015	Max 0,3	Max 0,55	Max 0,5	Max 0,05	Max 0,12	Max 0,05

The base material was welded using gas metal arc welding (GMAW) with active gas shield (MAG). The welding was performed in 36 passes using a double V preparation of the joint surfaces, Richter-Trummer [2012], Miranda [2010].

As mentioned before the first specimens were of the CT type according to ASTM E647 standard with its geometry shown in Figure 4.1.

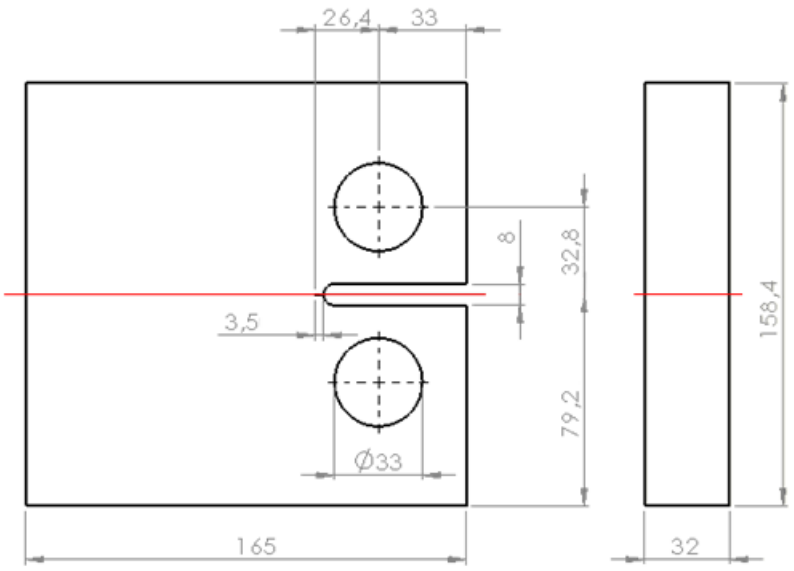


Figure 4.1: Geometry of the CT specimen

The red line in Figure 4.1 repesents the cut made and respective plane of study.

For the FEM calculations a Young's modulus of 210 GPa and Poisson's ratio of 0,3 were used. The yield strength of this steel was presented in a previous work (Richter-Trummer [2012]) and it is near 400 MPa.

The residual stress measurement was performed along a plane which included, weld material (WM), heat affected zone (HAZ) and base material (BM) like it is represented in the Figure 4.2.

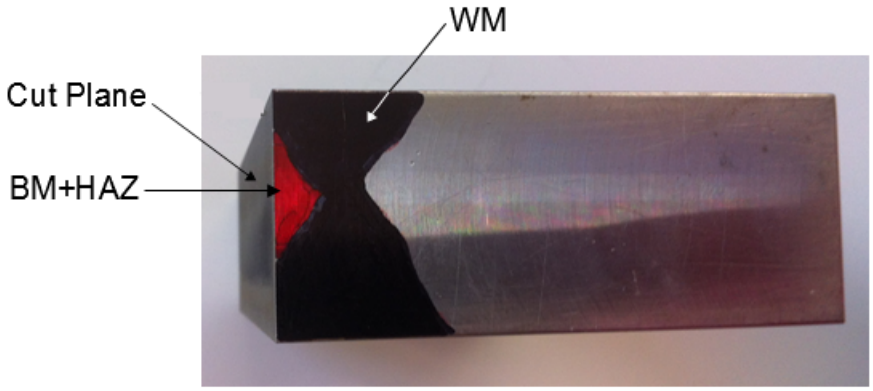


Figure 4.2: Plane of cut of CT specimen in the contour method

The other three specimens used in this work were provided by Cranfield University (Harry Coules and Paul Colegrove) and are S355NL steel plates with dimensions of 760 x 300 x 6 mm, with a weld deposit in the middle, seen in Figure 4.3.

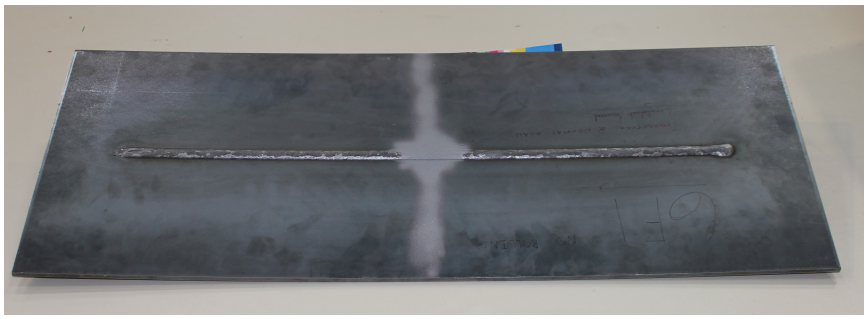


Figure 4.3: Welded plate specimen

The three specimens had a weld deposit done using the same parameters which are shown in Table 4.2.

Table 4.2: Welding parameters

Process	MIG (Pulsed), single pass
Power Supply	Fronius TransPuls Synergic 5000
Current	328 A
Voltage	35,1 V
Travel speed	500 mm/min
Filler wire feed speed	15 m/min
Contact Tip to Work Distance	13 mm
Gas Rate	10 ltr/min
Gas Composition	20% CO2, 2% O2, balance Ar
Filler Material	G3Si1

Two of the samples were not subjected to any post-weld treatment, while one was treated for residual stress reduction using a rolling technique. The rolling was done in a single pass at a speed of 500 mm/min and with a roller force of 150 kN.

4.2 CT Specimen

The CT specimen has already been used in previous works, with the purpose of studying a different topic and therefore was available at the beginning of this project. Also it constituted a great candidate for a first parametric study as the specimen has a very regular geometry, specially when compared with the welded plates specimens, as they presented a bulge due to the presence of the weld. In terms of complexity it is appropriate to start with a model that had a regular shape, such as the CT specimen and then evolve to more irregularly shaped specimens, such as the welded plates specimens.

The cutting and measuring of these specimens was done before and so the beginning point for this parametric study is the measured data of both cut halves surfaces, shown in Figure 4.4.

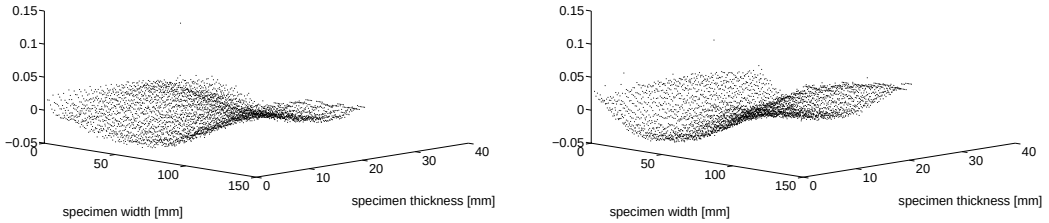


Figure 4.4: Measured data of both cut surfaces

From the measured surface relaxation to the actual residual stress present in the surface it is necessary to mathematically manipulate the data, which was done using MATLAB. Since the original measured data presents a very irregular surface, it is necessary to smooth the data. The smoothing operation is done through a MATLAB algorithm called “Spap2” and this algorithm only accepts regularly gridded surfaces, which results in the need to interpolate the data in order to obtain that same regular grid. A MATLAB algorithm has to be developed for this mathematical manipulation and it has to contain these 5 steps:

1. Interpolate both halves to a similar rectangular grid;
2. Calculate the middle plane of both halves and use it to align the interpolated data with Oxy plane and with each other;
3. Average both interpolated surfaces;
4. Smooth the surface in order to remove some of the measurement noise;
5. Write the smoothed interpolated surface relaxation to the FEM mesh.

The full algorithm created for the purpose of this study of the contour method with the CT specimen can be found in the appendix A of this dissertation but each step is briefly explained and shown.

Firstly using the MATLAB function “Griddata” and a user defined interpolation grid the original data is interpolated to a regular grid as shown in the following Figure 4.5. As the CT specimen is already a very geometrically regular specimen the interpolated surface does not look much different from the original data.

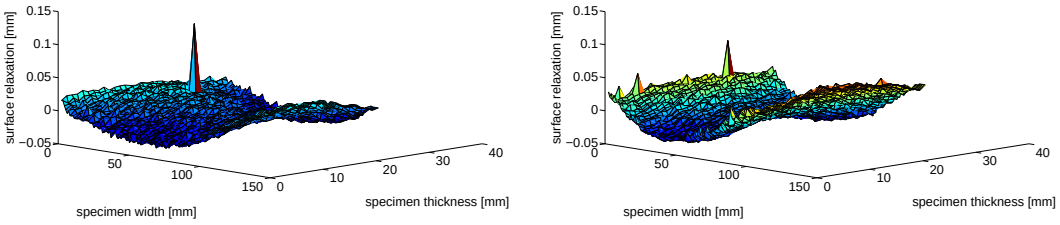


Figure 4.5: Measured data (both cut surfaces) in an interpolated grid

Having interpolated the data, the average plane of each cut surface has to be calculated. Figure 4.6 presents the surfaces along with the respective average planes.

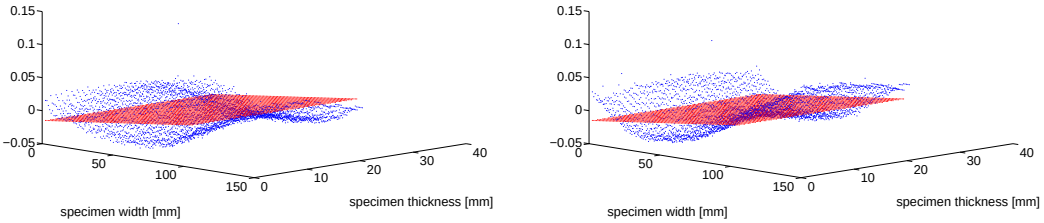


Figure 4.6: Average plane represented over the interpolated surfaces

Figure 4.6 represents schematically the rotation of the measured interpolated surface in one specific point and only in one dimension to better illustrate the principle. Point A is situated in the original surface and it has to rotate by α degrees in order to position the middle plane in the reference Oxy plane. A point in the new position is A* but as the angle is quite small this operation can be done by subtracting the value of the z coordinate in the original plane with the z coordinate of the equivalent point in the average plane. This results in the new point A** and introduces an error represented in the Figure 4.7 as the red line. As said before the angle α and the distances in reality are very small and so this error is also very small and can be ignored.

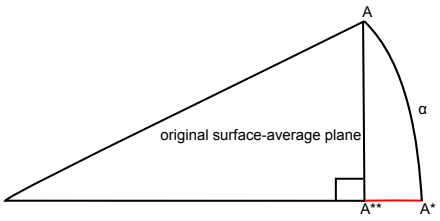


Figure 4.7: Plane rotation

After both planes have been aligned it is necessary to average them. An example of this averaged surface is shown in Figure 4.8.

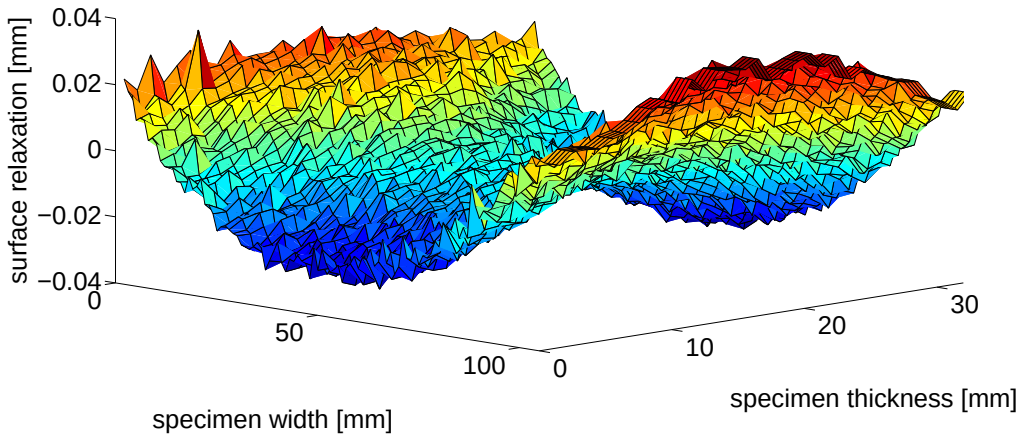


Figure 4.8: Average plane

But as it can be seen in the Figure 4.8 the amount of measurement noise is quite high and therefore it is required to perform a smoothing operation which is done using the MATLAB function “Spap2”. This function will be better studied in the next subsection. The result of the smoothing operation is shown in the Figure 4.9.

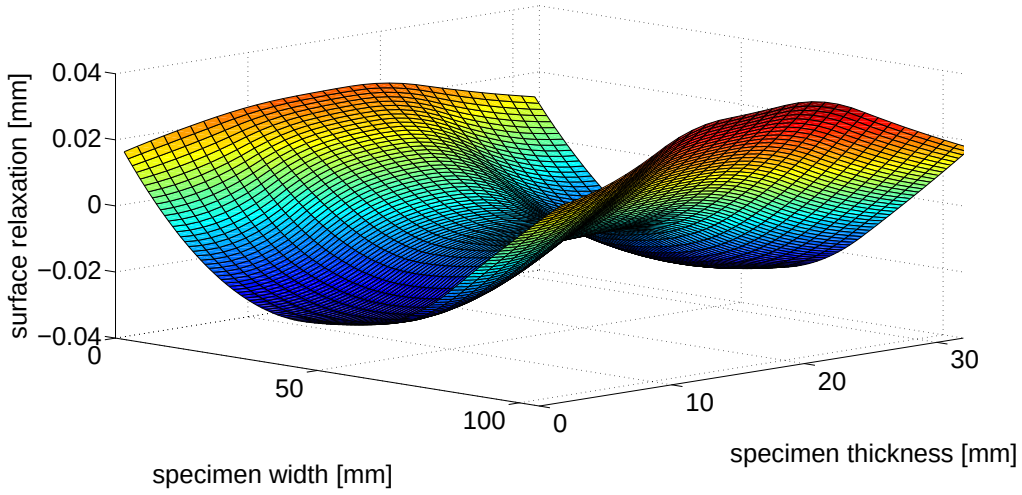


Figure 4.9: Smoothed surface

With this specimen the effect of different smoothing parameters was studied and they were fine tuned for the best result. Additionally the effect of a denser or less dense surface relaxation measurement grid was studied.

4.2.1 Parametric study of smoothing operation

As mentioned above the MATLAB function for smoothing is called "Spap2" and it can be written as:

$$\text{z_smooth=spap2}\left(\text{knots}, [kk], \{\text{x,y}\}, z\right); \tag{4.1}$$

where knots is an array which defines the number of polynomial pieces in each direction, k is the order of the polynomials used in each direction of the surface and {x,y} defines the grid over which the function will act, MathWorks [2011], Richter-Trummer [2008].

The value of k (order of the polynomial) is defined by two factors. Firstly the continuity in the first derivative has to be guaranteed, since stresses are to be calculated using the smooth displacement surface and secondly, in order to reduce the waviness in the surface, which would have a very noisy influence on the calculated stresses, the order has to be as low as possible. To guarantee these two conditions the polynomials have to be of second order. This is introduced in the function "Spap2" by setting k=3, MathWorks [2011].

Although the polynomial order can be defined *a priori*, the other parameters can be chosen using engineering judgment. To study both the density of the interpolation grid and the number of smoothing knots in each side it is required to run multiple times the contour method with different parametric variations each time. In this section the effect of the density of the interpolation grid is studied as well as the number of knots with the goal of obtaining the parameters for the best result possible and if possible create a guiding rule concerning these two parameters for future applications of the contour method.

In order to assess each result obtained from this parametric study it is necessary to have a mathematical relation that evaluates differences between each result. In this case it is the goodness of fit, which measures how much the smoothed surface resembles the original non smoothed surface. Besides the goodness of fit it is required to do a visual inspection, as what is intended is a solution that the represents all the measured data but that doesn't include all of the noise.

The expression for goodness of fit is:

$$\text{GOF} = \left(1 - \frac{\sum_{i=1}^{n}\left(z_i - \left(z_{smooth,i}\right)\right)^2}{\sum_{i=1}^{n}\left(z_i - \bar{z}\right)^2}\right) \times 100 \tag{4.2}$$

The value of goodness of fit that represents the total equality between the non smoothed data and the smoothed data is 100%, so the bigger the goodness of fit the closer are the two surfaces.

The first parameter to be studied was the number of smoothing knots in the x and y directions (knots array in eq. 4.1). The value of smoothing knots for each direction has to be a positive number and it is limited by $\text{length(x)} - \text{k} + 1$, where x is the input array in the respective direction and k as mentioned before is 3. In order to obtain result variations only

related to the changes in smoothing knots all of the other parameters, such as the type of interpolation and the density of the interpolation grid, where kept unchanged. The density of the interpolation grid used was the same density of the measurement grid, where every point is distanced 1 mm in both directions to the next point. This results in a matrix containing the surface relaxation with dimension {109,32} and so the limits for the number of smoothing knots are {107,28}.

The following Figure 4.10 and Figure 4.11 represents the stress map in MPa for minimum and maximum number of smoothing knots.

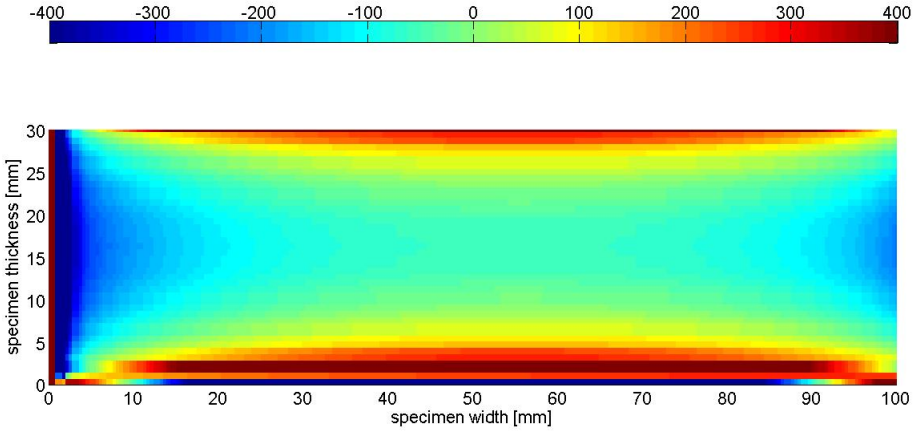


Figure 4.10: Residual stress map in MPa for minimum number of smoothing knots {1,1}

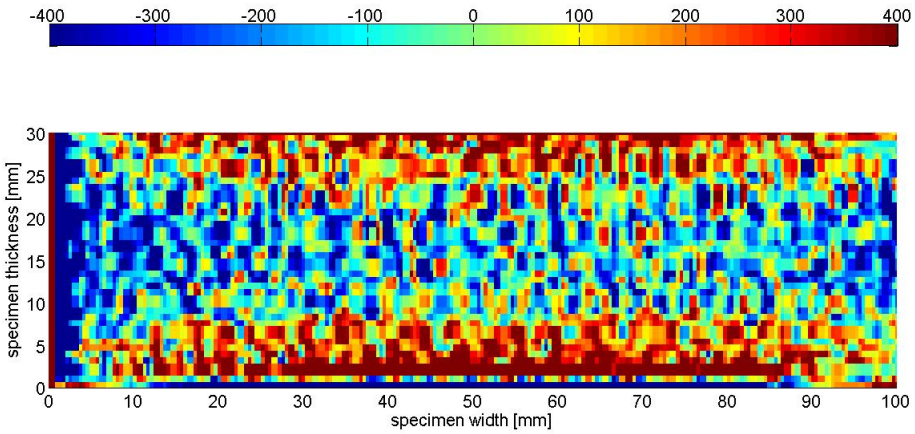


Figure 4.11: Residual stress map in MPa for maximum number of smoothing knots {107,28}

As it can be seen the effect of the number of smoothing knots is dramatic. In the first case the smoothed surface deviates too much from the original data. This is also proved by the value of GOF, as it was obtain the lowest value, 96.2807%.

In the limit situation, represented in Figure 4.11, the GOF is the highest value possible for this interpolation grid density, 99.8013%, but the result contains too much noise, showing stress results that are apart from the reality and only derive from measurement noise due to errors in the topography measurement done with the CMM.

The following Figure 4.12 shows the effect of the smoothing knots in the GOF values and it can be seen that between {1,1} and {10,10} the variation is more accentuated. Within these two values will be the optimal value as after {10,10} the noise in the measurement starts to be more apparent.

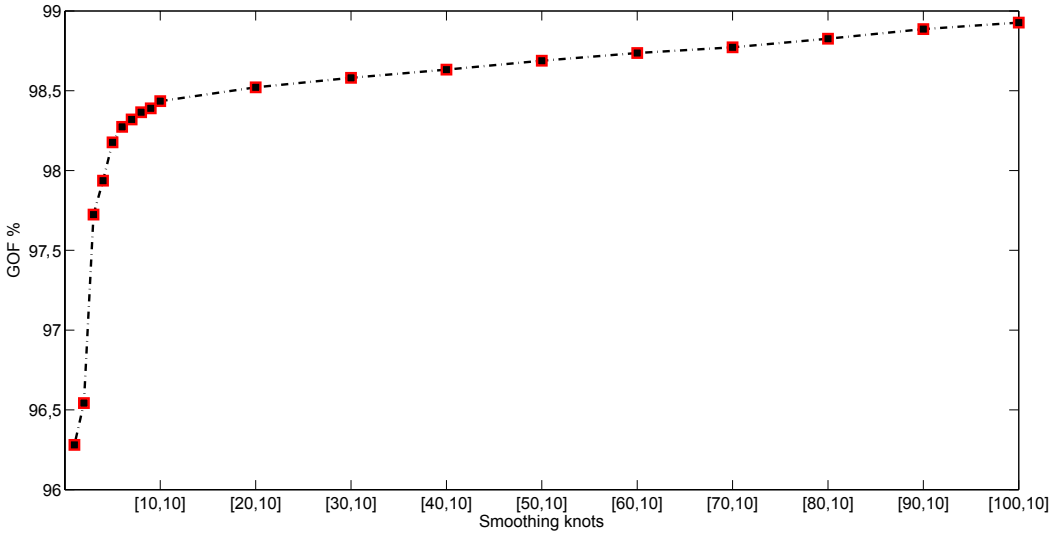


Figure 4.12: GOF variation with different smoothing knots

Eliminating the higher values of knots is an easy decision as the level of noise is quite obvious. However, within the range mentioned in the paragraph above it is much more difficult to determine what is real and what is noise. This decision is down to experience of the operator although the effect of varying this parameter within this range is not as dramatic as it was for the higher values of smoothing knots. This fact can be verified by Figure 4.13, where it is represented the difference between using {5,5} and {10,10} smoothing knots and the overall difference is very small, but still punctually getting to 100 MPa.

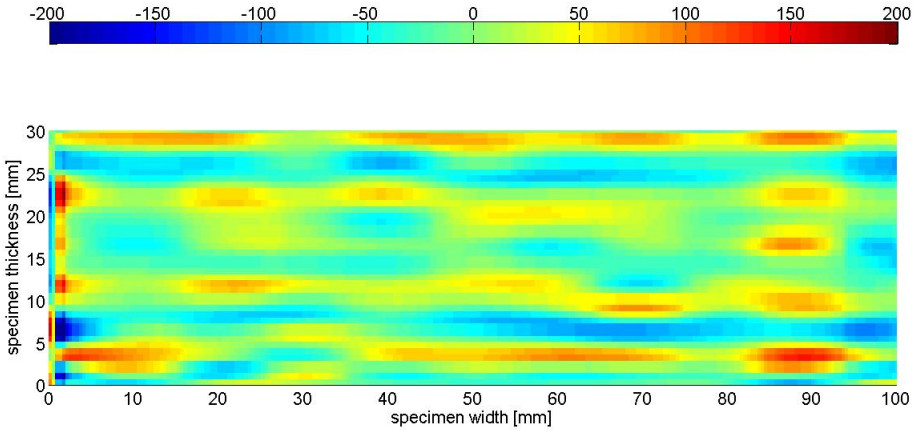


Figure 4.13: Difference between measured stress (MPa) for {5,5} and {10,10} smoothing knots

The author of this work opted for the {5,5} smoothing knots as the optimum value because it presented an acceptable GOF (>98%) and it seems to represent in a good way the measured surface, as it can be confirmed by Figure 4.14.

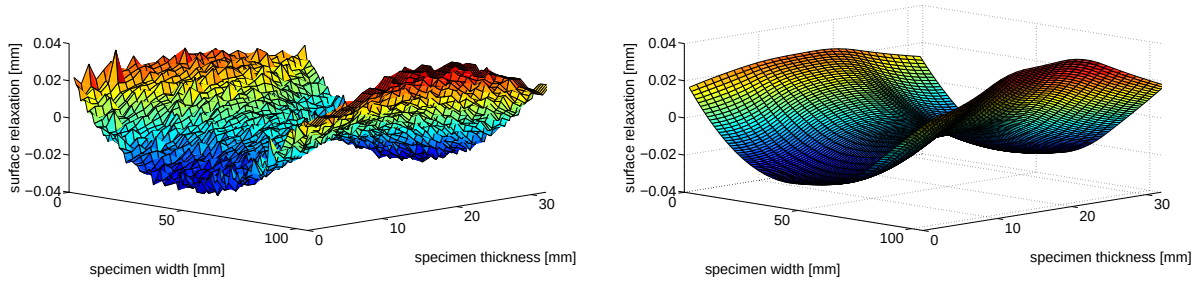


Figure 4.14: Surface relaxation for optimum number of smoothing knots (non-smoothed on the left and smoothed on the right)

Figure 4.15 compares the effect of the parametric variation using a two dimensional representation, with the values of the residual stress measured at mid width (~50 mm) for the minimum and maximum as well as the optimum values of smoothing knots.

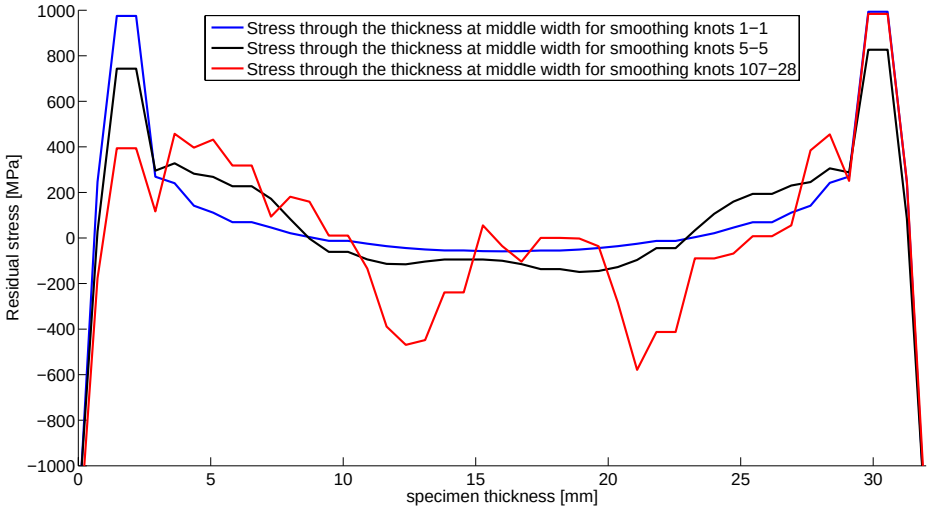


Figure 4.15: Residual stress through the thickness for different values of smoothing knots

An interesting and also obvious remark has to be done regarding the Figure 4.15: the contour measure is not valid for measuring at the edges of the specimen, because stress values go up to and over 1000 MPa surpassing by far the yield strength, and so if these values were considered as a real measurement it would imply large local plastic deformations. This measurement error in the edges may be due to the fact that the information was extrapolated to the boundaries creating “phantom” measurements. The stress information in the edges has to be discarded, in order to have a valid measurement.

With the smoothing knot parameter study and chosen the optimal value the attention is now turned to another parameter of the function “Spap2” which is the density of the interpolation grid. Figure 4.16 demonstrates in a simplistic 2-D schematic the interpolation grid along with a fictional surface in order to enlighten about the parameter in study.

This study was done in the same way as the one before by varying the interpolation grid conserving the values of the smoothing knots. In order to verify trends this parametric study was performed also using two different smoothing knot numbers.

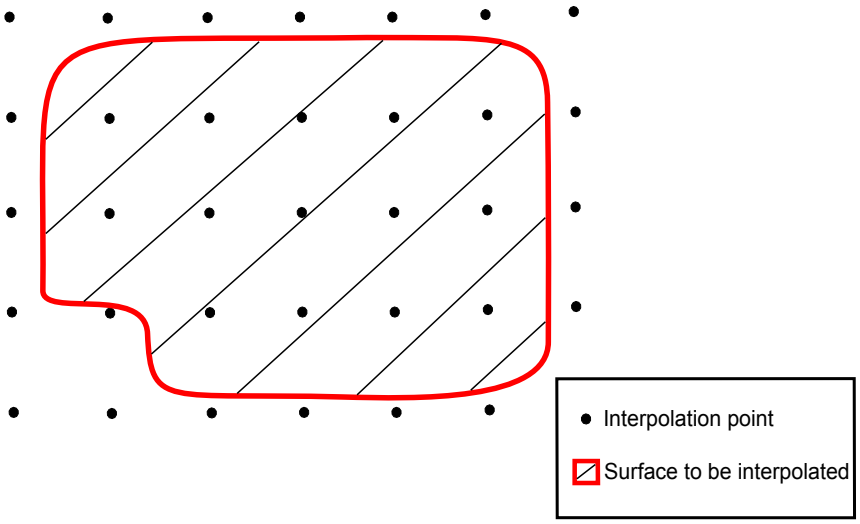


Figure 4.16: 2-D schematics of the interpolation containing the interpolation grid

A conclusion was very rapidly reached observing the results for different values of smoothing knots and interpolation grids. The two variables are independent even considering that the maximum limit number of smoothing knots varies with the density of the interpolation grid. In other words, the optimum value of smoothing knots reached in the study above is still valid for different interpolation grids. This fact is due to the value of smoothing knots being a geometric consideration because the value represents the number of polynomial pieces in the smoothing approximation. With the intention of better explaining this effect, a scheme of the smoothing operation in 2-D is shown in Figure 4.17.

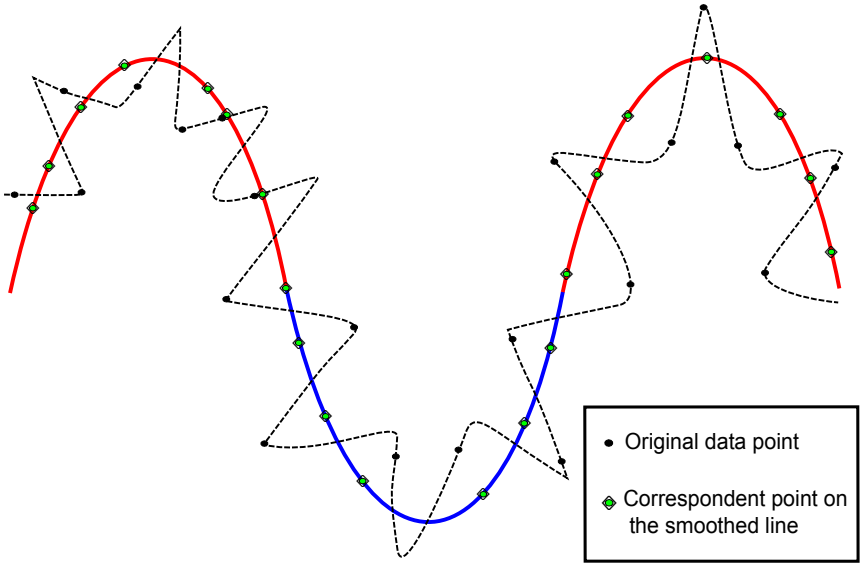


Figure 4.17: 2-D Schematic of the smoothing operation

Figure 4.17 presents a smoothed line in red and blue and the original line in black; the interpolation points (black dots) are also shown. The different colors in the smoothed line represent the three polynomial pieces. In the case shown in the scheme the number of smoothing knots is ideal as the obtained line follows the overall shape of the original surface and even if the number of interpolation points increases (denser interpolation grid) the ideal number of polynomial pieces will still be three.

The densities used to study their effect on the smoothing operation were; *(i)* a "normal density grid" where points are distanced from each other by 1 mm in both directions (the same density of the measurement), *(ii)* a "less dense" grid where points are distanced from each other by 2 mm in both directions, *(iii)* an "even less dense" grid where points are distanced from each other by 4 mm in both directions, *(iv)* a "denser" grid where points are distanced from each other by 0,5 mm in both directions and *(v)* an "even denser" grid where points are distanced from each other by 0,25 mm in both directions.

The GOF presents a variation which is quite intriguing, as it can be seen in Figure 4.18, because it was expected to increase with the density of the interpolation grid. This was expected as in theory with a denser grid there are more interpolation points for every measured point, which should result in a better approximation but the obtained effect is exactly the contrary.

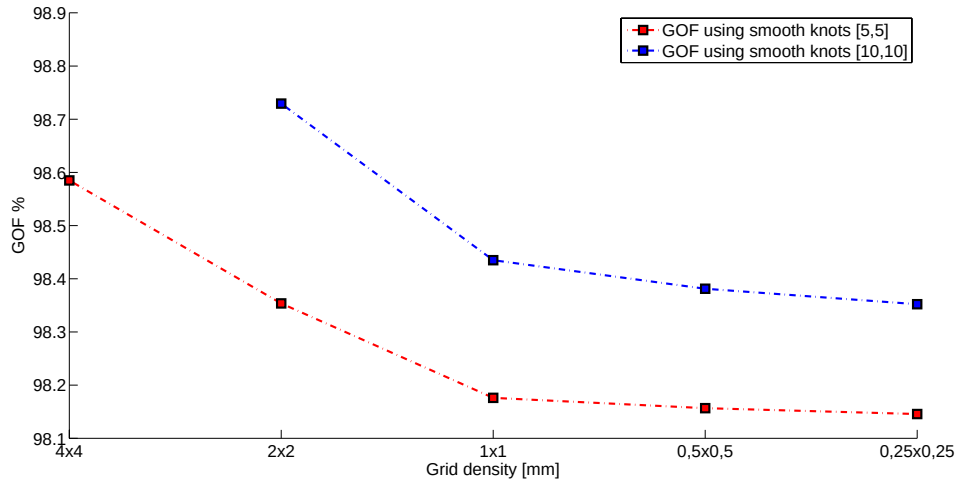


Figure 4.18: GOF variation with different interpolation densities

The behavior shown in Figure 4.18 can be explained when observing the interpolated surfaces for the extreme cases (Figure 4.19). In the case *(iii)*, "even less dense" grid, the interpolation grid is so sparse that the information present in many measured points is taken out, removing much of the noise but also not guarantying that part of the actual information required to obtain a valid result is not removed as well. In the case *(v)*, "even denser" grid, and especially in the specimen at hand where the measured mesh is very geometrically regular, the data is interpolated to intermediate points (points that do not exist in original

measurement).

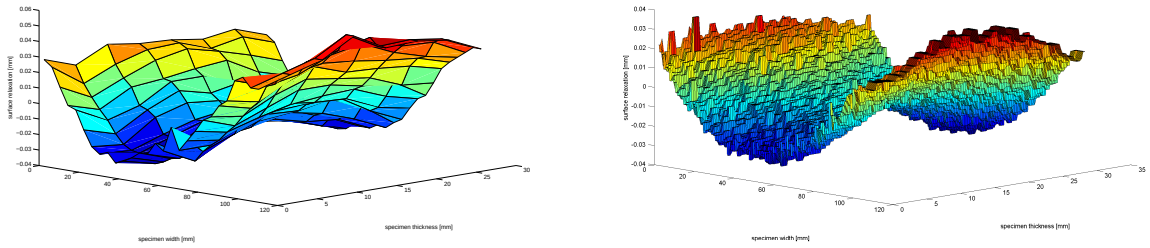


Figure 4.19: Interpolated surfaces using knots {5,5} for the extreme interpolation densities

It can be concluded that in order to obtain the best result possible the interpolation grid should have a similar density to the one used in the measurement. For this specific case it is the density mentioned above as "normal density" in which exist 104x19 points spaced between themselves by 1 mm in both directions.

The last parameter examined concerning the smoothing operation is the type of interpolation. MATLAB contains an interpolation function to perform this operation called "Griddata", function which interpolates in 4 distinct methods, "linear", "nearest", "cubic" and "v4". The "linear" uses a triangle-based linear interpolation, which is the default method for this function, or in other words, in case no method is specified MATLAB will use the "linear" method. "Cubic" uses a triangle-based polynomial interpolation with cubic degree, "nearest" uses a nearest neighbor interpolation and "v4" uses MATLAB 4 griddata method. The "cubic" and "v4" methods produce smooth surfaces while "linear" and "nearest" have discontinuities in the first and zero'th derivatives, respectively. More information about these methods can be found in the reference, MathWorks [2011].

Both parameters studied before (interpolation grid density and number of smoothing knots) were done using a "nearest" interpolation. The contour method was performed using the three other types of interpolations in order to figure which one would be the best choice for future works. The optimum parameters chosen before were used for these tests (smoothing knots {5,5} and a grid density of 104x19 interpolation points).

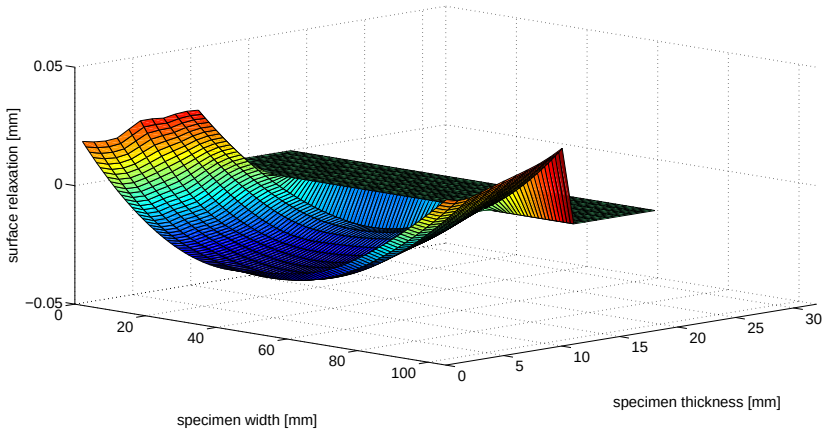


Figure 4.20: Smoothed surface relaxation using “linear” interpolation

Observing Figure 4.20 “linear” interpolation can be excluded as a possible technique for the contour method, as it fails to interpolate half of the information. The same is true for the “cubic” interpolation as the following Figure 4.21 reveals.

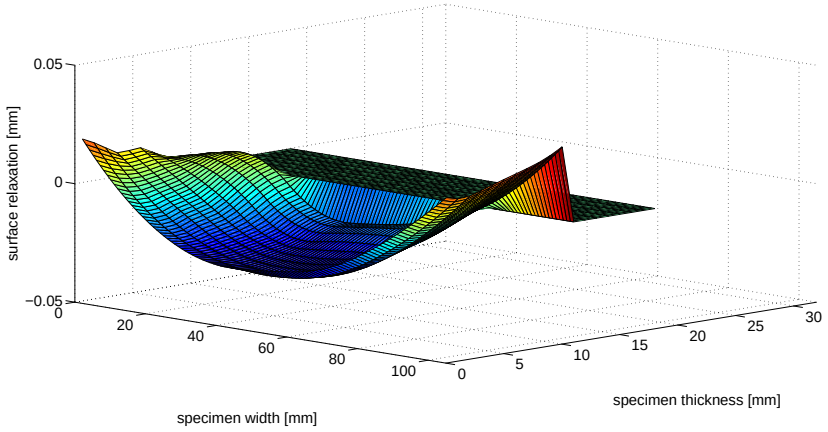


Figure 4.21: Smoothed surface relaxation using “cubic” interpolation

The “v4” interpolation method was able to interpolate all the information and it was obtained a stress map that resembles the one obtained when using the “nearest” method, as it can be seen in stress map (in MPa) presented in Figure 4.22.

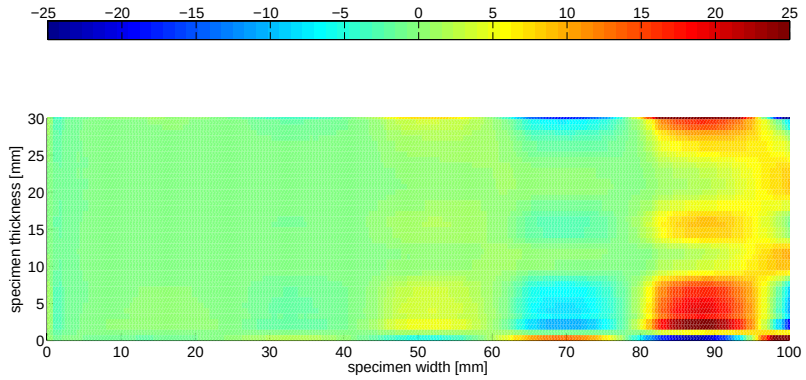


Figure 4.22: Difference in residual stress (MPa) between “v4” and “nearest” interpolation method

The goodness of fit is slightly higher for the “v4” method (98,3802%), but the difference is only of 0,2042% which does not justify the increase in interpolation time which is of the order of 4885,966% (from 0,082655 s to 4,12115 s). Although the interpolation time is only a small fraction of the time spent by the contour method it is still recommended to avoid this method of interpolation.

4.2.2 Parametric study of the CMM measurement grid

Besides the smoothing parameters it is also relevant to study the effect of a denser or less dense measurement grid, as the CMM measurement time is a precious commodity. The author of the present thesis is not aware of any published study on this effect on the contour measurement, leaving room for optimization.

To perform this study, information was removed from the matrix containing the original data, simulating that way measurements done with a less dense grid. The effect of the density along the width and thickness, separately as well as both combined, was verified. Also, a grid where points in interlock positions were removed, was studied.

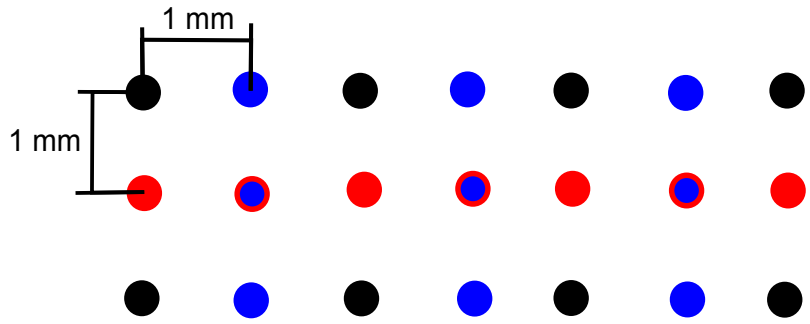


Figure 4.23: Measurement grid scheme

Figure 4.23 shows the points to be removed in each case. The points in blue, including the ones with red outline, are those to be removed when it is only intended to study the density of the gird along the width. The red points and the points in blue with red outline are the ones to be removed when it is intended to study the density along the thickness. The black points will be the remaining points when the density is cut by half in both directions. In the case of the removed interlock points, the remaining points in the grid will be the black ones and the blue with red outline points.

From the point of view of the goodness of fit there aren't great differences and the small improvements present in some cases were do to coincidentally removing the points furthest from the average surface.

To analyze the effect that the variations of the measurement grid it was constructed 2-D stress maps containing the difference between each obtained result and the reference, which was the stress map obtained using the optimum parameters discussed in the previous section. From these stress maps it was analyzed the difference through out the plane as well as the maximum values obtained.

Removing measurement points through the thickness and through the width separately resulted in greater stress differences throughout the entire surface than removing both at the same time. Removing interlock points also resulted in a worst result than reducing the density of the measurement grid in both directions. Figure 4.24 shows the differences of residual stress throughout the surface when using a measurement grid with half of the density in both directions (thickness and width) when compared with the original grid.

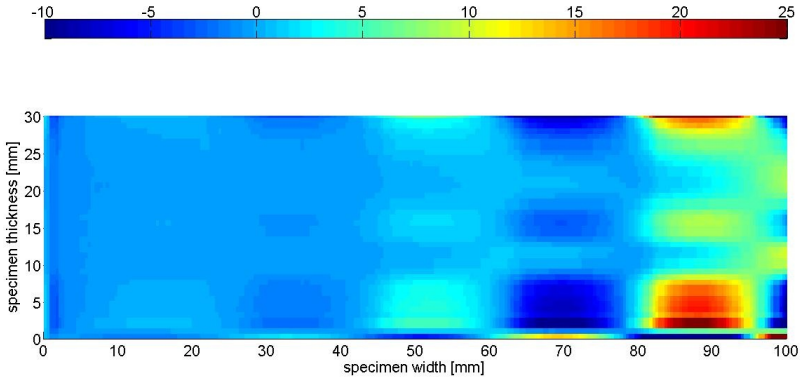


Figure 4.24: Difference of residual stress (MPa) between the original measurement grid and one with half the density in both directions

Regardless of any conclusion taken from the analysis of the measurement grid density reduction, one point has to be made, which is that the conclusions are only valid for this particular specimen and can only maybe be extrapolated for specimens with similar geometries and solicitations.

The biggest variation of residual stress is of the order of 25 MPa, which results in a maximum error of 6,25%, below 10%, which is a reference error value for residual stress measurements. This error is calculated taking into account the yield strength of the material. As the error is within acceptable values the reduced measurement grid can be considered safe to use for future similar specimens.

4.3 Welded Plate Specimens

The welded plates were the main object of the present study, and all of the steps of the contour method were performed on them. Each step was studied in order to search for possible problems and to attempt to present solutions.

4.3.1 WEDM cutting parameters

From the three welded plate specimens present available at the beginning of the work, one was intended to tune the cutting parameters in order to avoid problems with the contour measurements of the other two welded plates.

Cutting was performed at Autoconceptus with a Sodick 535L WEDM. A Ningbo 0,25 mm diameter wire was used to perform the cut. The wire was composed of hard brass with a tensile strength of 900 $\mathrm{N/mm^2}$and a maximum elongation of 3 %.

Figure 4.25 demonstrates the positioning of the plate in the WEDM machine. The specimen was clamped using pre-existing clamps but with the concern of securing the specimen as close to the cutting surface as possible, in order to decrease the elongation of the cut halves

and in that way avoiding a source of errors. The plate was aligned in the machine in order to obtain a perpendicular cut using a mechanical contact comparator.

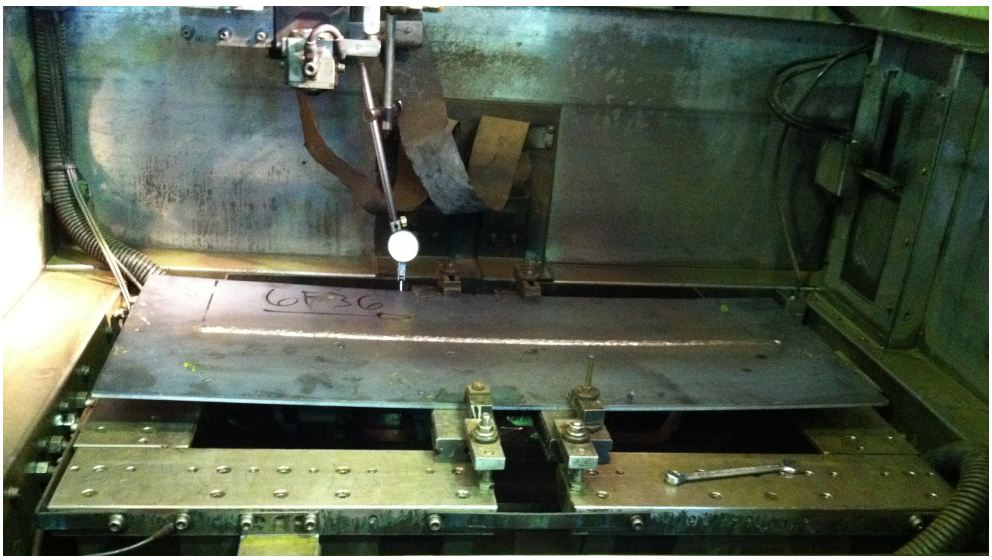


Figure 4.25: Specimen positioning in the WEDM machine using in house clamping system

The cut was performed at a speed of 7,5 mm/min until it reached the weld deposit when the line broke. To avoid scrapping the specimen the cut was restarted from the other end, now at a speed of 2,5 mm/min. As it reached the weld deposit again the wire broke one more time. Due to the non existence of a technique to separate the two halves without cutting through the deformed surfaces, it becomes impossible to measure the contour with a CMM and therefore to obtain the residual stress with the contour method.

A possible culprit for the wire breaking was the presence of slag in the welding deposit which has a much lower electrical conductivity than ordinary steel. As a way of better using the resources available for this dissertation it was decided to use this sample as testing bed for different cutting parameters and also to test a new clamping system which would prevent deflection upon cutting and in that way improve the measured results.

Figure 4.26 shows the first successful cut performed with the cutting test specimen. This cut was performed with the same clamps as before but now with a cleaned surface, which was obtained using a sand jet, and a cutting speed of 5 mm/min. The wire used was the same as before.

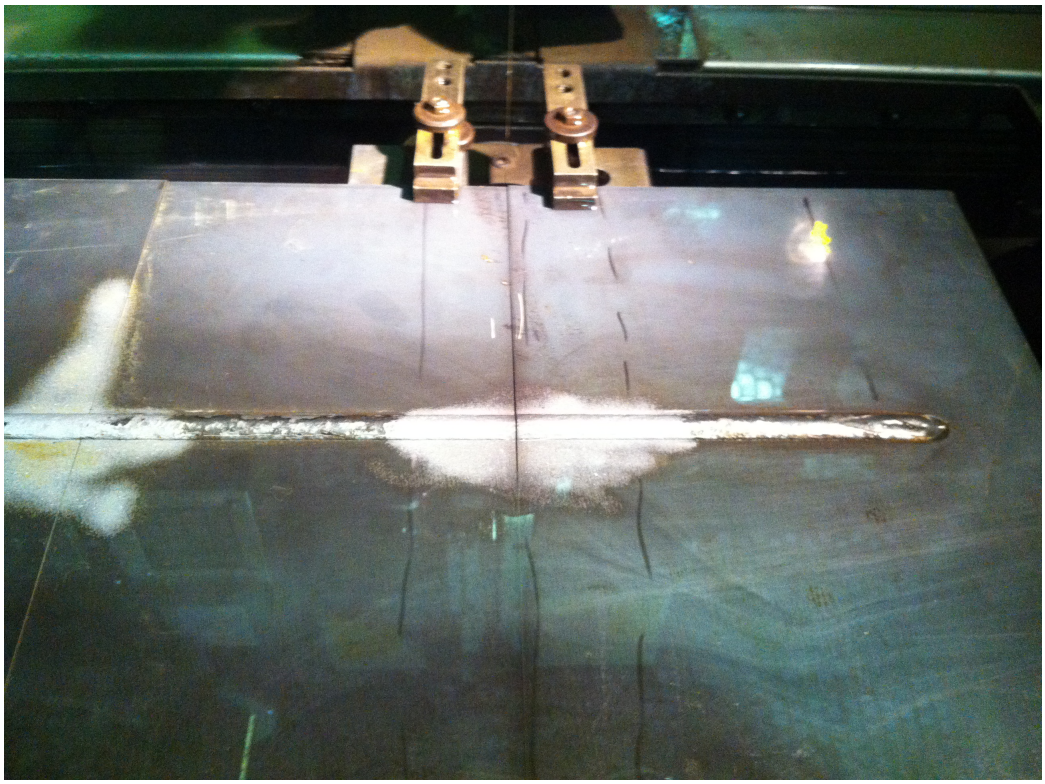


Figure 4.26: First successful specimen cut

With a successful cut performed a quarter length of the plate, it was then decided to measure the topography of the cut surfaces and perform the rest of the numerical procedures of the contour method. This quarter plate sample permitted building the ruling MATLAB code anticipating the measurement of the following samples, as well as checking the residual stress differences throughout the length of the welding bead. This code can be found in appendix B.

As a way of improving the results obtained with the contour measurement a clamping system was developed with the following requirements:

- be able to hold the specimen in both sides of the cut, very closely to the cutting line;
- distribute the holding force through several points in order to avoid introducing punctual plastification problems;
- low raw material and fabrication cost;

The clamps were fabricated out of DIN CK45 (EN C45E) steel and the fabrication drawings can be found in appendix C.

In order to assure that the plate and the clamps are perpendicular the plate was secured to the clamps in a bench vice as seen in Figure 4.27. The bolts were tied in a cross path and a holding force of one similar in all was applied to each bolt.



Figure 4.27: Mounting and alignment of clamping system

This clamping system allowed a reduction in preparation and alignment time in the CMM machine as the plate and clamps were aligned, being only required to fix the clamps to the machine with the necessary care to assure that the clamps are parallel to the cutting path, as seen in Figure 4.25 and Figure 4.26.

As the plate cut without the new clamping system was cut at quarter length of the plate it is not possible to do a direct results comparison with the plate cut with the new clamping system. In order to do a direct comparison properly it would be required at least one more plate specimen with similar characteristics in order to perform a cut at mid length without the new clamping system.

Taking into account the limitations of the comparison between the specimens cut with and without the new clamping system, described in the previous paragraph it is shown in Figure 4.28 the residual stress at mid thickness for both cases. The overall both curves are relatively similar, presenting a larger difference on the right side of the graph. As the length values increase the residual stress for the plate cut without the new clamping system decrease into negative values (compression) while the residual stress for the plate cut with the new clamping system maintains values closer to zero.

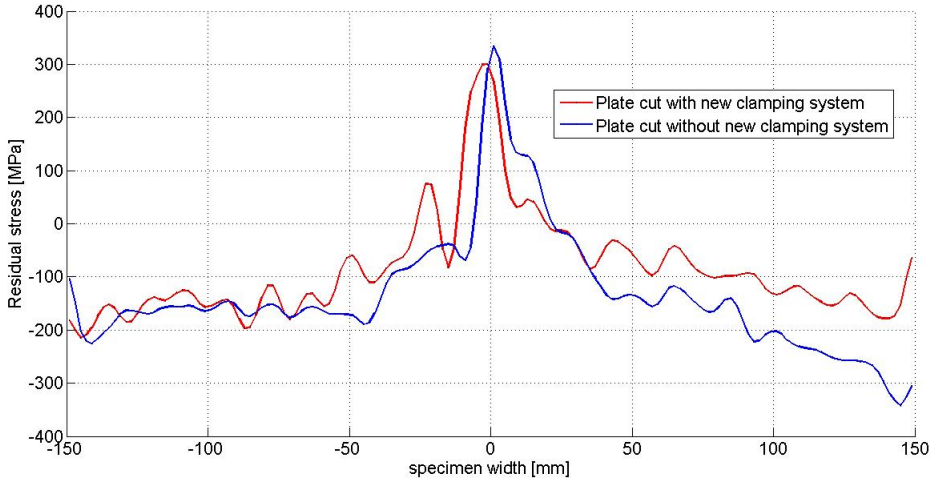


Figure 4.28: Residual stress measured at plate mid thickness

A preliminary rough approximation of the stress intensity factor distribution for a central crack perpendicular to the weld bead in such a plate is given as appendix D.

For a plate with a weld seam, the expected residual stress profile values would approach zero, when moving from the weld seam towards the free surfaces. The plate cut without the new clamping system is far from this expected profile; the region where it presents the larger difference with the expected profile (and also with the plate cut with the new clamping system) is the region which was cut first. A scheme of the cut is shown in Figure 4.29 where it is possible to observe the region cut first due to the cutting path and way. One possible explanation for this difference is that as the pre-existing clamps only hold the specimen in each side of the plate when the cut is performed the region in question is left with a large overhang for a longer period of time. As the new clamp system has more holding positions the overhang is diminished. This conclusion is not final as it requires validation as mentioned above.

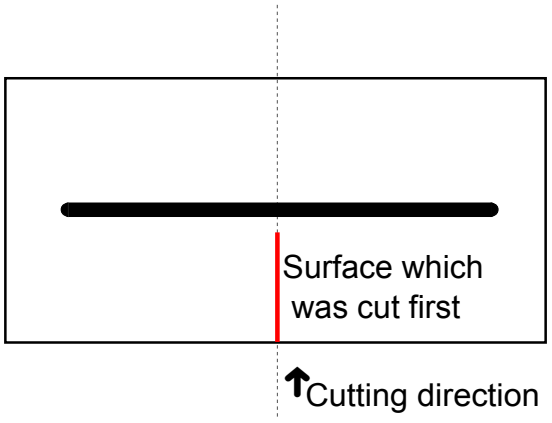


Figure 4.29: Scheme showing zone cutting path and direction

4.3.2 Parametric study of the smoothing operation

As in section 4.3.3 different parameters of the smoothing operation (number of smoothing knots, density of the interpolation grid, type of interpolation procedure) were studied in order to check for trends within the same type of specimens as well as more universal rules concerning the residual stress measurement by the contour method in general.

Firstly the number of smoothing knots and density of the interpolation grid were studied by varying its values while keeping the other parameters constant. The three densities of the interpolation grid used in this study were a 2mm x 0,5mm (length x thickness) spacing grid which is the same density as the CMM measurement grid, a denser grid with 1mm x 0,25mm spacing and a less dense with 4mm x 1mm spacing. The type of interpolation used was the "nearest" interpolation.

As the welded plate specimen presents a more irregular shape than the CT specimen it is of interest to show a representation of the interpolation grid over the smoothed average surface deformation to better understand the role played by the interpolation grid in the smoothing operation. Figure 4.30 shows this representation and it is visible that the interpolation grid when observed from above is seen as a rectangle larger than the actual cut surface.

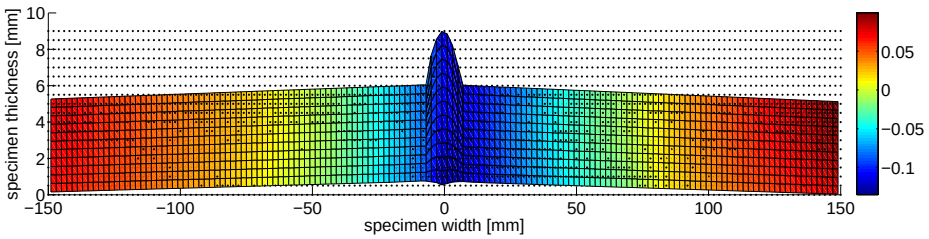


Figure 4.30: Interpolation grid over smoothed average surface deformation [mm]

Figure 4.31 represents the evolution of the goodness of fit with the increase of the number of smoothing knots for the three different interpolation grid densities for the specimen cut at quarter length. When comparing each curve in Figure 4.31 with the one in Figure 4.12 it is possible to verify that the shape of the curve is very similar although for the CT specimen the GOF keeps growing even that very slowly for bigger numbers of smoothing knots while in this new specimen there is a plateau at an average 99,2 % of GOF. The highest value of GOF was obtained for the {41-1} smoothing knots, which means that the best approximation to the pre-smoothing surface was obtained using 41 polynomial pieces along the length and 1 along the thickness.

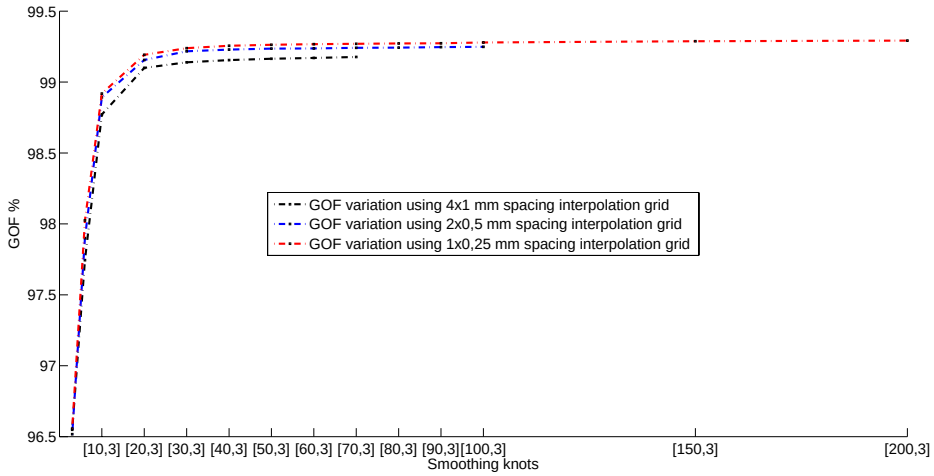


Figure 4.31: GOF for different numbers of smoothing knots

The conclusions reached in section 4.3.3 concerning the interpolation grid density are again valid for the welded plate specimen, for the same reasons, and so the recommended interpolation grid is the one with the same density as the CMM measurement grid (2x0,5 mm spacing).

Through visual comparison of the obtained stress maps for the different number of smoothing knots and interpolation grid densities it was concluded that the optimum stress measurement results from using {41-1} smoothing knots and an interpolation grid with 2x0,5mm spacing between interpolation points. Figure 4.32 shows the stress map obtained using this parameter combination.

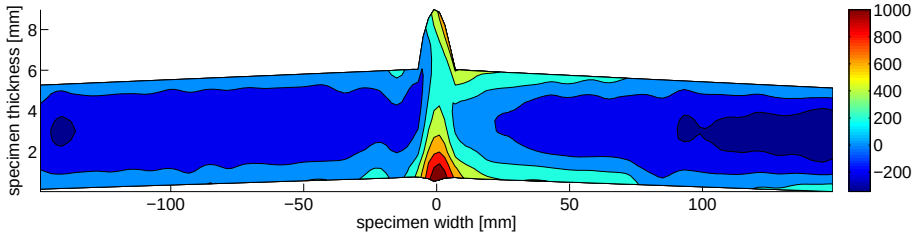


Figure 4.32: Stress map [MPa] using {41-1} smoothing knots and 2x0,5 mm interpolation grid density

Again it can be observed that nearer to the edges, especially in the area of the weld deposit the measured stress overpasses the yield strength of both the base and filler material (≈400 MPa for base material and ≈420 MPa for filler material). These high stresses can have been originated from local plastic deformation. Also as they are located near the edges it is possible that the CMM measurement is not completely reliable due to the uncertainty of the contact between the CMM tip and the surface close to the edge. This uncertainty is even more critical for thin specimens like the welded plates used in this study. Besides these trouble points the residual stress map obtained presents very credible results with traction

in the weld deposit and compression on the base material. Figure 4.33 shows the measured residual stress through the length at mid thickness and it can be observed that the profile of the residual stress is within the expected and the maximum values are lower than the yield strength.

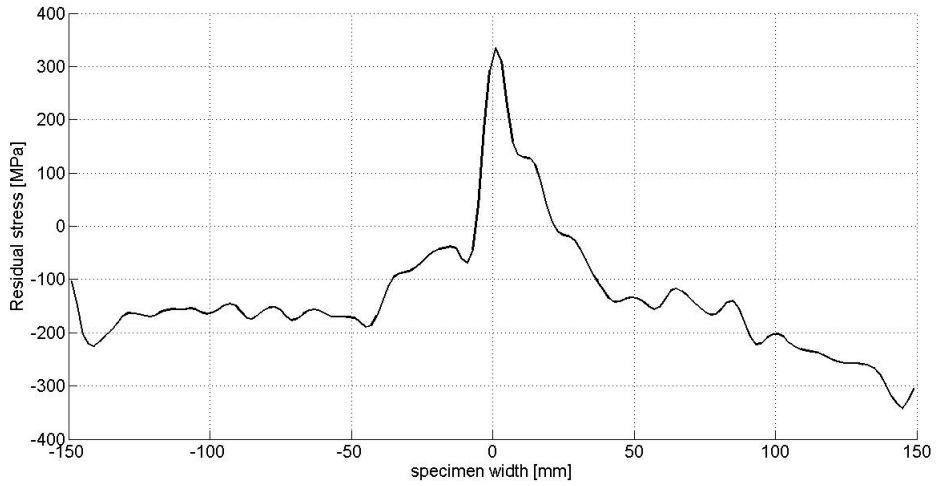


Figure 4.33: Residual stress measured at mid thickness

The conclusions reached for the density of interpolation grid and type of interpolation are valid for the rest of the welded plate specimens as well as any contour measurement specimen. Regarding the number of smoothing knots it was again tuned for the other two welded plate specimens (plates cut at mid length rolled and unrolled) reaching the same optimum parameter {41,1} number of smoothing knots. The value of smoothing knots is a more complex parameter to tune as it can not be completely defined *a priori* but only using trial and error although engineering judgment can help to reach a near optimum value.

When observing Figure 4.34 it is possible to predict that the optimum value for the smoothing knots along the thickness is one, as one curve along this direction seems sufficient to represent the surface. Along the width as the distance is larger it is necessary to analyze the interpolated surface with larger image amplification and the conclusion it is reached with this visual observation is that the number of smoothing knots in this direction will be ten or larger.

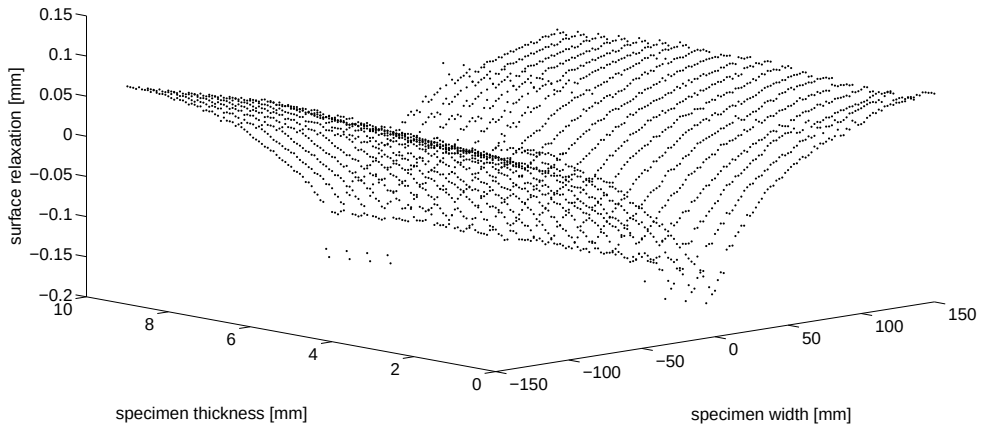


Figure 4.34: Average interpolated surface

4.3.3 Parametric study of the CMM measurement grid

Like in section 4.2.2 the effect of the density of the CMM measurement grid was studied by removing select data out of the CMM topography measurement. The residual stress obtained using all of the CMM measured data, Figure 4.32, is in this study taken as the reference, and the objective is to see if it is possible to obtain a very similar result with a less dense measurement grid. A scheme of the points to be removed in each following case is shown in Figure 4.23.

When observing the resulting residual stress maps for each case, it is possible to verify the point made in section 4.2.2 that a rule to reduce or not the density of the measurement grid can not me establish. This fact is due to the uncertainty of which information is left out, as with a lower density measurement grid the extrapolations are made over larger distances and in that way the deformations presented in certain areas are not related to the actual measurement in those areas but to deformations in neighboring areas instead.

In Figure 4.35 the stress maps for different cases of reduced measurement densities can be observed. Contrary to the conclusions taken from analyzing the results in the CT specimen, in the welded plate specimens the case where both the densities in directions of the thickness and of the length are reduced does not constitute the best result. The stress map obtained from reducing the measurement density in both directions is very similar to the one obtained from removing the measurement points along the length (Figure 4.35 a) and b)). These results present a larger area with very high values of normal stress (higher than the yield strength) and they were probably originated because the coincident points removed in these two case were the ones that presented a lower value of deformation and without these points the extrapolation was made from the remaining points which presented a higher value of deformation leading to higher values of residual stress obtained from the contour method.

Regarding the case of the removed interlock points the resultant stress map is similar to the ones in Figure 4.35 a) and b) and that were discussed in the paragraph above. This similarity may result from coincidentally the points removed around the area where the higher values of stress were the same resulting again in very high values of residual stress.

a)

b)

c)

d)

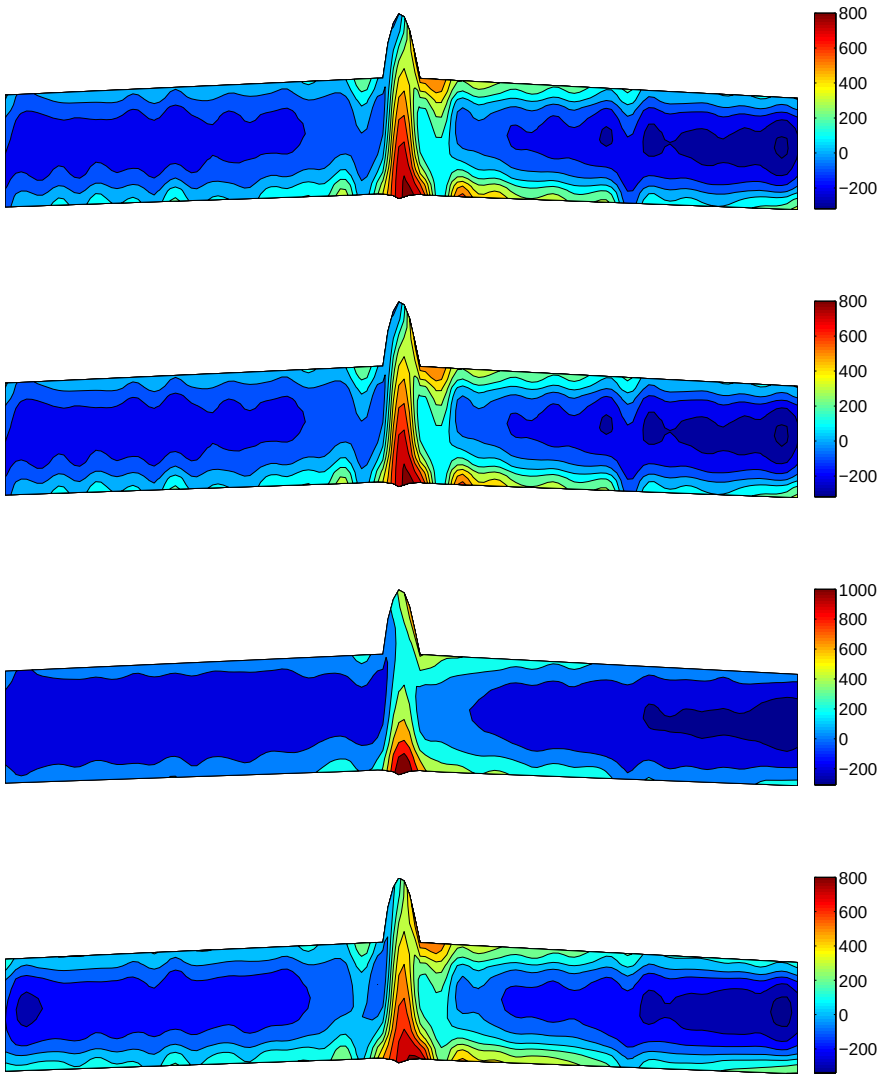


Figure 4.35: Stress maps [MPa] using different CMM measurement grids, a) removing points along the thickness and length, b) removing points along the length, c) removing points along the thickness, d) removing interlock points

From the four cases the one which is worth analyzing in greater depth is shown in Figure 4.35 c) where the measurement grid obtained had a 2 x 1 mm spacing between points (length x thickness). The overall profile of the stress map is very similar to the resultant of using the entire grid (2 x 0,5 mm spacing). Figure 4.36 shows the differences in stress throughout the entire surface. The highest difference is of 120 MPa which when compared to the base material yield strength (400 MPa) results in an error of 30 % which is more than double of the acceptable error for residual stress measurements (< 10 %), although it can be observed

that the point where this difference occurs is very close to the edge of the specimen. As the residual stress measured in this area is already not considered reliable it should instead be consider the differences within the center of the specimen. Further from the edges of the specimen the differences in residual stress measured are of around 40 MPa and this value constitutes an error of 7,14 % when compared to the filler material yield strength.

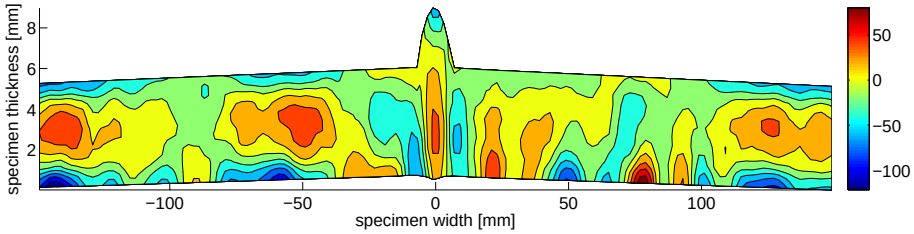


Figure 4.36: Difference in measured stress between using the entire CMM measurement grid and removing the points along the thickness

As at the time of the CMM measurements, the deformations to be obtained are still unknown it is complicated to judge *a priori* if the CMM measurement grid is dense enough for the purpose of performing the contour method and so it is recommended to use the maximum density possible within economic reason.

4.3.4 FEM considerations

The previous sections discussed several parameters within three steps of the contour method, the cut, the CMM measurement and the mathematical smoothing procedure, but one step was still not addressed which was the FEM calculations.

Upon having a matrix containing the deformation in a smoothed form it is necessary to introduce it in a FEM model and perform the elasticity calculations. The FEM calculation can be (depending on the model and the processing power of the equipment in use) the most time consuming of the mathematical procedures to transforms the CMM measured data into residual stress measurements. For this reason it is relevant to study the possibility of optimization within this step.

Figure 4.37 shows the original FEM mesh used for the measurements of the plate cut at quarter plate length. In the surface to be studied the mesh density is equal to CMM measurement grid (2 x 0,5 mm spacing). Near to the surface in study it is used a partition with a depth of 15 mm in order to obtain locally a denser mesh (elements C3D8R with dimensions 2 x 0,5 x 2 mm) and in that way perform the calculation much faster than if the whole model presented this mesh density.

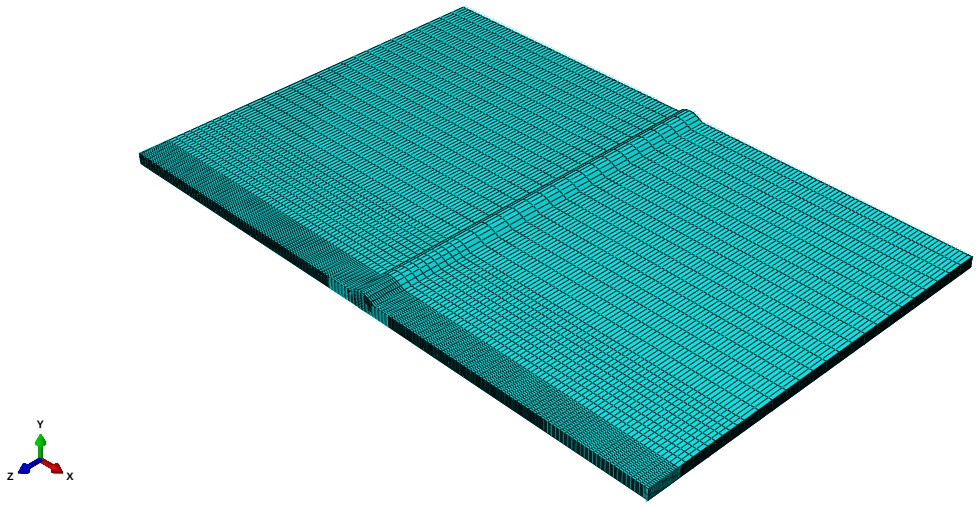


Figure 4.37: FEM model of quarter plate

One form of reducing the number of elements in the model and at the same time maintain the same mesh density in the surface of study is by using wedge elements (C3D6H) in a transition partition like it is shown in Figure 4.38. The model simplification can be seen by the difference in the number of elements (77400 elements originally and 48888 elements in the new model) which is of 63,16 %.

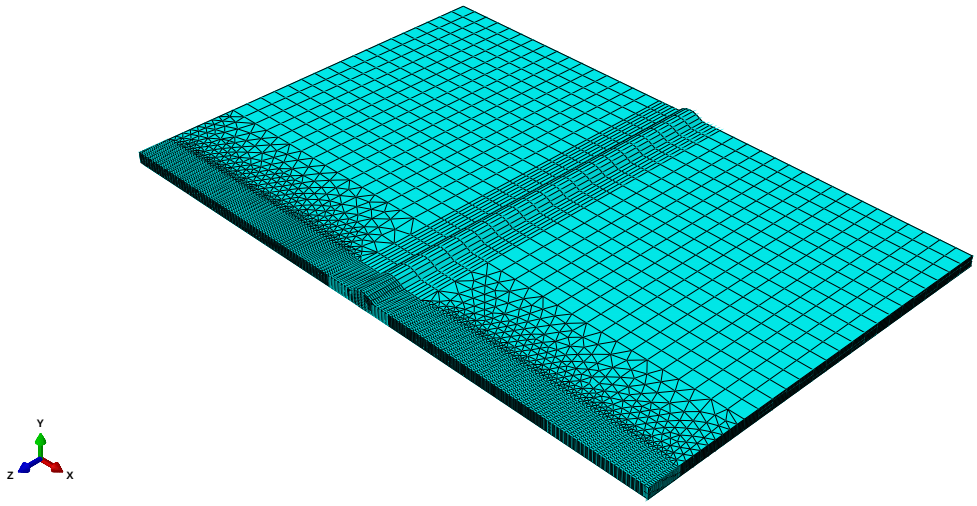


Figure 4.38: FEM model using wedge elements

Inspecting visually the results obtained from using the new optimized mesh it is possible to verify that the measured stress does not differ very much from the result using the original mesh. Figure 4.39 shows the differences in measured residual stress throughout the surface. The maximum value of difference was of approximately 60 MPa but it is situated in an edge area and so it is not relevant for the contour method. Within the surface of interest the maximum value of residual stress difference is of approximately 6 MPa which when compared to the yield strength presents an error of 1,5 %, value which is much lower than the maximum acceptable 10%.

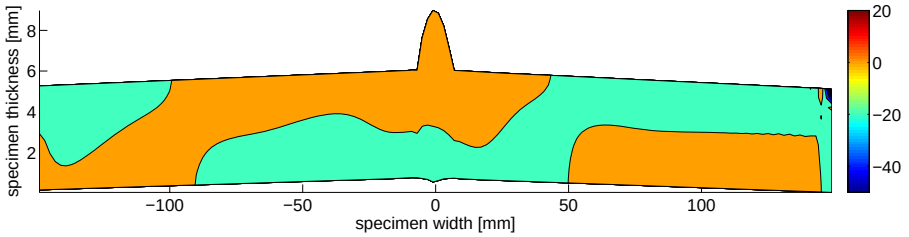


Figure 4.39: Difference in measured residual stress [MPa] between using optimized and original FEM mesh

Although the mesh was reasonably simplified the processing time for the models was not significantly reduced due to the fact that in this work it was used a high power computer (16 CPU's, 16 Gb of RAM memory and an SSD as main drive) and so using any of the meshes the processing time for each FEM calculation is less than one minute. If processing capability is a limitation it is recommended to use a simplified mesh as the overall time spent to obtain the residual stress results will diminish and the results will be within reasonable margin of error as seen in this experiment.

4.4 Rolling Technique

Of the three welded plates, one was heavily rolled to relieve residual stresses as described in section 4.1 in order to study the effect of this residual stress relief treatment with the contour method.

Figure 4.40 shows the residual stress map for both cases and difference is very drastic.

a)

b)

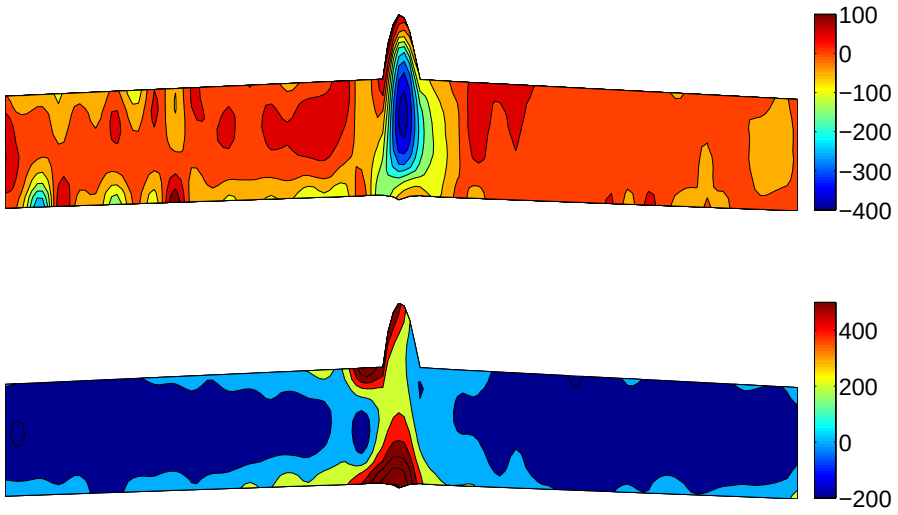


Figure 4.40: Residual stress (MPa) for rolled (a) and unrolled (b) specimen

It can be observed that the overall value of residual stress throughout the plate varies between the values -50 MPa and 50 MPa which is a lower variation than in the non-treated plate. Also a phenomena observed in this measurements is an inversion of the residual stress value as for example the weld seam which was under tension in the unrolled plate is under compression in the rolled plate. The areas where maximum values of residual stress remain the same (weld seam) only now they present contrary signal.

It is of interest to analyze in further detail the residual stress at mid thickness as in that way the areas of uncertainty of the contour measurement referred in section 4.2.1 and 4.3.3 are avoided. Figure 4.41 showcases the measurement at mid thickness for both rolled and unrolled specimen. In this representation it is more clearly visible the smaller variation of residual stress throughout the length of the plate with the exception of the weld seam where it is possible to see the inversion of the value.

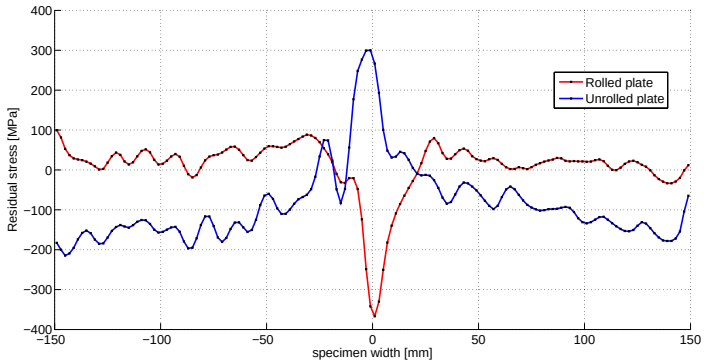


Figure 4.41: Residual stress measured at mid thickness for both rolled and unrolled plate

In terms of crack propagation it is expected that the rolled plate will outperform the unrolled as the residual stress in the overall plate is low and so it will not greatly influence the stress intensity factor and in the case of the weld seam as it presents large values of compression residual stress crack propagation will be prevented.

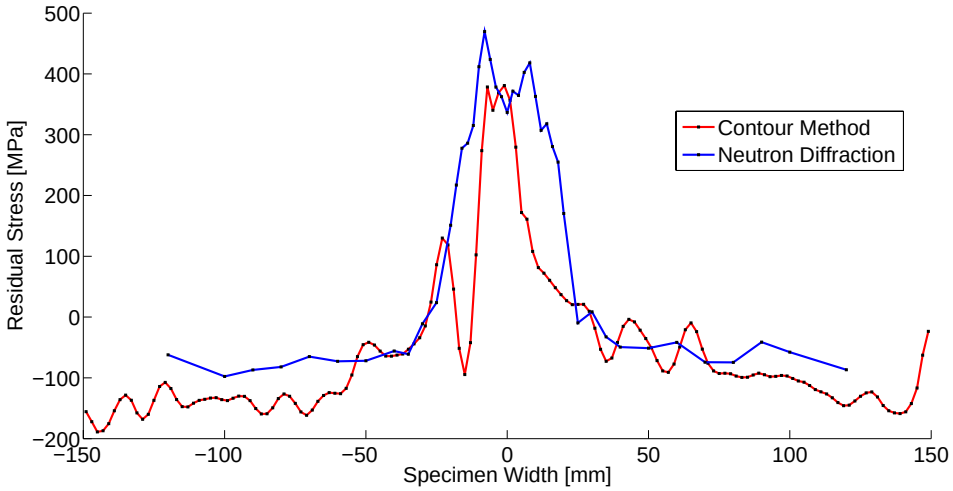
Chapter 5

Neutron Diffraction Comparison

Alongside the contour measurements performed at FEUP neutron diffraction measurements were performed for Cranfield University on the same specimens, at ILL (Institut Laue-Langevin, Grenoble, France). Diffraction measurements were performed in both longitudinal and transverse direction on the welded plates but as the contour method allowed only for measurement of normal residual stress it will only be considered the longitudinal direction diffraction measurement. The gauge volume on the longitudinal diffraction measurement is 2x2x2 mm and it is rotated by 45º relative to the plate. In order to compare the results it was selected the contour measurement data within a band of 2 mm in the center of the plate and the residual stress value was averaged within the thickness of this band.

Figure 5.1 shows the results for both techniques within the corresponding area.

a)



b)

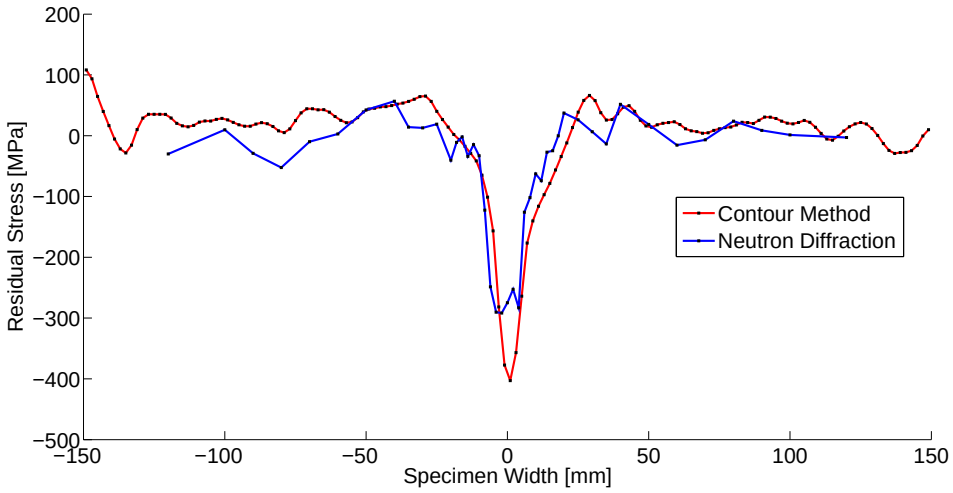


Figure 5.1: Residual stress measurement using contour method and neutron diffraction for unrolled plate (a) and rolled plate (b)

The residual stress values obtained by both techniques show good overall agreement with the biggest differences appearing in the non treated specimen.

Chapter 6

Economic and Legal Considerations

6.1 Cost Analysis

Economic considerations are of fundamental importance when considering the application of any technique in an industrial environment, being it either a manufacturing technique or an experimental or validation method. In order to facilitate an informed choice of residual stress measurement techniques, and turn feasible a future industrial application, this section roughly discusses the costs involved in performing this method.

The contour method may be divided into four major stages, cutting, surface topography measurement, data treatment and elastic calculations for obtaining stresses from displacements and each of this stages presents different costs which have to be accounted for.

The cutting was performed using a Sodick 535L WEDM at Autoconceptus. To cut the specimens a Ningbo 0,25 mm diameter wire was used. This hard brass wire is sold in coils, having been used wire from a 16 kg coil with a cost between 9 to 12 €/kg. As machine time is expensive due to both costs with the machine operator and machine devaluation over time it is important to take time into account. The cutting time was approximately 60 minutes to which has to be added the clamping time and specimen alignment which was different using or not using the clamp system developed during this work. Using only the pre-existing clamps the specimens had to be fixed and aligned in the machine tank which lead to a preparation time of roughly 30 min. Using the new clamping system the plate specimens were fixed and aligned with each other before arriving at Autoconceptus resulting in only having to align the clamps with the machine tank and in that way reducing preparation time to about 15 to 20 minutes. The potential for reducing WEDM preparation time was not completely explored as the heavy weight of the clamps caused difficulties in moving the specimens and clamps sets and in that way increased the preparation time over a potentially lighter clamp system.

For the cutting operation the total charge for one single specimen cut was 80 €.

In case of an increase in contour measurements and other procedures which involve cutting by WEDM it should be considered the acquisition of a WEDM. These machines are

manufactured by a different brands such as Sodick, Ona, Mitsubishi, Agiecut. In case a new machine is not justifiable, used WEDMs can be found on the market, such as for example an equal machine to the one used in this work (Sodick 535L) at the price of 27000 €, machinesbook [2011].

The measurement of the surface topography was also outsourced, due to the lack of a working CMM in the FEUP campus. The measurements were performed at CATIM and they may be divided into two stages, machine programming and the actual measurement. The cost of programming is higher than the cost of one measurement but if several measurements of similar specimens are executed the cost of programming over each sample will diminish as the same machine programming is valid for the different measurements.

The programming for the samples in question was of 518,72 €. The cost for each CMM topography measurement was 162,10 € before taxes.

The last two steps were performed in house and involved MATLAB programming as well as the use of a commercial FEM package. In terms of hardware, an available computer workstation with 16 CPU's, 16 Gb of RAM memory and an SSD as main drive was used; for cost analysis its depreciation should be considered. As this computer workstation is not completely necessary for the contour measurement and was only used because it was available at the workplace it devaluation will not be considered.

Considering these different factors and assuming an average salary of a mechanical engineer to be of 2000 €/month without taxes a cost for the last two method steps may be roughly estimated. Considering that in total the time spent with the contour method for both programming and measuring between 40 to 60 hours than the cost for this stage of the technique would be between 500 to 700 €.

	Cost
WEDM cut	80 €
CMM programming	650 € to 700 €
CMM measuring	200 €
Data treatment	500 € to 700 €
Total	1430 € to 1680 €

Table 6.1: Contour method approximated costs per measurement

The price per measurement will go down if more than one similar specimens is measured as the price of CMM programming and of MATLAB programming has to be divided by the number of measurements.

No attempt is made to estimate the real cost of a neutron diffraction measurement. Suffice to say that they require a neutron source, of which there are few worldwide, with an investment cost of the order of millions of Euros.

6.2 Legal Remarks

In order to study a future application of the contour method in industrial environment it is necessary to consider the legal limitations as the experimental technique is protected by a United States Patent no. 6,470,756 B1 dated 29$^{\text{th}}$ of October 2002. Legalities may introduce unforeseen costs due to lawsuits or due to the payment of royalties to the owner of the patent.

As the technique is protected by the patent mentioned above, in order to use the contour method in an industrial environment it would be necessary to contact the owner of the patent and discuss terms of usage including possible royalties. If this step is not taken, the user of the technique may be liable to lawsuit for infringement of United States intellectual property law.

Chapter 7

Concluding Remarks and Future Works

7.1 Conclusions

It was a goal of this work to measure normal residual stress in two specimens using the contour method; this was achieved successfully; proving that the technique can be used to obtain two dimensional residual stress maps.

Through parametric studies of the smoothing function performed in both the CT specimen and the welded plates specimens it was noted that the interpolation grid used should have the same density as the CMM measurement grid in order to obtain the best results.

Regarding the number of smoothing knots it was observed that it had a dramatic effect on the resultant stress calculation as with the increase in smoothing knots the smoothed surface resembles more closely the average interpolated surface (higher goodness of fit) but also introduces a higher level of calculation noise. In order to obtain the optimum stress result it is necessary to tune this parameter which can only be fully achieved through trial and error although through engineering judgment values close to optimum may be defined a *priori* with some experience.

Concerning the type of interpolation to use it was concluded that the recommended is the "nearest" type.

For the CT specimen the optimum parameters were;

- the number of smoothing knots had to be {5,5};
- the polynomials had to be of the second order;
- the interpolation grid had to have a 1x1 mm density (equal to the measurement density);
- the interpolation had to be of the "nearest" type.

The finite element mesh density should equal both CMM measurement grid and interpolation grid density as the spatial resolution is limited by the mesh density used in the FEM calculations until this density reaches the CMM measurement grid density. If the FEM mesh density

surpasses the CMM measurement grid density there is no spatial resolution enhancement because the added nodes will have deformation values obtained by interpolating deformation values from neighboring nodes and not real measured deformation.

It was verified that the contour method is not valid for measuring stresses close to free surfaces due to diverse errors induced while measuring the surface topography with the CMM. This fact may be of great concern for thin specimens.

From the CMM measurement grid reduction simulation it was concluded that it should be the densest possible within economic reason as it limits the spatial resolution.

The remarks made about smoothing function parameters and CMM measurement grid density were verified in the welded plate specimens.

For the welded plate specimens the optimum measurement was made with {41,1} number of knots and with similar rules concerning the polynomial order, interpolation grid density and type of interpolation as the ones made for the CT specimen.

Although it was not possible to confirm improvements in the measured residual stress due to the lack of similar specimens and due to the difference in location of the cut on both compared specimens differences were shown between the untreated plate clamped with the new clamping system and the plate clamped with the pre-existing machine clamps. The stress measured on the specimen clamped with the new clamping system had a stress profile close to expectations which may have been due to the smaller overhangs during cutting.

The plate rolled in a single pass at a speed of 500 mm/min and with a roller force of 150 kN presented lower values of measured residual stress and it also had a stress value inversion. The areas furthest from the weld seam which were under compression before treatment became tensioned areas and the weld seam which was under high values of residual tensile stress before treatment became a highly compressed area.

Comparing the results obtained by the contour method for the two welded plates cut at half length with the results for the same plates obtained using neutron diffraction technique it is possible to note that they present rather similar values within both techniques uncertainty. This similarity leads to the conclusion that the residual stress measured in these two plates are trustworthy representations of the residual stress present in the area subjected to measurement.

The simplified cost analysis performed within this study lead to an overall cost per measurement of the contour method to be below 2000 € for these specific specimens, orders of magnitude lower than real costs of neutron diffraction.

7.2 Future Works

Although the contour measurement is a technique developed over the last ten years there is still space for improvement.

The clamps developed in this work still need more experimentation in order to verify its effects on measured residual stress. Also the clamping system can be upgraded by using lighter alloys resulting in an overall weight saving and also the fixings and contact points between the clamps and the specimen can be improved.

A more detailed study should be done concerning applications of the contour method in the general industry. The concern of the study should be to point out the industries where the contour method would add value and also to implement the technique within a product life cycle. A cost analysis should be made in greater detail counting each different cost in each step and categorizing it (material cost, labor cost, machine devaluation cost, etc.).

References

J. Altenkirch, A. Steuwer, P. J. Withers, S. W. Williams, M. Poad, and S. W. Wen. Residual stress engineering in friction stir welds by roller tensioning. *Science and Technology of Welding and Joining*, 14(2):185–192, 2009.

ASTM. E647 standard test method for measurement of fatigue crack growth rates, 2008a.

ASTM. E837 standard practice for determining residual stresses by hole-drilling strain-gage method, 2008b.

P. J. Bouchard. *Residual Stresses in Lifetime and Structural Integrity Assessment*, pages 8134–8142. in: Encyclopedia of Materials: Science and Technology. Oxford, 2001.

Xiaohua Cheng, John W. Fisher, Henry J. Prask, Thomas Gnäupel-Herold, Ben T. Yen, and Sougata Roy. Residual stress modification by post-weld treatment and its beneficial effect on fatigue strength of welded structures. *International Journal of Fatigue*, 25(9-11):1259–1269, 2003.

S. B. Dronavalli. *Residual stress measurements and analysis by destructive and non destructive techniques*. PhD thesis, University of Nevada, Las Vegas, 2004.

Johnson Gregory. *Residual stress measurements using the contour method*. PhD thesis, Faculty of Engineering and Physical Sciences, University of Manchester, 2008.

HBM. Ry21 - hole-drilling rosette, December 2011. URL `http://www.hbm.com/en/menu/products/strain-gages-accessories/strain-gages-for-stress-analysis/single/categorie/strain-gages-universal-foil-strain-gages/product/hole-drilling-rosettes/backPID/strain-gages-for-stress-analysis/?geoip_cn=1&cHash=73ccc0dca88d5aeaeda48a29e75bd554`.

A. Hewat. *Neutron Diffraction and the Structure of New Materials*, pages 1–20. in: Encyclopedia of Materials: Science and Technology. Elsevier, Oxford, 2002.

K. H. Ho and S. T. Newman. State of the art electrical discharge machining (EDM). *International Journal of Machine Tools and Manufacture*, 43(13):1287–1300, 2003.

X. P. Jiang, X. Y. Wang, J. X. Li, D. Y. Li, C. S. Man, M. J. Shepard, and T. Zhai. Enhancement of fatigue and corrosion properties of pure Ti by sandblasting. *Materials Science and Engineering: A*, 429(1-2):30 – 35, 2006. doi: 10.1016/j.msea.2006.04.024.

A. Joseph, Sanjai K. Rai, T. Jayakumar, and N. Murugan. Evaluation of residual stresses in dissimilar weld joints. *International Journal of Pressure Vessels and Piping*, 82(9): 700–705, 2005.

machinesbook. Sodick aq 325l wire edm machine, October 2011. URL `http://machinesbook.com/ogloszenie,20111016215652,sodick_aq_325l_wire_edm_machine.html`.

S. S. Mahapatra and Amar Patnaik. Parametric optimization of wire electrical discharge machining (WEDM) process using taguchi method. *Journal of the Brazilian Society of Mechanical Sciences and Engineering*, 28:422–429, 2006.

K. Masubuchi. *Residual Stresses and Distortion in Welds*, pages 1–6. Elsevier, Oxford, 2005. (print) (updates).

MathWorks. Matlab documentation 2011, 2011. URL `http://www.mathworks.com/help/techdoc/`.

I. Milne, R. A. Ainsworth, A. R. Dowling, and A. T. Stewart. Assessment of the integrity of structures containing defects. *International Journal of Pressure Vessels and Piping*, 32 (1-4):3–104, 1988.

Roberto Manuel Canito Miranda. *Study of Fatigue Crack Propagation in Metallic Structures*. Mechanical engineering master thesis, Faculdade de Engenharia da Universidade do Porto, 2010.

Norliana Mohd Abbas, Darius G. Solomon, and Fuad Bahari. A review on current research trends in electrical discharge machining (EDM). *International Journal of Machine Tools and Manufacture*, 47(7-8):1214–1228, 2007.

D. V. Nelson. Effects of residual stress on fatigue crack propagation. *Residual stress effects in fatigue, ASTM STP 776*, pages 172–194, 1982.

A. P. Parker. *The mechanics of fracture and fatigue: an introduction*. E. & F.N. Spon, 1981.

M. Prime, R. Sebring, J. Edwards, D. Hughes, and P. Webster. Laser surface-contouring and spline data-smoothing for residual stress measurement. *Experimental Mechanics*, 44(2): 176–184, 2004.

M. B. Prime. Cross-sectional mapping of residual stresses by measuring the surface contour after a cut. *Journal of Engineering Materials and Technology*, 123(2):162–168, 2001.

M. B. Prime, H. Swenson, P. Pagliaro, and B. Zuccarello. Measuring multiple residual-stress components using the contour method and multiple cuts. Technical report, Los Alamos National Laboratory (LANL), 2009. LA-UR-09-01120.

Michael B. Prime. Residual stress measurement by successive extension of a slot: The crack compliance method. *Applied Mechanics Reviews*, 52(2):75–96, 1999.

Michael B. Prime. The contour method: A new approach in experimental mechanics. *Proceedings of the SEM Annual Conference*, pages 156 – 165, 2009.

A.B. Rhouma, H. Sidhom, C. Braham, J. Lédion, and M. E. Fitzpatrick. Effects of surface preparation on pitting resistance, residual stress, and stress corrosion cracking in austenitic stainless steels. *Journal of Materials Engineering and Performance*, 10(5):507–514, 2001.

João Eduardo Pinto Castro Ribeiro. *Caracterização Experimental e Numérica de Campos de Tensões Residuais Provocadas por Processos de Fabrico*. Doctorate thesis, Faculdade de Engenharia da Universidade do Porto, 2006.

V. Richter-Trummer. *Characterization of Different Alluminium Alloys of the Series 6000 and their Joining Processes*. Mechanical engineering master thesis, Faculdade de Engenharia da Universidade do Porto, February 2008.

V. Richter-Trummer. *Residual stress effects and damage tolerance behaviour of integral lightweight structures manufactured by FSW and HSM*. Doctorate thesis, Faculdade de Engenharia da Universidade do Porto, 2012.

V. Richter-Trummer and P. M. S. T. de Castro. The through-the-thickness measurement of residual stress in a thick welded steel compact tension specimen by the contour method. *The Journal of Strain Analysis for Engineering Design*, 46(4):315–322, 2011.

V. Richter-Trummer, Sérgio M. O. Tavares, Pedro M. G. P. Moreira, Miguel A. V. de Figueiredo, and Paulo M. S. T. de Castro. Residual stress measurement using the contour and the sectioning methods in a MIG weld: Effects on the stress intensity factor. *Ciência e Tecnologia dos Materiais*, 20:114–119, 2008.

G. S. Schajer. Measurement of non-uniform residual stresses using the hole-drilling method. Part I—stress valculation procedures. *Journal of Engineering Materials and Technology*, 110(4):338–343, 1988.

Shang Shin. FEM analysis of plasticity-induced error on measurement of welding residual stress by the contour method. *Journal of Mechanical Science and Technology*, 19(10): 1885–1890, 2005.

Simulia. ABAQUS 6.10 online documentation, 31 of October 2011 2010. URL https://www.sharcnet.ca/Software/Abaqus610/Documentation/docs/v6.10/index.html.

Eric Qiuli Sun. Shear Locking and Hourglassing in MSC Nastran, ABAQUS, and ANSYS. *VPD Conference - Proceedings*, 2006.

H. Tada and P. C. Paris. The stress intensity factor for a crack perpendicular to the welding bead. *International Journal of Fracture*, 21(4):279–284, 1983.

Y. S. Tarng, S. C. Ma, and L. K. Chung. Determination of optimal cutting parameters in wire electrical discharge machining. *International Journal of Machine Tools and Manufacture*, 35(12):1693–1701, 1995.

Tso-Liang Teng, Chin-Ping Fung, Peng-Hsiang Chang, and Wei-Chun Yang. Analysis of residual stresses and distortions in t-joint fillet welds. *International Journal of Pressure Vessels and Piping*, 78(8):523–538, 2001.

H. Terada. An analysis of the stress intensity factor of a crack perpendicular to the welding bead. *Engineering Fracture Mechanics*, 8(2):441–444, 1976.

A. Tolga Bozdana, Nabil N. Z. Gindy, and Hua Li. Deep cold rolling with ultrasonic vibrations - a new mechanical surface enhancement technique. *International Journal of Machine Tools and Manufacture*, 45(6):713–718, 2005.

R. A. Winholtz. *Residual Stresses: Macro and Micro Stresses*, pages 8148–8151. in: Encyclopedia of Materials: Science and Technology. Elsevier, Oxford, 2001.

P. J. Withers and H. Bhadeshia. Residual stress. Part 1 - Measurement techniques. *Materials Science and Technology*, 17(4):355–365, 2001.

P. J. Withers and P. J. Webster. Neutron and synchrotron x-ray strain scanning. *Strain*, 37 (1):19–33, 2001.

Philip J. Withers. *Residual Stresses: Measurement by Diffraction*, pages 8158–8169. in: Encyclopedia of Materials: Science and Technology. Elsevier, Oxford, 2001a.

Philip J. Withers. *Residual Stress: Definition*, pages 8110–8112. in: Encyclopedia of Materials: Science and Technology. Elsevier, Oxford, 2001b.

Philip J. Withers. Mapping residual and internal stress in materials by neutron diffraction. *Comptes Rendus Physique*, 8(7-8):806–820, 2007.

O. C. Zienkiewicz and R. L. Taylor. *The Finite Element Method*, volume 1: The Basis. Butterworth-Heinemann, fifth edition, 2000.

Appendix A

CT specimen

```
% program which takes the CMM (CATIM) output and interpolates it over the
% plates for plotting the deformation
% 27/09/2011 last modified 08/11/2011

% prepare the MatLab workspace
clear all, close all, clc

part=4; % part 1 is the geoemtry creation for the FEM mesh,
        % part 2 uses the FEM mesh for surface interpolation
        % part 3 writes the path for abaqus
        % part 4 reads the abaqus output

% input data
file{1}='raw_data/FEUP-MedPlaneza-ZonaCorteErosao_1-A.csv';
file{2}='raw_data/FEUP-MedPlaneza-ZonaCorteErosao_1-B.csv';

file_FEM='FEM/femap/FEM_nodes.inp';
fileID={'A','B'};

% Interpolation type
type_inter=2; %1 linear interpolation
              %2 nearest interpolation
              %3 cubic interpolation
              %4 v4 interpolation
              %5 comparison

% Downsizing Point Grid inputs
type_remov=0; %Which way removes points
              %0 does not remove any point
              %1 removes interlock points
              %2 removes entire columns
              %3 removes entire lines
              %4 removes entire columns and lines

removconst=2; %by how many times the mesh is downsized
              %2 removes 1/2

%  Smoothing parameters
knots={5,5}; % number of knots in X and Y directions
x=0.5:1:108.5;
y=0.5:1:31.5;
[X,Y]=meshgrid(x,y); % interpolation grid
```

```
43
44 if part ==1||3||4
45 %%%%%%%%%%%%%%%%%%%%%%%%%%%%%%%%%%%%%%%%%%%%%%%%%%%%%%%%%%%%%%%%%%%%%%%%%%%%
46
47 for k=1:2
48     clear Data_raw Data
49     % raw CMM measurement data
50     Data_raw=csvread(file{k},12,1);
51     Data_raw(:,2:5)=[];
52     Data(:,1)=Data_raw(1:3:length(Data_raw),1);
53     Data(:,2)=Data_raw(2:3:length(Data_raw),1);
54     Data(:,3)=Data_raw(3:3:length(Data_raw),1);
55
56     % finds data outside of the area to be measured and delets it
57     index=find(Data(:,1)>105.4);
58     Data(index,:)=[];
59
60     % Interpolation of the measured data points to a rectangular grid
61     if type_inter == 1
62         tic
63         Z_inter_lin{k} = griddata(Data(:,1),Data(:,2),Data(:,3),X,Y,'linear');
64         Linear_Interpolation_Time = toc;
65         Z{k} = Z_inter_lin{k};
66 %         disp('run linear')
67         show=['Interpolation time is ' num2str(Linear_Interpolation_Time)];
68         disp(show)
69
70     elseif type_inter == 2
71         tic
72         Z_inter_near{k} = griddata(Data(:,1),Data(:,2),Data(:,3),X,Y,'nearest');
73         Nearest_Interpolation_Time = toc;
74         Z{k} = Z_inter_near{k};
75 %         disp('run nearest')
76         show=['Interpolation time is ' num2str(Nearest_Interpolation_Time)];
77         disp(show)
78
79
80     elseif type_inter == 3
81         tic
82         Z_inter_cub{k} = griddata(Data(:,1),Data(:,2),Data(:,3),X,Y,'cubic');
83         Cubic_Interpolation_Time = toc;
84         Z{k} = Z_inter_cub{k};
85 %         disp('run cubic')
86         show=['Interpolation time is ' num2str(Cubic_Interpolation_Time)];
87         disp(show)
88
89     elseif type_inter == 4
90         tic
91         Z_inter_v4{k} = griddata(Data(:,1),Data(:,2),Data(:,3),X,Y,'v4');
92         V4_Interpolation_Time = toc;
93         Z{k} = Z_inter_v4{k};
94 %         disp('run V4')
95         show=['Interpolation time is ' num2str(V4_Interpolation_Time)];
96         disp(show)
97
98     elseif type_inter == 5
99         Z_inter_lin{k} = griddata(Data(:,1),Data(:,2),Data(:,3),X,Y,'linear');
100        Z_inter_near{k} = griddata(Data(:,1),Data(:,2),Data(:,3),X,Y,'nearest');
101        Z_inter_cub{k} = griddata(Data(:,1),Data(:,2),Data(:,3),X,Y,'cubic');
```

```
102         Z_inter_v4{k} = griddata(Data(:,1),Data(:,2),Data(:,3),X,Y,'v4');
103         Z{k} = Z_inter_near{k};
104 %         disp('run comparisson')
105     end
106
107     % Downsizing grid
108     if type_remov == 1
109         if removconst==4
110             for p1 = 1:length(Z{k}(1,:))
111                 if mod(p1,2) == 0
112                     for p2 = 1:length(Z{k}(:,1))
113                         if mod(p2,removconst) == 0
114                             Z_inter_near{k}(p2,p1) = NaN;
115                             Z_inter_lin{k}(p2,p1) = NaN;
116                             Z_inter_cub{k}(p2,p1) = NaN;
117                             Z_inter_v4{k}(p2,p1) = NaN;
118                             Z{k}(p2,p1) = NaN;
119                         end
120                     end
121                 end
122             end
123         end
124         if removconst==2
125             for p1 = 1:length(Z{k}(1,:))
126                 if mod(p1,2) ~= 0
127                     for p2 = 1:length(Z{k}(:,1))
128                         if mod(p2,removconst) == 0
129                             Z_inter_near{k}(p2,p1) = NaN;
130                             Z_inter_lin{k}(p2,p1) = NaN;
131                             Z_inter_cub{k}(p2,p1) = NaN;
132                             Z_inter_v4{k}(p2,p1) = NaN;
133                             Z{k}(p2,p1) = NaN;
134                         end
135                     end
136                 end
137                 if mod(p1,2) == 0
138                     for p2 = 1:length(Z{k}(:,1))
139                         if mod(p2,removconst) ~= 0
140                             Z_inter_near{k}(p2,p1) = NaN;
141                             Z_inter_lin{k}(p2,p1) = NaN;
142                             Z_inter_cub{k}(p2,p1) = NaN;
143                             Z_inter_v4{k}(p2,p1) = NaN;
144                             Z{k}(p2,p1) = NaN;
145                         end
146                     end
147                 end
148             end
149         end
150     elseif type_remov == 2
151         if removconst ~=1
152             for p1 = 1:length(Z{k}(:,1))
153                 if mod(p1,removconst) == 0
154                     Z_inter_near{k}(p1,:) = NaN;
155                     Z_inter_lin{k}(p1,:) = NaN;
156                     Z_inter_cub{k}(p1,:) = NaN;
157                     Z_inter_v4{k}(p1,:) = NaN;
158                     Z{k}(p1,:) = NaN;
159                 end
160             end
```

```
        end
    elseif type_remov == 3
    if removconst ~=1
        for p2 = 1:length(Z{k}(1,:))
            if mod(p2,removconst) == 0
                Z_inter_near{k}(:,p2) = NaN;
                Z_inter_lin{k}(:,p2) = NaN;
                Z_inter_cub{k}(:,p2) = NaN;
                Z_inter_v4{k}(:,p2) = NaN;
                Z{k}(:,p2) = NaN;
            end
        end
    end
    elseif type_remov == 4
         for p1 = 1:length(Z{k}(1,:))
            if mod(p1,removconst) == 0
                Z_inter_near{k}(:,p1) = NaN;
                Z_inter_lin{k}(:,p1) = NaN;
                Z_inter_cub{k}(:,p1) = NaN;
                Z_inter_v4{k}(:,p1) = NaN;
                Z{k}(:,p1) = NaN;
            end
         end
        for p2 = 1:length(Z{k}(:,1))
            if mod(p2,removconst) == 0
                Z_inter_near{k}(p2,:) = NaN;
                Z_inter_lin{k}(p2,:) = NaN;
                Z_inter_cub{k}(p2,:) = NaN;
                Z_inter_v4{k}(p2,:) = NaN;
                Z{k}(p2,:) = NaN;
             end
        end
    end
end
        indX=find(isnan(Z{1}(:,1)));
        indY=find(isnan(Z{1}(1,:)));
        Z{1}(indX,:) = [];
        Z{2}(indX,:) = [];
        X(indX,:)=[];
        Y(indX,:)=[];
        y(indX)=[];
        Z{1}(:,indY) = [];
        Z{2}(:,indY) = [];
        X(:,indY)=[];
        Y(:,indY)=[];
        x(indY)=[];

for k=1:2
    % calculate centroid
    x0 = mean(Data)';

    % translate the points around the centroid
    XYZ_trans = [(Data(:, 1) - x0(1)) (Data(:, 2) - x0(2)) ...
        (Data(:, 3) - x0(3))];

    [U, S, V] = svd(XYZ_trans, 0);

    % find the smallest singular value in S and extract the
    % corresponding right singular vector from V
```

```
220     [s, ii] = min(diag(S));
221     a = V(:, ii);   % Direction cosines of the normal to the best-fit
222                     % plane.
223
224     for n=1:length(Data)
225         plane(n)=x0(3)-a(1)/a(3)*(Data(n,1)-x0(1))-a(2)/a(3)*...
226             (Data(n,2)-x0(2));
227     end
228     % plotting comparrison
229     if type_inter ==  5
230         figure(10+k), hold on
231         subplot(2,2,1); surf(X,Y,Z_inter_lin{k})
232         titlestring=['Complete Raw Data Linear Interpolation side ' num2str(k)];
233         Title(titlestring)
234         view(50,25)
235         subplot(2,2,2);surf(X,Y,Z_inter_near{k})
236         titlestring=['Complete Raw Data Nearest Interpolation side ' num2str(k)];
237         Title(titlestring)
238         view(50,25)
239         subplot(2,2,3);surf(X,Y,Z_inter_cub{k})
240         titlestring=['Complete Raw Data Cubic Interpolation side ' num2str(k)];
241         Title(titlestring)
242         view(50,25)
243         subplot(2,2,4);surf(X,Y,Z_inter_v4{k})
244         titlestring=['Complete Raw Data V4 Interpolation side ' num2str(k)];
245         Title(titlestring)
246         view(50,25)
247         namestring=['analyzed_data/Different_interpolations_side_' num2str(k)];
248         saveas(gcf,namestring,'pdf')
249
250         figure(18+k), hold on
251         titlestring=['Complete Raw Data cub side ' num2str(k)];
252         Title(titlestring)
253         surf(X,Y,Z_inter_cub{k})
254         view(50,25)
255
256         figure(12+k), hold on
257         subplot(2,2,1);surf(X,Y,Z_inter_near{k}-Z_inter_lin{k})
258         titlestring=['Difference Between Nearest and Linear Interpolation side ' num2str(k)];
259         Title(titlestring)
260         view(50,25)
261         subplot(2,2,2);surf(X,Y,Z_inter_near{k}-Z_inter_cub{k})
262         titlestring=['Difference Between Nearest and Cubic Interpolation side ' num2str(k)];
263         Title(titlestring)
264         view(50,25)
265         subplot(2,2,3);surf(X,Y,Z_inter_near{k}-Z_inter_v4{k})
266         titlestring=['Difference Between Nearest and V4 Interpolation side ' num2str(k)];
267         Title(titlestring)
268         view(50,25)
269         namestring=['analyzed_data/Interpolation_comparissons_side_' num2str(k)];
270         saveas(gcf,namestring,'pdf')
271     else
272         figure(14+k), hold on
273 %         titlestring=['Surface Side ' num2str(k)];
274 %         Title(titlestring)
275         surf(X,Y,Z{k})
276         xlabel('specimen width [mm]')
277         ylabel('specimen thickness [mm]')
278         zlabel('surface relaxation [mm]')
```

```
        view(45,20)
        namestring=['analyzed_data/Interpolation_results_side_' num2str(k)];
        saveas(gcf,namestring,'pdf')

        figure(100+k), hold on
%         titlestring=['Surface side ' num2str(k) ' and midle plane'];
%         Title(titlestring)
        plot3(X,Y,Z{k},'b.')
        plot3(Data(:,1),Data(:,2),plane,'r.')
        xlabel('specimen width [mm]')
        ylabel('specimen thickness [mm]')
        view(45,20)
        namestring=['analyzed_data/Measured_points_side_' num2str(k) '_with_midle_plane'];
        saveas(gcf,namestring,'pdf')
    end
end



% importing nodes
allnodes=csvread('FEM/nodes.inp',1,0);
nodeset_=importdata('FEM/surface_node_set.inp');
nodeset=unique(nodeset_.data);
nodeset(7845:7856)=[];
for n=1:length(nodeset)
    nodes(n,:) = allnodes(find(allnodes(:,1)==nodeset(n)),:);
end

% couting surface nodes
[d1,d2]=size(nodeset_.data);
number_surface_nodes=d1*d2;

% calculates the average of both specimen halfs
average_surface=(Z{1}+Z{2})./2;

% eliminates some errors
average_surface(find(average_surface(:,:)>0.04))=NaN;

if part ==1
    % smooths the gridded data
    k=3; % quadratic spline
    surf_smooth_av=spap2(knots,[k k],{x,y},average_surface');

    if type_inter ==  5
        average_surface_lin=(Z_inter_lin{1}+Z_inter_lin{2})./2;
        average_surface_cub=(Z_inter_cub{1}+Z_inter_cub{2})./2;
        average_surface_near=(Z_inter_near{1}+Z_inter_near{2})./2;
        average_surface_v4=(Z_inter_v4{1}+Z_inter_v4{2})./2;

        surf_smooth_av_lin=spap2(knots,[k k],{x,y},average_surface_lin');
        surf_smooth_av_cub=spap2(knots,[k k],{x,y},average_surface_cub');
        surf_smooth_av_near=spap2(knots,[k k],{x,y},average_surface_near');
        surf_smooth_av_v4=spap2(knots,[k k],{x,y},average_surface_v4');
        for nn=1:size(X,2)
            for mm=1:size(X,1)
                smooth_surface_lin(mm,nn)=fnval(surf_smooth_av_lin,...
                    {X(mm,nn),Y(mm,nn)});
                smooth_surface_cub(mm,nn)=fnval(surf_smooth_av_cub,...
                    {X(mm,nn),Y(mm,nn)});
```

```
338                 smooth_surface_near(mm,nn)=fnval(surf_smooth_av_near,...
339                     {X(mm,nn),Y(mm,nn)});
340                 smooth_surface_v4(mm,nn)=fnval(surf_smooth_av_v4,...
341                     {X(mm,nn),Y(mm,nn)});
342             end
343         end
344     end
345
346
347     for nn=1:size(X,2)
348         for mm=1:size(X,1)
349             smooth_surface(mm,nn)=fnval(surf_smooth_av,...
350                 {X(mm,nn),Y(mm,nn)});
351         end
352     end
353
354     for nn=1:length(nodes)
355         smooth_result(nn)=fnval(surf_smooth_av,{nodes(nn,2),...
356             nodes(nn,4)});
357     end
358
359     smooth_result=smooth_result-mean(smooth_result);
360
361     if part ==1
362         % plotting
363         figure(1), hold on
364 %         Title('Average Surface')
365         surf(X,Y,average_surface)
366         xlabel('specimen width [mm]')
367         ylabel('specimen thickness [mm]')
368         zlabel('surface relaxation [mm]')
369         view(45,20)
370         saveas(gcf,'analyzed_data/Average_surface','pdf')
371
372         figure(2), hold on
373         Title('Average Surface')
374         plot3(X,Y,average_surface,'k.')
375         xlabel('specimen width [mm]')
376         ylabel('specimen thickness [mm]')
377         zlabel('surface relaxation [mm]')
378         view(45,20)
379         saveas(gcf,'analyzed_data/Average_surface_plot3','pdf')
380
381         figure(3)
382         Title('Average Smooth Surface')
383         set(gca,'FontSize',16)
384         surf(X,Y,smooth_surface)
385         xlabel('specimen width [mm]')
386         ylabel('specimen thickness [mm]')
387         zlabel('surface relaxation [mm]')
388         view(45,20)
389         axis([0 105 0 32 -0.04 0.04])
390         saveas(gcf,'analyzed_data/Average_Smooth_Surface','pdf')
391
392         if type_inter ==  5
393             figure(21), hold on
394             subplot(2,2,1); surf(X,Y,average_surface_lin)
395             xlabel('specimen width [mm]','Rotation',-25)
396             ylabel('specimen thickness [mm]','Rotation',15)
```

```
397             zlabel('surface relaxation [mm]')
398             Title('Smooth surface with Linear Interpolation')
399             view(50,25)
400             subplot(2,2,2);surf(X,Y,average_surface_near)
401             xlabel('specimen width [mm]','Rotation',-25)
402             ylabel('specimen thickness [mm]','Rotation',15)
403             zlabel('surface relaxation [mm]')
404             Title('Smooth surface with Nearest Interpolation')
405             view(50,25)
406             subplot(2,2,3);surf(X,Y,average_surface_cub)
407             xlabel('specimen width [mm]','Rotation',-25)
408             ylabel('specimen thickness [mm]','Rotation',15)
409             zlabel('surface relaxation [mm]')
410             Title('Smooth surface with Cubic Interpolation')
411             view(50,25)
412             subplot(2,2,4);surf(X,Y,average_surface_v4)
413             xlabel('specimen width [mm]','Rotation',-25)
414             ylabel('specimen thickness [mm]','Rotation',15)
415             zlabel('surface relaxation [mm]')
416             Title('Smooth surface with V4 Interpolation')
417             view(50,25)
418             saveas(gcf,'Average_surface_different_interpolation','pdf')
419
420             figure(22), hold on
421             subplot(2,2,1); surf(X,Y,smooth_surface_lin)
422             xlabel('specimen width [mm]','Rotation',-25)
423             ylabel('specimen thickness [mm]','Rotation',15)
424             zlabel('surface relaxation [mm]')
425             Title('Smooth surface with Linear Interpolation')
426             view(50,25)
427             subplot(2,2,2);surf(X,Y,smooth_surface_near)
428             xlabel('specimen width [mm]','Rotation',-25)
429             ylabel('specimen thickness [mm]','Rotation',15)
430             zlabel('surface relaxation [mm]')
431             Title('Smooth surface with Nearest Interpolation')
432             view(50,25)
433             subplot(2,2,3);surf(X,Y,smooth_surface_cub)
434             xlabel('specimen width [mm]','Rotation',-25)
435             ylabel('specimen thickness [mm]','Rotation',15)
436             zlabel('surface relaxation [mm]')
437             Title('Smooth surface with Cubic Interpolation')
438             view(50,25)
439             subplot(2,2,4);surf(X,Y,smooth_surface_v4)
440             xlabel('specimen width [mm]','Rotation',-25)
441             ylabel('specimen thickness [mm]','Rotation',15)
442             zlabel('surface relaxation [mm]')
443             Title('Smooth surface with V4 Interpolation')
444             view(50,25)
445             saveas(gcf,'Smooth_surface_different_interpolation','pdf')
446         end
447     end
448
449     % Goodness of fit
450     average_surface=inpaint_nans(average_surface,0);
451     sum_smooth=0;
452     sum_origin=0;
453     for nn=1:size(X,1)
454         for mm=1:size(X,2)
455
```

```
456             sum_smooth=sum_smooth+(smooth_surface(nn,mm)-...
457                 average_surface(nn,mm))^2;
458             sum_origin=sum_origin+(average_surface(nn,mm)-...
459                 nanmean(nanmean(smooth_surface)))^2;
460
461         end
462     end
463     GOF=1-sum_smooth/sum_origin;
464
465 %     clc
466     disp(strcat('The goodness of fit for this surface is ',...
467         num2str(GOF*100),'%'))
468
469
470     % Writes the Abaqus input file with the obtained deformation
471     fid1 = fopen('FEM/1/displacement.inp', 'w');
472     fprintf(fid1, '*BOUNDARY, TYPE=DISPLACEMENT, OP=MOD\n');
473     for nn=1:length(smooth_result)
474         fprintf(fid1, strcat('\t        ',num2str(nodes(nn,1)),',\t',...
475             num2str(2),',\t,\t',num2str(smooth_result(nn)),' \n'));
476     end
477     fclose(fid1)
478
479       % Writes the Abaqus input file non deformed
480     fid1 = fopen('FEM/1/originaldisplacement.inp', 'w');
481     fprintf(fid1, '*BOUNDARY, TYPE=DISPLACEMENT, OP=MOD\n');
482     for nn=1:length(smooth_result)
483         fprintf(fid1, strcat('\t        ',num2str(nodes(nn,1)),',\t',...
484             num2str(2),',\t,\t',num2str(nodes(nn,4)),' \n'));
485     end
486     fclose(fid1)
487
488 end
489
490 end
491 %%%%%%%%%%%%%%%%%%%%%%%%%%%%%%%%%%%%%%%%%%%%%%%%%%%%%%%%%%%%%%%%%%%%%%%%%%%%%%%%
492
493 %%%%%%%%%%%%%%%%%%%%%%%%%%%%%%%%%%%%%%%%%%%%%%%%%%%%%%%%%%%%%%%%%%%%%%%%%%%%%%%%
494 if part == 3
495     % writes a path with all the nodes from the surface. Afterwards, the
496     % stresses on this nodes will be retrieved
497     fid1 = fopen('FEM/pathB.txt', 'w');
498     for j=1:length(nodes(:,1))
499         fprintf(fid1, strcat(num2str(nodes(j,1)),', '));
500     end
501     fclose(fid1)
502 end
503 %%%%%%%%%%%%%%%%%%%%%%%%%%%%%%%%%%%%%%%%%%%%%%%%%%%%%%%%%%%%%%%%%%%%%%%%%%%%%%%%
504
505 %%%%%%%%%%%%%%%%%%%%%%%%%%%%%%%%%%%%%%%%%%%%%%%%%%%%%%%%%%%%%%%%%%%%%%%%%%%%%%%%
506 if part == 4
507     % import stress from the created abaqus report and plots them
508     DELIMITER = ' ';
509     HEADERLINES = 2;
510     newData1 = importdata('FEM/abaqus.rpt', DELIMITER,...
511         HEADERLINES);
512     stress22=-newData1.data(:,2);
513     stress22_qq=-newData1.data(:,:);
514
```

```
515     % eliminates teh extrapolated node values
516     indexes=find(nodes(:,2)>106);
517     stress22(indexes)=[];
518     nodes(indexes,:)=[];
519
520     figure(3)
521     plot3(nodes(:,2),nodes(:,4),stress22,'k.')
522
523     % interpolate the obtained data to a rectangular grid
524     x=linspace(0,105,265);
525     y=linspace(0,32,45);
526     [X,Y]=meshgrid(x,y);
527     stressRS=griddata(nodes(:,2),nodes(:,4),stress22,X,Y,'nearest');
528
529     figure(31)
530     set(gca,'FontSize',16)
531     surf(X,Y,stressRS)
532     view([-22 89])
533     axis equal
534     xlabel('specimen width [mm]','FontSize',12,'Rotation',18)
535     ylabel('specimen thickness [mm]','FontSize',12,'Rotation',-70)
536     colorbar('location','NorthOutside','FontSize',14)
537     set(gca,'CLim',[-400 400])
538     saveas(gcf,'analyzed_data/RScontourmap3D',...
539         'jpg')
540
541     figure(32)
542     set(gca,'FontSize',16)
543     surf(X,Y,stressRS)
544     view([-0.5 90])
545     axis equal
546     axis([0 100 0 30])
547     xlabel('specimen width [mm]','FontSize',12)
548     ylabel('specimen thickness [mm]','FontSize',12)
549     colorbar('location','NorthOutside','FontSize',14)
550     set(gca,'CLim',[-400 400])
551     saveas(gcf,'analyzed_data/RScontourmap',...
552         'jpg')
553
554     figure(33)
555     set(gca,'FontSize',16)
556     surf(X,Y,stressRS,'LineStyle','none')
557     view([-0.5 90])
558     axis equal
559     axis([0 100 0 30])
560     xlabel('specimen width [mm]','FontSize',12)
561     ylabel('specimen thickness [mm]','FontSize',12)
562     colorbar('location','NorthOutside','FontSize',14)
563     set(gca,'CLim',[-400 400])
564     saveas(gcf,'analyzed_data/RScontourmap_no_lines',...
565         'jpg')
566
567     save('variables.mat','X','Y','stressRS')
568 end
569 %%%%%%%%%%%%%%%%%%%%%%%%%%%%%%%%%%%%%%%%%%%%%%%%%%%%%%%%%%%%%%%%%%%%%%%%%%%%%%%%
```

Appendix B

MATLAB contour method code for welded plate specimen

```
% program which takes the CMM (CATIM) output and interpolates it over the
% plates for plotting the deformation
% 10/11/2011 last modified 11/11/2011

% prepare the MatLab workspace
clear all, close all, clc

% Interpolation type
type_inter=2; %1 linear interpolation
              %2 nearest interpolation
              %3 cubic interpolation
              %4 v4 interpolation

% Downsizing Point Grid inputs
% ------------------------------------------------------------------------
type_remov=0; %Which way removes points
              %0 does not remove any point
              %1 removes interlock points
              %2 removes entire lines
              %3 removes entire columns
              %4 removes entire columns and lines

removconst=2; %by how many times the mesh is downsized
              %2 removes 1/2

% ------------------------------------------------------------------------
%  Smoothing parameters
knots={45,5}; % number of knots in X and Y directions
x=-150:2:150;
y=0:0.5:9;
[X,Y]=meshgrid(x,y); % interpolation grid

%%%%%%%%%%%%%%%%%%%%%%%%%%%%%%%%%%%%%%%%%%%%%%%%%%%%%%%%%%%%%%%%%%%%%%%%%%%%
%%%%%%%%%%%%%%%%%%%%%%%%%%%%%%%%%%%%%%%%%%%%%%%%%%%%%%%%%%%%%%%%%%%%%%%%%%%%
% ------------------------------------------------------------------------
% parts of the code below were taken from:
% ML_PhD_VRT_CTsteel_contour_1_v01_simplifiedCodeForShowing.M
%
% Created        V. Richter-Trummer 13/07/2010
```

```
% ------------------------------------------------------------------


part=1; % part 1 is the geoemtry creation for the FEM mesh,
        % part 2 writes the path for abaqus
        % part 3 reads the abaqus output

% input data
file{1}='raw_data/LMD20115009158-10_IDMEC-MedPlacaSoldadura-A.csv';
file{2}='raw_data/LMD20115009158-20_IDMEC-MedPlacaSoldadura-B.csv';

%%%%%%%%%%%%%%%%%%%%%%%%%%%%%%%%%%%%%%%%%%%%%%%%%%%%%%%%%%%%%%%%%%%%%%%%%%%

for k=1:2
    clear Data_raw Data
    % raw CMM measurement data
    Data_raw_left=csvread(file{k},0,0);
    Data_raw_right=csvread(file{k},0,1);

    Data_left(:,1)=Data_raw_left(1:3:length(Data_raw_left),1);
    Data_left(:,2)=Data_raw_left(2:3:length(Data_raw_left),1);
    Data_left(:,3)=Data_raw_left(3:3:length(Data_raw_left),1);
    Data_right(:,1)=Data_raw_right(1:3:length(Data_raw_right),1);
    Data_right(:,2)=Data_raw_right(2:3:length(Data_raw_right),1);
    Data_right(:,3)=Data_raw_right(3:3:length(Data_raw_right),1);
    Data(1:length(Data_left(:,1)),1)=Data_left(:,1);
    Data(1:length(Data_left(:,1)),2)=Data_left(:,2);
    Data(1:length(Data_left(:,1)),3)=Data_left(:,3);
    Data(length(Data_left(:,1))+1:length(Data_left(:,1))*2,1)=Data_right(:,1);
    Data(length(Data_left(:,1))+1:length(Data_left(:,1))*2,2)=Data_right(:,2);
    Data(length(Data_left(:,1))+1:length(Data_left(:,1))*2,3)=Data_right(:,3);

    Data(find(Data(:,3)<-1),:)=[];

    if k==1
        data_plate_A=Data;
    elseif k==2
        data_plate_B=Data;
    end
end

    tol=0.2;
    contador_X=0;
    for x_sort=-149:2:149
        contador_X=contador_X+1;
        organizerA=find(data_plate_A(:,1)>x_sort-tol & ...
            data_plate_A(:,1)<x_sort+tol);
        [a,b]=sort(data_plate_A(organizerA,2),'descend');
        measured_A_matrix_y(:,contador_X)=a;
        organizerB=find(data_plate_B(:,1)>x_sort-tol & ...
            data_plate_B(:,1)<x_sort+tol);
        [a,b]=sort(data_plate_B(organizerB,2),'descend');
        measured_B_matrix_y(:,contador_X)=a;
    end
    count=0;
    for nn=1:length(measured_A_matrix_y(1,:))/2
        for mm=1:length(measured_A_matrix_y(:,1))
            count=count+1;
            measured_A_matrix_x(mm,nn)=data_plate_A(count,1);
```

```
            measured_A_matrix_z(mm,nn)=data_plate_A(count,3);
        end
    end
    count=length(data_plate_A(:,1));
    for nn=length(measured_A_matrix_y(1,:))/2+1:length(measured_A_matrix_y(1,:))
        for mm=1:length(measured_A_matrix_y(:,1))
            count=count-1;
            measured_A_matrix_x(mm,nn)=data_plate_A(count,1);
            measured_A_matrix_z(mm,nn)=data_plate_A(count,3);
        end
    end
    count=0;
    for nn=1:length(measured_B_matrix_y(1,:))/2
        for mm=1:length(measured_B_matrix_y(:,1))
            count=count+1;
            measured_B_matrix_x(mm,nn)=data_plate_B(count,1);
            measured_B_matrix_z(mm,nn)=data_plate_B(count,3);
        end
    end
     count=length(data_plate_B(:,1));
    for nn=length(measured_B_matrix_y(1,:))/2+1:length(measured_B_matrix_y(1,:))
        for mm=1:length(measured_B_matrix_y(:,1))
            count=count-1;
            measured_B_matrix_x(mm,nn)=data_plate_B(count,1);
            measured_B_matrix_z(mm,nn)=data_plate_B(count,3);
        end
    end

% importing nodes
allnodes=csvread('FEM/Nodes.inp',1,0);
nodeset_=importdata('FEM/surface_nodes.inp');
nodeset=unique(nodeset_.data);
ins=[];
for n=1:length(nodeset)
    if isnan(nodeset(n))
        ins=[ins n];
    end
end
nodeset(ins)=[];
for n=1:length(nodeset)
    nodes(n,:) = allnodes(find(allnodes(:,1)==nodeset(n)),:);
end

    FEMnodes=allnodes(find(allnodes(:,4)==190),:);
    tol=0.2;
    contador_X=0;
    for x_sort=-149:1:-7
        contador_X=contador_X+1;
        aux_2=find(FEMnodes(:,2)>x_sort-tol & ...
            FEMnodes(:,2)<x_sort+tol);
        [a,b]=sort(FEMnodes(aux_2,3),'descend');
            nodes_list=FEMnodes(aux_2(b),1);
        node_ID_A(:,contador_X)=nodes_list;
    end

%    Quarter Plate with Wedge elements 0.5x1
node_ID_middle(:,1)=[541,3779,3780,3781,3782,3783,3784,3785,3786,3787,3788,552];
node_ID_middle(:,2)=[540,3769,3770,3771,3772,3773,3774,3775,3776,3777,3778,553];
node_ID_middle(:,3)=[37,3759,3760,3761,3762,3763,3764,3765,3766,3767,3768,554];
```

```
node_ID_middle(:,4)=[539,3749,3750,3751,3752,3753,3754,3755,3756,3757,3758,40];
node_ID_middle(:,5)=[36,3739,3740,3741,3742,3743,3744,3745,3746,3747,3748,555];
node_ID_middle(:,6)=[538,3729,3730,3731,3732,3733,3734,3735,3736,3737,3738,41];
node_ID_middle(:,7)=[35,3719,3720,3721,3722,3723,3724,3725,3726,3727,3728,556];
node_ID_middle(:,8)=[537,3709,3710,3711,3712,3713,3714,3715,3716,3717,3718,42];
node_ID_middle(:,9)=[34,3699,3700,3701,3702,3703,3704,3705,3706,3707,3708,557];
node_ID_middle(:,10)=[536,3689,3690,3691,3692,3693,3694,3695,3696,3697,3698,43];
node_ID_middle(:,11)=[33,3679,3680,3681,3682,3683,3684,3685,3686,3687,3688,558];
node_ID_middle(:,12)=[535,3669,3670,3671,3672,3673,3674,3675,3676,3677,3678,44];
node_ID_middle(:,13)=[32,3659,3660,3661,3662,3663,3664,3665,3666,3667,3668,559];
node_ID_middle(:,14)=[534,3649,3650,3651,3652,3653,3654,3655,3656,3657,3658,560];

    contador_x=0;
    for x_sort=7:1:149
        contador_x=contador_x+1;
        aux_2=find(FEMnodes(:,2)>x_sort-tol & ...
            FEMnodes(:,2)<x_sort+tol);
        [a,b]=sort(FEMnodes(aux_2,3),'descend');
            nodes_list=FEMnodes(aux_2(b),1);
        node_ID_B(:,contador_x)=nodes_list;
    end
    node_ID=[node_ID_A node_ID_middle node_ID_B];
    for nn=1:size(node_ID,2)
        for mm=1:size(node_ID,1)
            c=find(FEMnodes(:,1)==node_ID(mm,nn));
            matrix_x(mm,nn)=nodes(c,2);
            matrix_y(mm,nn)=nodes(c,3);
        end
    end


     % Downsizing grid
    if type_remov == 1
        if removconst==4
            for p1 = 1:length(measured_A_matrix_x(1,:))
                if mod(p1,2) == 0
                    for p2 = 1:length(measured_A_matrix_x(:,1))
                        if mod(p2,removconst) == 0
                            measured_A_matrix_x(p2,p1) = NaN;
                            measured_A_matrix_y(p2,p1) = NaN;
                            measured_A_matrix_z(p2,p1) = NaN;
                            measured_B_matrix_x(p2,p1) = NaN;
                            measured_B_matrix_y(p2,p1) = NaN;
                            measured_B_matrix_z(p2,p1) = NaN;
                        end
                    end
                end
            end
        end
        if removconst==2
            for p1 = 1:length(measured_A_matrix_x(1,:))
                if mod(p1,2) ~= 0
                    for p2 = 1:length(measured_A_matrix_x(:,1))
                        if mod(p2,removconst) == 0
                            measured_A_matrix_x(p2,p1) = NaN;
                            measured_A_matrix_y(p2,p1) = NaN;
                            measured_A_matrix_z(p2,p1) = NaN;
                            measured_B_matrix_x(p2,p1) = NaN;
                            measured_B_matrix_y(p2,p1) = NaN;
```

```
                        measured_B_matrix_z(p2,p1) = NaN;
                    end
                end
            end
            if mod(p1,2) == 0
                for p2 = 1:length(measured_A_matrix_x(:,1))
                    if mod(p2,removconst) ~= 0
                        measured_A_matrix_x(p2,p1) = NaN;
                        measured_A_matrix_y(p2,p1) = NaN;
                        measured_A_matrix_z(p2,p1) = NaN;
                        measured_B_matrix_x(p2,p1) = NaN;
                        measured_B_matrix_y(p2,p1) = NaN;
                        measured_B_matrix_z(p2,p1) = NaN;
                    end
                end
            end
        end
    end
elseif type_remov == 2
    if removconst ~=1
        for p1 = 1:length(measured_A_matrix_x(:,1))
            if mod(p1,removconst) == 0
                measured_A_matrix_x(p1,:) = NaN;
                measured_A_matrix_y(p1,:) = NaN;
                measured_A_matrix_z(p1,:) = NaN;
                measured_B_matrix_x(p1,:) = NaN;
                measured_B_matrix_y(p1,:) = NaN;
                measured_B_matrix_z(p1,:) = NaN;
            end
        end
    end
    indX=find(isnan(measured_A_matrix_x(:,1)));
    indY=find(isnan(measured_A_matrix_x(1,:)));
elseif type_remov == 3
    if removconst ~=1
        for p2 = 1:length(measured_A_matrix_x(1,:))
            if mod(p2,removconst) == 0
                measured_A_matrix_x(:,p2) = NaN;
                measured_A_matrix_y(:,p2) = NaN;
                measured_A_matrix_z(:,p2) = NaN;
                measured_B_matrix_x(:,p2) = NaN;
                measured_B_matrix_y(:,p2) = NaN;
                measured_B_matrix_z(:,p2) = NaN;
            end
        end
    end
    indX=find(isnan(measured_A_matrix_x(:,1)));
    indY=find(isnan(measured_A_matrix_x(1,:)));
elseif type_remov == 4
     for p1 = 1:length(measured_A_matrix_x(1,:))
        if mod(p1,removconst) == 0
            measured_A_matrix_x(:,p1) = NaN;
            measured_A_matrix_y(:,p1) = NaN;
            measured_A_matrix_z(:,p1) = NaN;
            measured_B_matrix_x(:,p1) = NaN;
            measured_B_matrix_y(:,p1) = NaN;
            measured_B_matrix_z(:,p1) = NaN;
        end
     end
```

```
        for p2 = 1:length(measured_A_matrix_x(:,1))
            if mod(p2,removconst) == 0
                measured_A_matrix_x(p2,:) = NaN;
                measured_A_matrix_y(p2,:) = NaN;
                measured_A_matrix_z(p2,:) = NaN;
                measured_B_matrix_x(p2,:) = NaN;
                measured_B_matrix_y(p2,:) = NaN;
                measured_B_matrix_z(p2,:) = NaN;
             end
        end
        indX=find(isnan(measured_A_matrix_x(:,1)));
        indY=find(isnan(measured_A_matrix_x(1,:)));
    end

    % Rebuilding originial Data matrix
    count=0;
    for nn=1:length(measured_A_matrix_y(1,:))
        for mm=1:length(measured_A_matrix_y(:,1))
            count=count+1;
            new_data_plate_A(count,:)=[measured_A_matrix_x(mm,nn) ...
                measured_A_matrix_y(mm,nn) measured_A_matrix_z(mm,nn)];
            new_data_plate_B(count,:)=[measured_B_matrix_x(mm,nn) ...
                measured_B_matrix_y(mm,nn) measured_B_matrix_z(mm,nn)];
        end
    end
    ind=find(isnan(new_data_plate_A(:,1)));
    new_data_plate_A(ind,:)=[];
    ind2=find(isnan(new_data_plate_B(:,1)));
    new_data_plate_B(ind2,:)=[];

% Alignment of both halves
% ------------------------------------------------------------------------
    % calculate centroid
    x0 = mean(new_data_plate_A)';

    % translate the points around the centroid
    XYZ_trans = [(new_data_plate_A(:, 1) - x0(1)) (new_data_plate_A(:, 2) - x0(2)) (new_data_plate_A(:, 3) - x

    [U, S, V] = svd(XYZ_trans, 0);

    % find the smallest singular value in S and extract the
    % corresponding right singular vector from V
    [s, ii] = min(diag(S));
    a = V(:, ii);   % Direction cosines of the normal to the best-fit
                    % plane.

    for n=1:length(new_data_plate_A)
        plane_plate_A(n)=x0(3)-a(1)/a(3)*(new_data_plate_A(n,1)-x0(1))-a(2)/a(3)*...
            (new_data_plate_A(n,2)-x0(2));
    end
    % Alignment
    new_data_plate_A(:,3)=new_data_plate_A(:,3) - plane_plate_A';

    % calculate centroid
    x0 = mean(new_data_plate_B)';

    % translate the points around the centroid
    XYZ_trans = [(new_data_plate_B(:, 1) - x0(1)) (new_data_plate_B(:, 2) - x0(2)) (new_data_plate_B(:, 3) - x

```

```
335     [U, S, V] = svd(XYZ_trans, 0);
336
337     % find the smallest singular value in S and extract the
338     % corresponding right singular vector from V
339     [s, ii] = min(diag(S));
340     a = V(:, ii);   % Direction cosines of the normal to the best-fit
341                     % plane.
342
343     for n=1:length(new_data_plate_B)
344         plane_plate_B(n)=x0(3)-a(1)/a(3)*(new_data_plate_B(n,1)-x0(1))-a(2)/a(3)*...
345             (new_data_plate_B(n,2)-x0(2));
346     end
347      % Alignment
348     new_data_plate_B(:,3)=new_data_plate_B(:,3) - plane_plate_B';
349 % --------------------------------------------------------------------
350
351 figure(119), hold on
352 plot3(new_data_plate_A(:,1),new_data_plate_A(:,2),new_data_plate_A(:,3),'r.')
353 plot3(new_data_plate_B(:,1),new_data_plate_B(:,2),new_data_plate_B(:,3),'b.')
354
355 if type_inter==1
356     Z_plate_A=griddata(new_data_plate_A(:,1),new_data_plate_A(:,2) ...
357         ,new_data_plate_A(:,3),X,Y,'linear');
358     Z_plate_B=griddata(-new_data_plate_B(:,1),new_data_plate_B(:,2) ...
359         ,new_data_plate_B(:,3),X,Y,'linear');
360
361 elseif type_inter==2
362     Z_plate_A=griddata(new_data_plate_A(:,1),new_data_plate_A(:,2) ...
363         ,new_data_plate_A(:,3),X,Y,'nearest');
364     Z_plate_B=griddata(-new_data_plate_B(:,1),new_data_plate_B(:,2) ...
365         ,new_data_plate_B(:,3),X,Y,'nearest');
366
367 elseif type_inter==3
368     Z_plate_A=griddata(new_data_plate_A(:,1),new_data_plate_A(:,2) ...
369         ,new_data_plate_A(:,3),X,Y,'cubic');
370     Z_plate_B=griddata(-new_data_plate_B(:,1),new_data_plate_B(:,2) ...
371         ,new_data_plate_B(:,3),X,Y,'cubic');
372
373 elseif type_inter==4
374     Z_plate_A=griddata(new_data_plate_A(:,1),new_data_plate_A(:,2) ...
375         ,new_data_plate_A(:,3),X,Y,'v4');
376     Z_plate_B=griddata(-new_data_plate_B(:,1),new_data_plate_B(:,2) ...
377         ,new_data_plate_B(:,3),X,Y,'v4');
378 end
379
380 % calculates the average of both specimen halfs
381 average_surface=(Z_plate_A+Z_plate_B)./2;
382
383 mean_average_surface_lines=mean(average_surface,1);
384
385 i=0;
386 for m=1:length(X(:,1))
387     for n=1:length(X(1,:))
388         i=i+1;
389         new_Data(i,:) = [X(m,n) Y(m,n) average_surface(m,n)];
390     end
391 end
392 XYZ=[new_Data(:,1),new_Data(:,2),new_Data(:,3)];
393
```

```
% calculate centroid
x0 = mean(XYZ)';

% translate the points around the centroid
XYZ_trans = [(XYZ(:, 1) - x0(1)) (XYZ(:, 2) - x0(2)) ...
    (XYZ(:, 3) - x0(3))];

[U, S, V] = svd(XYZ_trans, 0);

% find the smallest singular value in S and extract the
% corresponding right singular vector from V
[s, ii] = min(diag(S));
a = V(:, ii);   % Direction cosines of the normal to the best-fit
                % plane.

for n=1:length(new_Data)
    average_plane(n)=x0(3)-a(1)/a(3)*(new_Data(n,1)-x0(1))-a(2)/a(3)*...
        (new_Data(n,2)-x0(2));
end

figure(103),hold on
Title('Average Interpolated Surface with middle plane')
plot3(new_Data(:,1),new_Data(:,2),new_Data(:,3),'b.')
plot3(new_Data(:,1),new_Data(:,2),average_plane,'r.')
view([-29 40]);

figure(102),hold on
Title('Middle planes before and after alignment')
plot3(new_Data(:,1),new_Data(:,2),average_plane,'b.')
view([-29 40]);

new_Data(:,3)=new_Data(:,3) - average_plane';

XYZ=[new_Data(:,1),new_Data(:,2),new_Data(:,3)];

% Testing again for allginment
% calculate centroid
x0 = mean(XYZ)';

% translate the points around the centroid
XYZ_trans = [(XYZ(:, 1) - x0(1)) (XYZ(:, 2) - x0(2)) ...
    (XYZ(:, 3) - x0(3))];

[U, S, V] = svd(XYZ_trans, 0);

% find the smallest singular value in S and extract the
% corresponding right singular vector from V
[s, ii] = min(diag(S));
a = V(:, ii);   % Direction cosines of the normal to the best-fit
                % plane.

for n=1:length(new_Data)
    average_plane(n)=x0(3)-a(1)/a(3)*(new_Data(n,1)-x0(1))-a(2)/a(3)*...
        (new_Data(n,2)-x0(2));
end

i=0;
for m=1:length(X(:,1))
    for n=1:length(X(1,:))
```

```
453         i=i+1;
454         X(m,n)= new_Data(i,1);
455         Y(m,n)= new_Data(i,2);
456         average_surface(m,n)= new_Data(i,3);
457     end
458 end
459 % % % % % %
460
461 figure(99),hold on
462 Title('Both Interpolated Surfaces')
463 plot3(X,Y,Z_plate_A,'b.')
464 plot3(X,Y,Z_plate_B,'r.')
465 view([-29 40]);
466
467 figure(119),hold on
468 % Title('Average Interpolated Surface and both measured plates')
469 plot3(X,Y,average_surface,'k.')
470 set(gca,'FontSize',16)
471 set(gcf, 'Position', get(0,'Screensize')); % Maximize figure
472 xlabel('specimen width [mm]','Rotation',0)
473 ylabel('specimen thickness [mm]','Rotation',-35)
474 zlabel('surface relaxation [mm]','Rotation',90)
475 view([-12 20]);
476 saveas(gcf,'analyzed_data/Measured_plates_and_average','pdf')
477
478 figure(120),hold on
479 % Title('Average Interpolated Surface')
480 plot3(X,Y,average_surface,'k.')
481 view([-29 40]);
482
483 figure(121),hold on
484 % Title('Average Interpolated Surface')
485 plot3(X,Y,average_surface,'k.')
486 view([-29 40]);
487
488 figure(101),hold on
489 Title('Average Interpolated Surface')
490 surf(X,Y,average_surface)
491 view([10 52]);
492
493 figure(102),hold on
494 Title('Difference between before and after allignment of Average Surface')
495 plot3(new_Data(:,1),new_Data(:,2),average_plane,'r.')
496 view([-50 20]);
497 saveas(gcf,'analyzed_data/Before_and_after_alignment_of_average_surface','pdf')
498
499 if part ==1
500     % smooths the gridded data
501     k=3; % quadratic spline
502     surf_smooth_av=spap2(knots,[k k],{x,y},average_surface');
503     for nn=1:size(matrix_x,2)
504         for mm=1:size(matrix_x,1)
505             smooth_surface(mm,nn)=fnval(surf_smooth_av,...
506                 {matrix_x(mm,nn),matrix_y(mm,nn)});
507         end
508     end
509      for nn=1:length(nodes)
510         smooth_result(nn)=fnval(surf_smooth_av,{nodes(nn,2),...
511             nodes(nn,3)});
```

```
512         smooth_result_to_write(nn)=smooth_result(nn)+nodes(nn,4);
513     end
514
515     smooth_result=smooth_result-mean(smooth_result);
516
517     interpolated_smooth_surface=griddata(matrix_x,matrix_y ...
518         ,smooth_surface,X,Y,'nearest');
519
520     % Goodness of fit
521     average_surface=inpaint_nans(average_surface,0);
522     sum_smooth=0;
523     sum_origin=0;
524     for nn=1:size(X,1)
525         for mm=1:size(X,2)
526
527             sum_smooth=sum_smooth+(interpolated_smooth_surface(nn,mm)-...
528                 average_surface(nn,mm))^2;
529             sum_origin=sum_origin+(interpolated_smooth_surface(nn,mm)-...
530                 nanmean(nanmean(smooth_surface)))^2;
531
532         end
533     end
534     GOF=1-sum_smooth/sum_origin;
535
536
537     figure(120), hold on
538     set(gca,'FontSize',16)
539 %     Title('Average Smooth Surface and Interpolation Grid')
540     set(gcf, 'Position', get(0,'Screensize')); % Maximize figure
541     surf(matrix_x,matrix_y,smooth_surface)
542     xlabel('specimen width [mm]','Rotation',-25)
543     ylabel('specimen thickness [mm]','Rotation',15)
544     zlabel('surface relaxation [mm]')
545     view([48 37])
546 %     colorbar('location','NorthOutside','FontSize',14)
547     saveas(gcf,'analyzed_data/Average_Smooth_Surface_and_Interpolation_Grid_3D','pdf')
548
549     figure(121), hold on
550     set(gca,'FontSize',16)
551 %     Title('Average Smooth Surface and Interpolation Grid')
552     set(gcf, 'Position', get(0,'Screensize')); % Maximize figure
553     surf(matrix_x,matrix_y,smooth_surface)
554     xlabel('specimen width [mm]','Rotation',0)
555     ylabel('specimen thickness [mm]','Rotation',90)
556     zlabel('surface relaxation [mm]')
557     view([-0.5 90])
558     colorbar('location','EastOutside','FontSize',14)
559     saveas(gcf,'analyzed_data/Average_Smooth_Surface_and_Interpolation_Grid','pdf')
560
561
562     disp(strcat('The goodness of fit for this surface is ',...
563         num2str(GOF*100),'%'))
564
565
566     % Writes the Abaqus input file with the obtained deformation
567     fid1 = fopen('FEM/1/displacement.inp', 'w');
568     fprintf(fid1, '*BOUNDARY, TYPE=DISPLACEMENT, OP=MOD\n');
569     for nn=1:length(smooth_result)
570         fprintf(fid1, strcat('\t        ',num2str(nodes(nn,1)),',\t',...
```

```
571             num2str(3),',\t,\t',num2str(smooth_result_to_write(nn)),' \n'));
572     end
573     fclose(fid1)
574
575     % Writes the Abaqus input file non deformed
576     fid1 = fopen('FEM/1/originaldisplacement.inp', 'w');
577     fprintf(fid1, '*BOUNDARY, TYPE=DISPLACEMENT, OP=MOD\n');
578     for nn=1:length(smooth_result)
579         fprintf(fid1, strcat('\t        ',num2str(nodes(nn,1)),',\t',...
580             num2str(2),',\t,\t',num2str(nodes(nn,4)),' \n'));
581     end
582     fclose(fid1)
583 end
584 %%%%%%%%%%%%%%%%%%%%%%%%%%%%%%%%%%%%%%%%%%%%%%%%%%%%%%%%%%%%%%%%%%%%%%%%%%%%%%%
585
586 %%%%%%%%%%%%%%%%%%%%%%%%%%%%%%%%%%%%%%%%%%%%%%%%%%%%%%%%%%%%%%%%%%%%%%%%%%%%%%%
587 if part == 2
588     % writes a path with all the nodes from the surface. Afterwards, the
589     % stresses on this nodes will be retrieved
590     fid1 = fopen('FEM/pathB.txt', 'w');
591     for j=1:length(nodes(:,1))
592         fprintf(fid1, strcat(num2str(nodes(j,1)),', '));
593     end
594     fclose(fid1)
595 end
596 %%%%%%%%%%%%%%%%%%%%%%%%%%%%%%%%%%%%%%%%%%%%%%%%%%%%%%%%%%%%%%%%%%%%%%%%%%%%%%%
597
598 %%%%%%%%%%%%%%%%%%%%%%%%%%%%%%%%%%%%%%%%%%%%%%%%%%%%%%%%%%%%%%%%%%%%%%%%%%%%%%%
599 if part == 3
600     % import stress from the created abaqus report and plots them
601     DELIMITER = ' ';
602     HEADERLINES = 2;
603     newData1 = importdata('FEM/abaqus.rpt', DELIMITER,...
604         HEADERLINES);
605     stress33=-newData1.data(:,2);
606     stress33_qq=-newData1.data(:,:);
607
608     % Ploting
609     figure(3)
610     plot(nodes(:,2),nodes(:,3),'k.')
611
612     aux_nodes=csvread('FEM/Nodes.inp',1,0);
613     FEMnodes=aux_nodes(find(aux_nodes(:,4)==190),:);
614     tol=0.2;
615     contador_X=0;
616     for x_sort=-149:1:-7
617         contador_X=contador_X+1;
618         aux_2=find(FEMnodes(:,2)>x_sort-tol & ...
619             FEMnodes(:,2)<x_sort+tol);
620         [a,b]=sort(FEMnodes(aux_2,3),'descend');
621             nodes_list=FEMnodes(aux_2(b),1);
622         node_ID_A(:,contador_X)=nodes_list;
623     end
624
625 %    Quarter Plate with Wedge elements 0.5x1
626 node_ID_middle(:,1)=[541,3779,3780,3781,3782,3783,3784,3785,3786,3787,3788,552];
627 node_ID_middle(:,2)=[540,3769,3770,3771,3772,3773,3774,3775,3776,3777,3778,553];
628 node_ID_middle(:,3)=[37,3759,3760,3761,3762,3763,3764,3765,3766,3767,3768,554];
629 node_ID_middle(:,4)=[539,3749,3750,3751,3752,3753,3754,3755,3756,3757,3758,40];
```

```
node_ID_middle(:,5)=[36,3739,3740,3741,3742,3743,3744,3745,3746,3747,3748,555];
node_ID_middle(:,6)=[538,3729,3730,3731,3732,3733,3734,3735,3736,3737,3738,41];
node_ID_middle(:,7)=[35,3719,3720,3721,3722,3723,3724,3725,3726,3727,3728,556];
node_ID_middle(:,8)=[537,3709,3710,3711,3712,3713,3714,3715,3716,3717,3718,42];
node_ID_middle(:,9)=[34,3699,3700,3701,3702,3703,3704,3705,3706,3707,3708,557];
node_ID_middle(:,10)=[536,3689,3690,3691,3692,3693,3694,3695,3696,3697,3698,43];
node_ID_middle(:,11)=[33,3679,3680,3681,3682,3683,3684,3685,3686,3687,3688,558];
node_ID_middle(:,12)=[535,3669,3670,3671,3672,3673,3674,3675,3676,3677,3678,44];
node_ID_middle(:,13)=[32,3659,3660,3661,3662,3663,3664,3665,3666,3667,3668,559];
node_ID_middle(:,14)=[534,3649,3650,3651,3652,3653,3654,3655,3656,3657,3658,560];


    contador_X=0;
        for x_sort=7:1:149
        contador_X=contador_X+1;
        aux_2=find(FEMnodes(:,2)>x_sort-tol & ...
            FEMnodes(:,2)<x_sort+tol);
        [a,b]=sort(FEMnodes(aux_2,3),'descend');
            nodes_list=FEMnodes(aux_2(b),1);
        node_ID_B(:,contador_X)=nodes_list;
        end
    node_ID=[node_ID_A node_ID_middle node_ID_B];
    for nn=1:size(node_ID,2)
        for mm=1:size(node_ID,1)
            c=find(FEMnodes(:,1)==node_ID(mm,nn));
            matrix_stress(mm,nn)=stress33(c);
            matrix_x(mm,nn)=nodes(c,2);
            matrix_y(mm,nn)=nodes(c,3);
        end
    end

% Ploting
    figure(33)
    set(gca,'FontSize',16)
    surf(matrix_x,matrix_y,matrix_stress)
    xlabel('specimen width [mm]','Rotation',0)
    ylabel('specimen thickness [mm]','Rotation',0)
    zlabel('Normal stress [MPa]')
    colorbar('location','NorthOutside','FontSize',14)
    set(gcf, 'Position', get(0,'Screensize')); % Maximize figure
    saveas(gcf,'analyzed_data/Stress_Map','jpg')

    figure(34)
    set(gca,'FontSize',16)
    surf(matrix_x,matrix_y,matrix_stress)
    xlabel('specimen width [mm]','Rotation',0)
    ylabel('specimen thickness [mm]','Rotation',90)
    zlabel('Normal stress [MPa]')
    view([-0.5 90])
    colorbar('location','EastOutside','FontSize',14)
    set(gcf, 'Position', get(0,'Screensize')); % Maximize figure
    saveas(gcf,'analyzed_data/Stress_Map_Plane','jpg')

    figure(35)
    set(gca,'FontSize',16)
    surf(matrix_x,matrix_y,matrix_stress,'LineStyle','none')
    xlabel('specimen width [mm]','Rotation',0)
    ylabel('specimen thickness [mm]','Rotation',90)
    zlabel('Normal stress [MPa]')
```

```
689     view([-0.5 90])
690     colorbar('location','EastOutside','FontSize',14)
691     set(gcf, 'Position', get(0,'Screensize')); % Maximize figure
692     saveas(gcf,'analyzed_data/Stress_Map_Plane_no_lines','jpg')
693
694     save('stress.mat','matrix_x','matrix_y','matrix_stress')
695 end
```

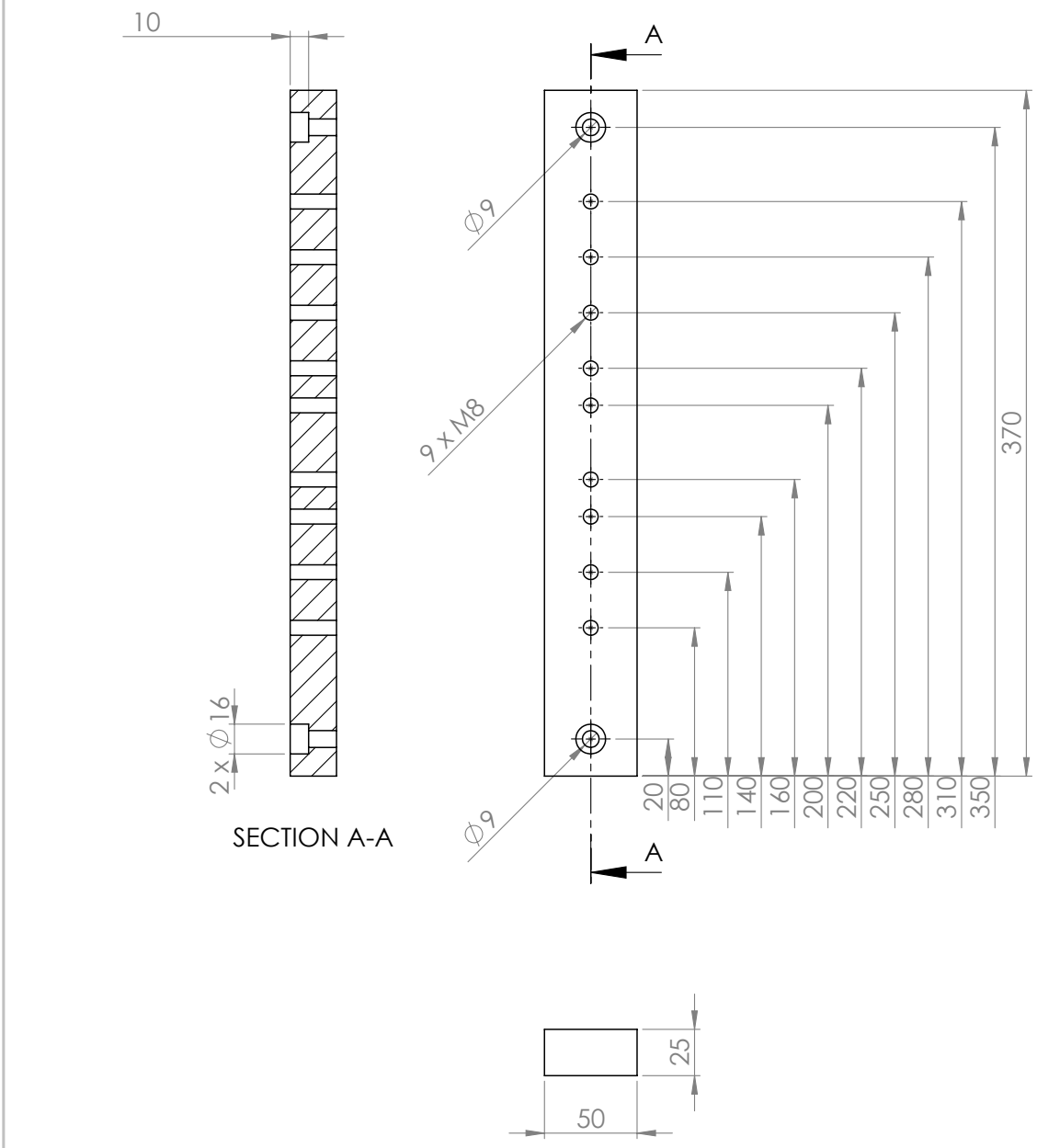
Appendix C

Fabrication drawings for the clamping system

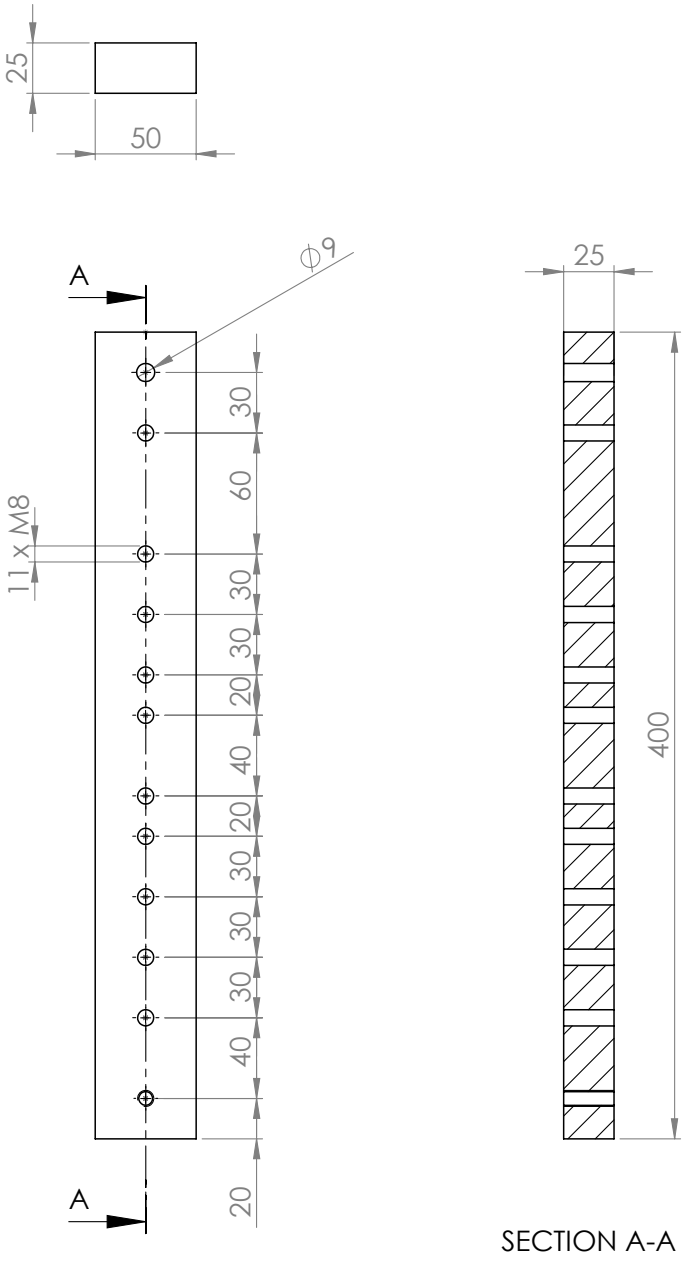
In this appendix it is presented the fabrication drawings of the clamping system (Figure C.1) developed and used in this work.



Figure C.1: Clamping system



UNLESS OTHERWISE SPECIFIED: DIMENSIONS ARE IN MILLIMETERS SURFACE FINISH: TOLERANCES: LINEAR: ANGULAR:		FINISH:			DEBUR AND BREAK SHARP EDGES	DO NOT SCALE DRAWING	REVISION
	NAME	SIGNATURE	DATE			TITLE:	
DRAWN							
CHK'D							
APPV'D							
MFG							
Q.A				MATERIAL:		DWG NO. Newbridge1	A4
				WEIGHT:		SCALE:1:3	SHEET 1 OF 1



SECTION A-A

UNLESS OTHERWISE SPECIFIED: DIMENSIONS ARE IN MILLIMETERS SURFACE FINISH: TOLERANCES: LINEAR: ANGULAR:		FINISH:			DEBUR AND BREAK SHARP EDGES	DO NOT SCALE DRAWING	REVISION
	NAME	SIGNATURE	DATE			TITLE:	
DRAWN							
CHK'D							
APPV'D							
MFG							
Q.A				MATERIAL:		DWG NO. Newbridge2	A4
				WEIGHT:		SCALE:1:3	SHEET 1 OF 1

Appendix D

Residual stress effect on stress intensity factor

In this appendix the effect of residual stress on the stress intensity factor of an infinite plate is demonstrated by using residual stress distributions found in Terada [1976] and Tada and Paris [1983] and comparing with an infinite plate free of residual stress. A rough approximation between these proposed residual stress distributions and that measured by the contour method on a weld plate, at mid thickness, is performed in this appendix.

The normal residual stress field due the presence of a welding seam along the line perpendicular to the joint may be represented by:

$$\sigma(x) = \sigma_{Max} f\left(x\right) \tag{D.1a}$$

$$\sigma(\xi) = \sigma_{Max} f\left(\xi\right) = \sigma_{Max} f\left(\frac{x}{c}\right) \tag{D.1b}$$

where c is the point along the line perpendicular to the joint where the residual stress curve intersects the zero value.

According to Terada [1976], $f\left(\xi\right)$ has to satisfy the following conditions.

(a) The residual stress has to self balance;

$$\int_{-\infty}^{\infty} f\left(\xi\right) d\xi = 0 \tag{D.2a}$$

(b) The residual stress distribution is symmetric with respect to the center line of the joint;

$$f\left(\xi\right) = f\left(-\xi\right) \tag{D.2b}$$

(c) The maximum value of unity occurs at x= 0;

(d) The effect of welding diminishes as the distance from it increases;

$$f(\xi) \to 0 \quad as \quad \xi \to \infty \tag{D.2c}$$

The proposed distributions are:

$$f_{Terada}(\xi) = e^{\left(-0{,}5\xi^2\right)}\left(1-\xi^2\right) \tag{D.3a}$$

$$f_{Tada\ and\ Paris}(\xi) = \frac{1-\xi^2}{1+\xi^4} \tag{D.3b}$$

In order to approximate the residual stress fields proposed with the actual measurement obtained with the contour method at mid thickness the values must be: $\sigma_{Max} = 300$ MPa and $c = 35$ mm.

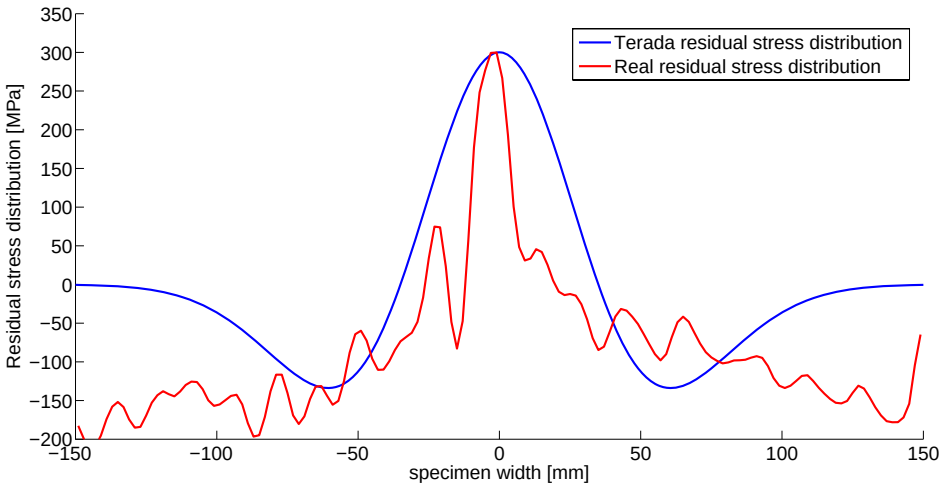


Figure D.1: Residual stress field

Using the weight function technique (see, e.g. Parker [1981]) the stress intensity factor, K is given by:

$$K = \int_{-a}^{a} \sigma(x).w(x,a)dx \tag{D.4}$$

where w(x,a) is the weight function which is given by:

$$w(x,a) = \frac{E}{2K}\frac{\delta v(x,a)}{\delta a} \tag{D.5}$$

In the case of an infinite plate in the absence of residual stress the stress intensity factor and displacement are:

$$\begin{cases} K = & \sigma\sqrt{\pi a} \\ v(x,a) = & \frac{2\sigma}{E}\sqrt{a^2-x^2} \end{cases} \tag{D.6}$$

Replacing D.6 in D.5 the weight function will become:

$$w(x,a) = \sqrt{\frac{a}{\pi}}\frac{1}{\sqrt{a^2-x^2}} \tag{D.7}$$

The stress intensity factor for an infinite plate with the proposed residual stress fields will be:

$$K_{Terada}\left(a\right) = \int_{-a}^{a} 300.e^{\left(-0{,}5\left(\frac{x}{35}\right)^2\right)}\left(1-\left(\frac{x}{35}\right)^2\right)\sqrt{\frac{a}{\pi}}\frac{1}{\sqrt{a^2-x^2}}dx \tag{D.8a}$$

$$K_{Tada\ and\ Paris}\left(a\right) = \int_{-a}^{a} 300\frac{1-\left(\frac{x}{35}\right)^2}{1+\left(\frac{x}{35}\right)^4}\sqrt{\frac{a}{\pi}}\frac{1}{\sqrt{a^2-x^2}}dx \tag{D.8b}$$

If a 200 MPa remote tension (like it is shown in Figure D.2) is added to the residual stress already present in the plate the stress intensity factor will become:

$$K_{Terada}\left(a\right) = \int_{-a}^{a}\left(200+300.e^{\left(-0{,}5\left(\frac{x}{35}\right)^2\right)}\left(1-\left(\frac{x}{35}\right)^2\right)\right)\sqrt{\frac{a}{\pi}}\frac{1}{\sqrt{a^2-x^2}}dx \tag{D.9a}$$

$$K_{Tada\ and\ Paris}\left(a\right) = \int_{-a}^{a}\left(200+300\frac{1-\left(\frac{x}{35}\right)^2}{1+\left(\frac{x}{35}\right)^4}\right)\sqrt{\frac{a}{\pi}}\frac{1}{\sqrt{a^2-x^2}}dx \tag{D.9b}$$

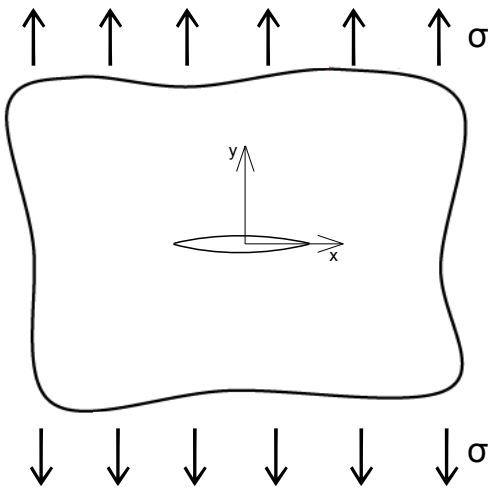


Figure D.2: Scheme of infinite plate under remote tension

The stress intensity factor evolution with the increase in crack length may now be represented for the Terada distribution using c=35, together with the K solution for the infinite plate without residual stresses, Figure D.3.

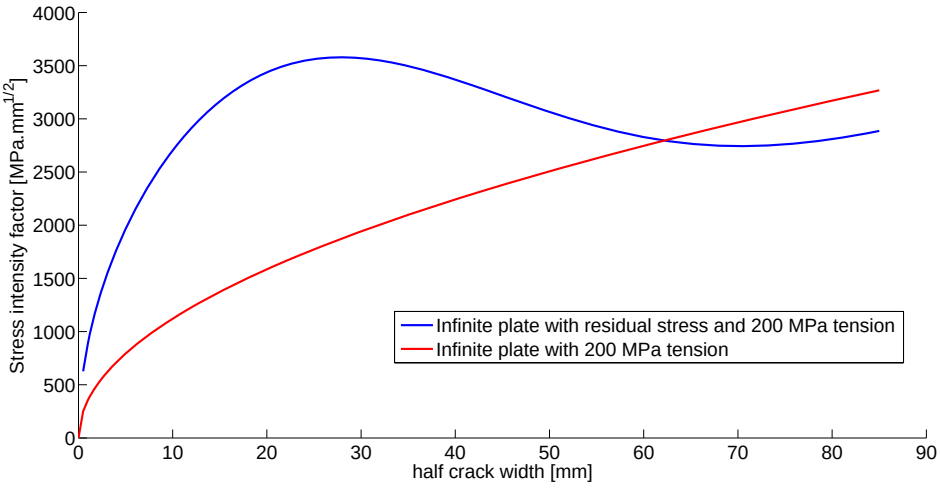


Figure D.3: Stress intensity factor evolution with crack length

Although rigorous for the infinite plate, this is of course a very rough approximation for dealing with the present finite plate. This appendix just aims at showing how a possible approach to the problem could be performed, once the required tools, as relevant weight function are in place.

The Terada model is applicable to a 1D problem, where residual stress distribution along a line is known and self-equilibrating. In the contour method, a full field analysis is made instead, and the self-equilibrium is achieved on the plane. The identification of a line for comparison with the Terada model will therefore be always a rough approximation, as it is unlikely that the real residual stresses along the chosen line will be self-equilibrating.